ABSTRACT

Title of Dissertation: DEVELOPMENT AND PLASTICITY OF THE FUNCTIONAL LAMINAR MESOSCALE ORGANIZATION OF THE PRIMARY AUDITORY CORTEX

Krystyna Lisa Solarana, Doctor of Philosophy, 2016

Dissertation directed by: Professor Patrick O. Kanold, Department of Biology

Early sensory experience is fundamental for proper structural and functional organization of the brain. A brain region that particularly relies on sensory input during a critical period of development is the primary auditory cortex (A1). The functional architecture of A1 in adult mammals has been widely studied on a macroscale and single-cell level, and it is evident that this sensory area is characterized by a tonotopic gradient of frequency preference and that individual auditory neurons are tuned to complex features of acoustic stimuli. However, the development of microcircuits within A1 and how experience shapes this mesoscale organization during different plasticity windows is not known. The work in this dissertation uses *in vivo* two-photon calcium imaging in mice to investigate how the population dynamics of auditory neurons within thalamorecipient layer 4 and supragranular layers 2/3 change over development – from before ear opening, through

the critical period for auditory spectral tuning, and on to mature adult circuitry. Furthermore, this dissertation explores how brief visual deprivation has the power to initiate compensatory, cross-modal plasticity mechanisms and restructure network circuitry in the adult auditory cortex, after the critical period for developmental plasticity has closed. Results from these studies fill crucial gaps in our understanding of experience-dependent cortical circuit development and refinement by showing that the spatial representation of sound frequency is shaped by sensory experience, teasing apart the underlying laminar-specific differences in microcircuitry changes, and indicating an overall dissociation of plasticity of single-cell, mesoscale, and macroscale network properties.

DEVELOPMENT AND PLASTICITY OF THE FUNCTIONAL LAMINAR
MESOSCALE ORGANIZATION OF THE PRIMARY AUDITORY CORTEX


by


Krystyna Lisa Solarana


Dissertation submitted to the Faculty of the Graduate School of the
University of Maryland, College Park, in partial fulfillment
of the requirements for the degree of
Doctor of Philosophy
2016


Advisory Committee:
Professor Patrick O. Kanold, Chair
Distinguished Professor Catherine Carr
Assistant Professor Daniel Butts
Associate Professor Joshua Singer
Associate Professor Matthew Roesch

# Acknowledgments

First and foremost, I would like to express my deepest gratitude to my husband, Brandon, for the unconditional love, unwavering encouragement, and endless patience he has provided since day one of graduate school. Thank you for consistently stepping up and never complaining when I stayed in lab late to get more work done, and for witnessing all my doubts and frustrations and never letting me give up.

An enormous thank you to my parents, Lucy and Jan, and my brother, Adam, for being a constant source of loving support and encouraging words, and for always believing in me and encouraging me to persevere.

This dissertation would not have been possible without the help of past and present Kanold Lab members, particularly Aminah, Rongkang, Zac, Ji, Ying, Dan N, Dan W, Nik F, Shahzeib, Kevin, and Phil. Thank you for your encouragement, coding help, troubleshooting assistance, editing, and endless cell clicking.

I would also like to thank my mentor, Dr. Patrick Kanold, for his guidance, support, and endless creative ideas during my graduate studies, and for helping me to improve as a scientist, writer, and speaker.

Lastly, I would like to thank the members of my dissertation committee: Dr. Catherine Carr, Dr. Dan Butts, Dr. Joshua Singer, and Dr. Matt Roesch, for their support and intellectual insight throughout my graduate training.

# Table of Contents

# List of Tables

# List of Figures

# List of Abbreviations

| | |
|---|---|
| A1 | Primary auditory cortex |
| AAF | Anterior auditory field |
| AAV | Adeno-associated virus |
| ACSF | Artificial cerebrospinal fluid |
| ACX | Auditory cortex |
| AII | Secondary auditory cortex |
| BF | Best Frequency |
| Ca2+ | Calcium |
| CF | Characteristic frequency |
| dB | Decibels |
| EAM | External auditory meatus |
| eIPSC | Evoked inhibitory post-synaptic current |
| EPSC/P | Excitatory post-synaptic current/potential |
| F | Fluorescence |
| FOV | Field of view |
| FRA | Frequency response area |
| GABA | Gamma-amino butyric acid |
| GCaMP | GFP-calmodulin fusion protein |
| GECI | Genetically engineered calcium indicator |

| | |
|---|---|
| GFAP | Glial fibrillary acidic protein |
| GFP | Green fluorescent protein |
| IC | Inferior colliculus |
| ICV | Intracerebroventricular |
| IHC | Immunohistochemistry |
| IPSC/P | Inhibitory post-synaptic current/potential |
| IQR | Interquartile range |
| K+ | Potassium |
| L2/3 | Layer 2/3 |
| L4 | Layer 4 |
| LGN | Lateral geniculate nucleus |
| LSPS | Laser scanning photostimulation |
| LTD | Long-term depression |
| LTP | Long-term potentiation |
| mEPSC | Miniature excitatory postsynaptic current |
| MGN | Medial geniculate nucleus |
| mIPSC | Miniature inhibitory postsynaptic current |
| NC | Noise correlations |
| P# | Postnatal days |
| PV | Parvalbumin |
| RF | Receptive field |

| | |
|---|---|
| ROI | Region of interest |
| S1 | Primary Somatosensory Cortex |
| SAM | Sinusoidally-amplitude modulated |
| SC | Signal correlations |
| SEM | Standard error of the mean |
| SNR | Signal to noise ratio |
| SP | Subplate |
| SPL | Sound pressure level |
| SR-101 | Sulforhodamine-101 |
| STD | Standard deviation |
| STDP | Spike timing dependent plasticity |
| Thy-1 | Thymus cell antigen 1 promoter |
| USV | Ultrasonic vocalization |
| V1 | Primary visual Cortex |

# Chapter 1: Introduction

Early experience of the world shapes the structural and functional organization of the brain. The ability of neural circuits to rewire in response to external sensory input allows the mammalian brain to adapt to its environment and is a fundamental feature of sensory cortices, particularly during specific critical periods in early development. The primary visual (V1) (Wiesel and Hubel, 1963, 1965; Hensch, 2005), somatosensory (S1) (Van der Loos and Woolsey, 1973; Fox, 1992; Feldman et al., 1999; Feldman, 2000, 2009), and auditory (A1) (Zhang et al., 2001, 2002; Chang and Merzenich, 2003; de Villers-Sidani et al., 2007; Insanally et al., 2009; Barkat et al., 2011; Polley et al., 2013; Schreiner and Polley, 2014) cortices have routinely been used as model systems for studying the relationship between the sensory periphery and cortical circuitry, and have allowed both common and distinct underlying plasticity mechanisms to be identified. Within each of these primary sensory cortical areas there exists a highly ordered topographical representation of the periphery – as a rostrocaudally-oriented tonotopic gradient in A1 (Woolsey, 1942; Goldstein et al., 1970; Merzenich et al., 1975; Bandyopadhyay et al., 2010; Hackett et al., 2011; Winkowski and Kanold, 2013; Kanold et al., 2014), an orderly map of facial whiskers within the barrel cortex (Woolsey and Van der Loos, 1970; Chen-Bee et al., 2012), and alternating ocular dominance and orientation columns in V1 (Hubel and Wiesel, 1962, 1977; Garrett et al., 2014; Kremkow et al., 2016). While topographical organization begins to emerge during prenatal development – through

both intrinsic molecular cues and activity-dependent processes – the visual, acoustic, and somatosensory environmental stimulation encountered during early postnatal life restructure and refine the rudimentary connectivity and are crucial for experience-dependent plasticity and proper cortical circuit formation.

To better understand plasticity and delineate specific critical period windows for different stimulus features, diverse sensory deprivation studies have been conducted for the auditory, visual, and somatosensory systems, yet these paradigms do not produce uniform results across and within cortical areas. Distinct differences in plasticity likely arise due to the developmental stage studied (e.g. early postnatal vs. adult), the degree of deprivation (e.g. partial vs. full; peripheral ablation), and the complex projection patterns within laminae (e.g. L4 vs. L2/3). Therefore, to understand the distinct changes observed within these sensory cortices as a response to various sensory exposure or deprivation paradigms, it is important to review thalamocortical and cortico-cortical circuit development, the laminar organization of stimulus feature processing, as well as mechanisms of passive vs. attention-specific synaptic plasticity.

## *Cortical Circuitry*

### The "canonical" sensory cortical circuit

In the adult cerebral cortex, there exists a "canonical" microcircuit in which a serial relay of input allows for sequentially more complex stages of neural computation and sensory processing (Atencio et al., 2009; Atencio and Schreiner,

2010). Within the auditory cortex, this hierarchical structure of connectivity begins when highly ordered ascending thalamic input from the medial geniculate nucleus (MGN) enters thalamorecipient layer 4 (L4), which then sends feed-forward projections to supragranular layers 2 and 3 (L2/3) (**Fig. 1.1a**) (Atencio et al., 2009). Specific thalamic nuclei of other sensory systems likewise send excitatory input to their respective cortical region, including dorsal lateral geniculate (dLGN) input to L4 of V1, and ventrobasal (VB) input to L4 of S1. This circuitry is much more complex, however, as thalamic projections innervate every cortical layer, the densest of which terminate in middle layers (Douglas et al., 2004). Layer 6 and the most superficial cortical layer, L1, are also directly innervated by thalamic projections (Wu et al., 2008). Layer 6 neurons then send feedback projections to the MGN and are proposed to modulate thalamic responses (Wu et al., 2008).

In the adult, the vertical thalamocortical axonal projection to L4 is predominantly columnar (Feldmeyer et al., 1999; Feldmeyer, 2012) such that peripherally organized input is largely preserved topographically in cortical layer 4. However, confined within a column axons show extensive arborization (Feldmeyer, 2012). The potent excitatory influence of thalamic input on L4 activity has been heavily studied, since the amount of cortico-cortical input to this layer far outnumbers thalamic synapses, which roughly account for only 5-15% of total projections (Gil et al., 1999; Bruno and Sakmann, 2006; Douglas and Martin, 2007; Schoonover et al., 2014). The success of thalamic input in driving L4 neurons can perhaps best be explained by a model in which convergent and synchronous thalamic input within the characteristic columnar structure determines thalamocortical efficacy (Schoonover et

3

al., 2014). The requirement of intracortical recurrent connectivity in increasing gain of this input has been debated (Bruno and Sakmann, 2006), but silencing of intracortical excitatory circuits has revealed that laminar connections can amplify thalamocortical signal and preserve feedforward tuning while simultaneously integrating additional inputs and elongating receptive fields (Li et al., 2013b).

A laminar transformation of stimulus information has been described in L2/3 of A1 (Atencio et al., 2009; Atencio and Schreiner, 2010; Winkowski and Kanold, 2013), which results from the fact that these neurons receive a convergence of columnar, tonotopically-organized L4 input and substantial intralaminar and long-range cortico-cortical connections (Oviedo et al., 2010; Meng et al., 2015). For a pyramidal cell located in L2/3 of cat V1, over 70% of excitatory input originates from intralaminar connectivity (Binzegger et al., 2004; Douglas and Martin, 2007). Likewise in A1, L2/3 neurons receive significant intralaminar inputs from other L2/3 neurons in addition to the feed-forward input they receive from L4 neurons (Barbour and Callaway, 2008; Oviedo et al., 2010; Winkowski and Kanold, 2013; Meng et al., 2015). Recurrent feedback loops within L2/3 allow for a wider sampling and integration of diverse synaptic inputs and signal amplification, supporting the generation of more complex receptive fields (Douglas et al., 1995; Chance et al., 1999; Douglas and Martin, 2007), and might foster processing of more natural environmental stimuli such as vocalizations over pure tones (Nelken, 2004; Kanold et al., 2014). L2/3 neurons also project to infragranular layers 5/6, which send reciprocal projections back to the thalamus. This feedback allows the cortex to enhance thalamic transmission and even alter thalamic receptive fields (Briggs and Usrey, 2008).

## Subplate and thalamocortical connectivity

Thalamic innervation of cortical layer 4 requires long-range growing axons in the developing brain to traverse subcortical areas, target the correct cortical area and enter the cortical plate, terminate within the correct layer, and then segregate to form whisker-specific, eye-specific, or frequency-specific clusters. The earliest thalamic afferent growth is directed by molecular gradients that act to guide growing fibers to the appropriate cortical region (Molnar and Blakemore, 1995). Prior to entering the cortical plate, thalamic axons pause and accumulate in the subplate (SP), a transitory population of neurons located in the cortical white matter (Shatz and Luskin, 1986; Allendoerfer and Shatz, 1994). SP neurons are a morphologically distinct class of cells that provide the first postsynaptic target for growing thalamic axons prior to their innervation of the cortical plate (McConnell et al., 1989; Molnar et al., 1998). The role of SP neurons as a cellular scaffold and integral intermediate relay for feed-forward transmission is supported by numerous tracing and ablation studies in which subplate removal resulted in improper formation of cortical organization (Ghosh et al., 1990; Ghosh and Shatz, 1992, 1993; Allendoerfer and Shatz, 1994; Katz and Shatz, 1996; Catalano and Shatz, 1998; Kanold et al., 2003; Kanold, 2004; Yang et al., 2009; Kanold and Luhmann, 2010; Tolner et al., 2012; Viswanathan et al., 2012).

In the visual system, subplate ablation during early development prevents LGN axon targeting of L4 of V1 (Ghosh et al., 1990), precludes the anatomical segregation of thalamic axons according to eye preference (Ghosh and Shatz, 1992), and thus results in a deficient maturation of thalamocortical synapses. These

anatomical abnormalities have profound functional consequences, as evidenced by the absence of orientation columns and poorly tuned and weak responses to visual stimuli in V1 (Kanold et al., 2003; Kanold, 2004; Kanold and Luhmann, 2010). Furthermore, studies in rat S1 have shown that subplate ablation disrupts barrel column formation in L4 and impairs the strengthening of thalamocortical inputs to L4 neurons (Tolner et al., 2012).

From this thorough evidence in V1 and S1, it can be speculated that subplate is also required for the strengthening of synaptic transmission and establishment of proper functional architecture in A1, and that critical circuitry changes are occurring during early sensory development. In fact, it has been shown that following subplate ablation in cats, MGN axons, like LGN axons, display abnormal trajectories and grow past the auditory region within the white matter (Ghosh and Shatz, 1993). With subplate intact, *in vitro* studies in mice show that MGN projections to SP neurons increase and strengthen between postnatal (P) days 2-13, and that SP neurons can induce action potentials in L4 neurons at these early ages (Zhao et al., 2009), even prior to the onset of hearing. Coincident to the formation of strong functional excitatory connections between SP and L4, thalamocortical axons grow into the cortical plate and have reached their target cortical layer 4 by P8 (in S1) and have begun branching (Hoerder-Suabedissen and Molnar, 2015). During this intermediate stage, L4 neurons receive excitatory projections from SP and from MGN (**Fig. 1.1a**). These inputs interact and promote strengthening (or weakening) of thalamocortical synapses during the critical period, which has been proposed to occur by exploiting spike-timing dependent (STDP) learning rules (Kanold and Shatz, 2006). In what has
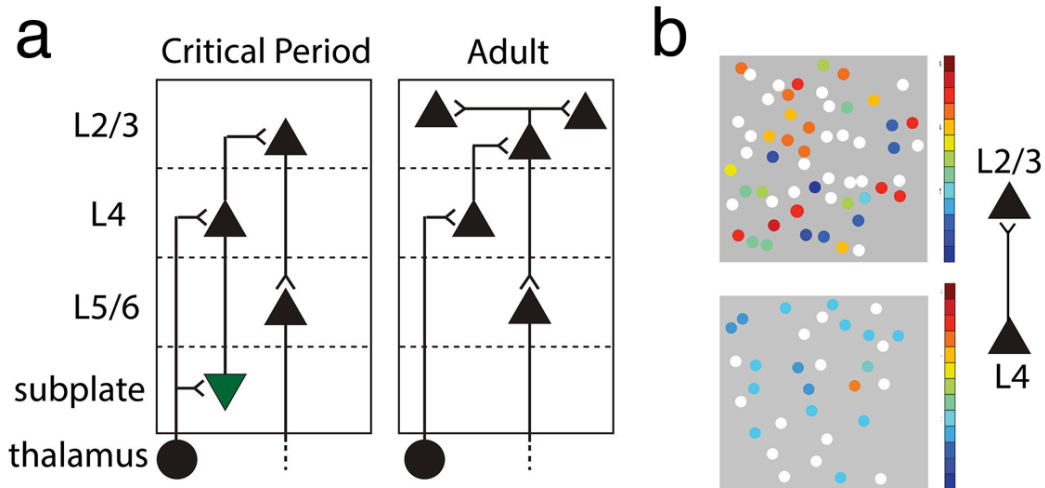
**Figure 1.1. Schematic of the "canonical" cortical circuit during early postnatal development and in the adult.** (**a**) Subplate neurons receive thalamic input and project into the developing cortical plate, mostly to L4, and are required for the maturation of synapses in L4. Subplate neurons mostly die off after the first three weeks of postnatal development, and in the adult cortex, ascending thalamic input is first processed in L4. Supragranular layer 2/3 neurons receive L4 input, as well as a large amount of intra-laminar input. (**b**) A spatial diagram of BF variability for auditory neurons in two imaging planes in thalamorecipient L4 and supragranular L2/3. Color indicates BF (low frequencies in blues, and higher frequencies in reds), and white circles denote unresponsive cells. Note the homogeneity of responses in L4 compared to the local heterogeneity of responses in L2/3.

been described as a "teacher circuit" (Butts and Kanold, 2010), SP neurons create an intermediate circuit that allows pre- and post-synaptic spiking activity to sequentially occur within the potentiating window on the fast time scales necessary to elicit STDP. SP neurons only have a short time in order to "teach" layer 4 neurons to appropriately

respond to MGN inputs, as they begin to die off shortly after birth and are at least 80% absent by P21 in mice. Those that survive persist within layer 6 of mature cortex.

As a result of these ongoing circuitry changes occurring during early postnatal development, it is likely that SP neurons impart their stimulus preference to L4 neurons and that a rudimentary tonotopic map exists within SP, which is then projected to L4 (Kanold, 2009). In fact, electrophysiology experiments in the Kanold lab have shown that SP neurons show sound-evoked responses in A1 prior to L4 neurons (Wess et al., 2011). This evidence demonstrates that subplate is integrated into early circuitry, is involved in spontaneous and sound-evoked activity before and during ear opening and the onset of functional hearing (~P12), and influences the maturation of thalamocortical and intracortical connectivity.

Spontaneous network activity is a crucial step in activity-dependent assembly of early cortical connectivity, and is thought to pattern the initial coarse topography within sensory cortices by evoking correlated activity between groups of cells (Feller et al., 1996; Katz and Shatz, 1996; Butts, 2002). In the ferret visual cortex, prominent waves of activity were observed at eye opening that were characterized by strong noise correlations, which suggests a high degree of common input at this early stage preceding experience-dependent refinement (Smith et al., 2015). Neighboring excitatory neurons in early development are electrically coupled via gap junctions (Yao et al., 2016), but do not exhibit preferential functional connectivity (Ko et al., 2013). Furthermore, the feedforward ascending input that is largely confined within columns in the adult appears to "color outside the lines" during development, as axon

collaterals in L4 and L2/3 project over columnar borders (Bender et al., 2003; Feldmeyer, 2012). In V1, experience of visual stimuli is required to reorganize the arrangement of local synaptic connections such that stronger connections preferentially form between neurons tuned to similar stimulus features, whereas differentially tuned neurons lose synaptic connectivity (Ko et al., 2013). This circuit refinement and decrease in noise correlation over development might serve to improve discrimination of stimulus parameters but relies on stimulus exposure (Smith et al., 2015). Thus, while molecular gradients initiate cortical organization and spontaneous waves form the crude wiring patterns within cortex via activity-dependent processes, patterned sensory input is required for the proper formation of circuit subnetworks and an accurate topographical representation of the sensory periphery processed by each modality.

## *Auditory Processing*

### The primary auditory pathway

Sound waves enter the external auditory meatus as mechanical vibrations and are transformed into electrochemical signals within the cochlea of the inner ear. This function is attributed to hair cells, the sensory cell of the cochlea, which through their deflection allow the influx of potassium ($K^+$) and then calcium ($Ca^{2+}$), neurotransmitter release, and initiate the propagation of acoustic information through the primary auditory pathway. Hair cells are maximally stimulated along different portions of the basilar membrane of the cochlea. At the stiff base, hair cells respond

to high frequencies, whereas those at the more flexible apex transduce low frequencies. Thus, the topographic spatial representation of sound frequency (tonotopy) is first established within the cochlea and is preserved throughout the sequential stages of feedforward auditory processing within the primary auditory pathway.

Auditory nerves transfer this signal to the cochlear nuclei, whose neurons then target the superior olive. The superior olive receives input from both ears and functions in comparing interaural intensity and temporal differences to determine localization of sound. Next, the inferior colliculus (IC) of the midbrain integrates the convergent input it receives, and can activate reflexes such as fast orientation to sound sources via contact with the superior colliculus. Prior to reaching cortical processing layers, auditory input that has rapidly traversed this pathway is relayed through the MGN of the thalamus. Thus with all these sequential processing stages involved not just in relaying auditory input but also serving their respective decoding functions, it seems reasonable that ACX neurons act as more than just frequency detectors.

Much is known about the different developmental stages of these sequential processing areas, which are likely to affect auditory cortical response development and refinement. In mice, cochlear structures are present at birth but mature in size by P8-10 (Mikaelian and Ruben, 1965). In CBA-J mice, cochlear potentials appear in some animals at P8 and in all by P10, and reach adult like values by P14 (Mikaelian and Ruben, 1965). During this time, the structural maturation of the cochlea (as well as hair cells and spiral ganglion cells) begins at the basal end and proceeds to the apex

(Romand, 1987; Romand and Ehret, 1990). The external auditory meatus (EAM) in CBA-J mice begins to open around P9 and is fully open by P12 (Mikaelian and Ruben, 1965), but opens slightly later in C57BL/6 mice used in these studies, specifically between P12-13 (Willott and Shnerson, 1978; Shnerson and Pujol, 1983). The middle ear cavity of mice is filled with a gelatinous substance, most of which disappears by P9-10 in CBA-J mice (Mikaelian and Ruben, 1965). In studies characterizing earlier development of inner ear structures, the EAM was surgically opened so sound could reach the inner ear with less impedance (Shnerson and Pujol, 1983). Just before natural ear opening in C57 mice, only high-intensity stimuli of moderately low frequencies could evoke responses in IC neurons, but just after hearing onset (P12-14) thresholds were reduced and responses to higher frequency tones could be evoked (Willott and Shnerson, 1978). The emergence of low frequency sensitivity prior to high frequency tuning is interesting given that the basal, high-frequency end of the cochlea matures prior to the apical, low-frequency end (Romand, 1987). Studies have shown that this incongruity occurs due to a developmental shift in the tonotopic organization of the cochlea, causing basal regions of the cochlea to gradually respond to higher frequencies during early hearing development (Echteler et al., 1989; Mills and Rubel, 1998). Thus, while the base of the cochlea responds maximally to low frequencies at hearing onset, it progressively responds to higher frequencies. Tuning properties within IC neurons were considered mature by P15-17, just several days after ear opening (Willott and Shnerson, 1978).

## Functional processing within the auditory cortex

The functional architecture of the auditory cortex (ACX) in adult mammals has been widely studied, and several key features are evident: 1) auditory neurons can be tuned to simple and complex features of acoustic stimuli, 2) the existence of a rostrocaudally-oriented preferred-frequency gradient is well-established, and 3) individual neuronal tuning and organization on a wider scale are influenced by external acoustic stimuli – both during the critical period in development (around P12-15 in mice) and in certain cases in adulthood (Stiebler et al., 1997; Read et al., 2002; Takahashi et al., 2006; Barkat et al., 2011; Hackett et al., 2011; Guo et al., 2012a).

Electrophysiological recordings have for a long time dominated the field of auditory research, and have led to the discovery of topographic organization within specific auditory cortex areas in monkeys (Merzenich and Brugge, 1973; Morel et al., 1993), cats (Woolsey, 1942; Merzenich et al., 1975; Reale and Imig, 1980), ferrets (Bizley et al., 2005), rats (Polley et al., 2007), mice (Stiebler et al., 1997; Hackett et al., 2011; Guo et al., 2012a), and within many other mammals (Read et al., 2002; Schreiner and Winer, 2007). Frequency-preference gradients in ACX reflect the tonotopically organized MGB projections into L4, which are first established in the cochlea and are preserved through all stages of feed-forward auditory processing. While it is clear that ACX neurons are tuned to complex features of acoustic stimuli, the fine-scale organization of ACX is less understood, largely because it has mostly been probed with a limited stimulus set (e.g., tones, noise) and severely constrained electrophysiological techniques. These techniques allow reliable recordings from a

limited number of neurons at a time with coarse spatial sampling, which precludes the probing of fine-scale organization. Additionally, these methods also involve pooling of local (perhaps heterogenous) neuronal responses, and have a selection bias towards strongly responsive electrode penetration sites.

New imaging techniques allowing visualization of large neuronal populations at a high spatial resolution have begun to reveal a far greater complexity of processing in ACX than previously appreciated (Bandyopadhyay et al., 2010; Castro and Kandler, 2010; Rothschild et al., 2010; Winkowski and Kanold, 2013). *In vivo* two-photon calcium imaging in mice has shown that the smooth tonotopy characterized by microelectrode mapping studies breaks down at fine spatial scales, and that frequency preferences of local neighboring neurons are quite heterogeneous, and can vary by several octaves (Bandyopadhyay et al., 2010; Castro and Kandler, 2010; Rothschild et al., 2010). This local heterogeneity of responses, particularly in supragranular layers 2/3, is thought to arise as a result of differing connectivity patterns across ACX layers within columnar microcircuits, which may have specific advantages in the hierarchical laminar transformation of auditory information integration (Atencio et al., 2009; Atencio and Schreiner, 2010; Watkins et al., 2014) and might provide the substrate for processing of more natural behaviorally-relevant stimuli (Nelken, 2004; Kanold et al., 2014).

Layer 4 receives its principal input from topographically organized thalamic afferents, and thus one would expect that it might retain a clearer frequency-gradient organization. On the other hand, the more complex spectrotemporal receptive fields that are characteristic of L2/3 neurons could arise from the abundance of local

13

intralaminar connections, including input from spectrally distinct columns and long-distance cortico-cortical projections to this layer (Hackett et al., 2011; Watkins et al., 2014). Neighboring spines on individual L2/3 neuronal dendritic arbors can have a wide range of frequency selectivity, with 55% of spines demonstrating broad tuning (Chen et al., 2011). Studies often classify a substantial amount of ACX neurons as "unresponsive" due to the fact that these neurons either do not respond to pure tones or do not exhibit the classic "V-shape" tuning structure, but there is evidence that these neurons are actually highly selective for complex acoustic stimuli resulting from the nonlinear integration of the multitude of synaptic inputs these neurons receive (Sadagopan and Wang, 2009). Furthermore, studies using $GABA_A$ agonist muscimol and antagonist picrotoxin effectively showed that increasing intracortical inhibition preferentially disinhibited responses to characteristic frequency (CF) stimuli, whereas reversing this inhibition allowed return of broad frequency intracortical inputs to neurons and widened receptive fields (Kaur et al., 2004). This suggests that while feedforward projections determine peak frequency tuning preference of neurons and maintain tonotopy on a coarse scale, lateral intracortical inputs can either broaden spectral tuning via excitatory synapses (Kaur et al., 2004; Happel et al., 2010), or conversely promote sharpening via inhibitory inputs.

Recent two-photon calcium imaging has also revealed that neural response properties within L2/3 are more heterogenous than L4 responses on a local scale (**Fig. 1.1b**), which is consistent with L4 being the first to receive tonotopically structured thalamic inputs before further processing in L2/3 (Winkowski and Kanold, 2013), and can potentially be explained by the heterogeneous synaptic tuning of individual

14

spines of L2/3 neurons (Chen et al., 2011). Winkowski *et al*. further showed that signal correlations between pairs of neurons in L4 were higher than in L2/3, which indicate that these neurons are more strongly driven by shared feed-forward inputs, while neurons in L2/3 were found to have higher noise correlations between neuronal pairs, suggestive of more cortical interconnectivity.

## Auditory cortex critical period plasticity

During development, in what is known as a critical period (CP), neuronal circuits are at their most malleable state and connections are established and modified based on the sensory stimulation we encounter (Katz and Shatz, 1996; Hensch, 2005). Numerous studies have found that during the critical period of auditory development, manipulation of environmental acoustic inputs results in receptive field distortions and wide-scale restructuring of ACX organization, as evidenced by alterations in the tonotopic map and disruption of binaural integration (Zhang et al., 2001; Insanally et al., 2009; Popescu and Polley, 2010; Barkat et al., 2011; Polley et al., 2013; Caras and Sanes, 2015).

Rats have served as the predominant rodent model for studying A1 CP plasticity, and studies exposing rodents to different sound stimuli in early postnatal development have amassed a wealth of knowledge of the auditory critical period for plasticity, which is now better appreciated to be a succession of developmental windows specific to different stimulus features such as frequency preference, tuning bandwidth, and sweep direction selectivity (King et al., 2015). In normally-reared rats, A1 neurons show adult-like excitatory responses to tones at P14, just several

days after they first display tone-evoked responses at P11 (de Villers-Sidani et al., 2007; Insanally et al., 2009). With respect to response latency and threshold, the most significant maturation is seen from P11-P14. On the macroscale, neuronal frequency tuning is highly overlapping in early development, with more adult-like tonotopy observed by P22 (Zhang et al., 2001). Interestingly, discrepancies related to the maturation of frequency selectivity have been reported. While several studies indicate that frequency selectivity of A1 neurons progressively sharpens with age (Zhang et al., 2001; Chang and Merzenich, 2003; Chang et al., 2005; Carrasco et al., 2013), other studies in rat have shown that bandwidth actually increases with age, peaks around P16-18, and remains broad at older ages (de Villers-Sidani et al., 2007; Insanally et al., 2009). These latter studies found that neurons at P14 had the most narrow tuning, which could not be accounted for by response thresholds as thresholds were comparable to the older mice examined (Insanally et al., 2009). This is paralleled with findings in developing cats showing that young animals have the narrowest tuning, which broadens sharply from P9-P40 (Eggermont, 1996).

Passive exposure to pure tones during early development results in overrepresentation of frequency tuning to those sounds when the window is between P9-28 in rats (Zhang et al., 2001). In this study, P9 litters were exposed to 25 ms-pulsed monotone stimuli at 4- or 19-kHz played at 60-70 dB SPL for 10-16 hours a day until rats reached P28 (Zhang et al., 2001). In a similar experiment by de Villers-Sidani et al., the authors used a shifting 3-day window of tone exposure to precisely delineate the onset and closure of the critical period for spectral selectivity in rats. They observed maximal expansion of A1 tuning to the experimental frequency when

16

rats were exposed to 250-ms long 7 kHz tones at 70 dB SPL between P11-13 (de Villers-Sidani et al., 2007). A subsequent study by Insanally et al. used frequency-modulated (FM) sweeps to investigate the effects of complex sound experience on cortical development. While they found a similar early window for spectral selectivity, they further differentiated distinct subsequent sensitive periods for tuning bandwidth and sweep direction (Insanally et al., 2009).

Similarly in mice, studies exposing young postnatal litters to 100 ms-pulsed 7- or 20-kHz tones at 73-78 dB for 3-day intervals (P8-11, P12-15, and P16-19) found significant tonotopic reorganization only when mice were exposed in the P12-15 window (Barkat et al., 2011). Interestingly, tone-exposure changes to frequency representation were not observed in the two auditory processing stages preceding cortex. Kittens exposed to a loud (80 dB) tonal stimulus continuously for 5-8 hours a day from birth to P50 or P75 (Moore and Aitkin, 1975) and mice reared with repetitive clicks (Sanes and Constantine-Paton, 1985) did not exhibit changes in tonotopic organization within the inferior colliculus, and mice reared with a pure tone stimulus showed no frequency distribution shift within the thalamus (Barkat et al., 2011), which suggests that topographic organization within these two areas is established prior to sensory exposure. However, exposure-induced tuning changes at the single cell level were found in both the inferior colliculus (Sanes and Constantine-Paton, 1983, 1985) and thalamus (Barkat et al., 2011).

The influence of sensory deprivation on cortical development has been investigated in the visual system by binocular lid suture (Wiesel and Hubel, 1965; Crair et al., 1998), binocular enucleation (Crowley and Katz, 1999), or rearing

animals in complete darkness (Timney et al., 1980; Mower, 1991; Fagiolini and Hensch, 2000). While these studies found poorly differentiated spatial receptive fields in V1 of visually-deprived animals (Wiesel and Hubel, 1965), both orientation and ocular dominance columns emerged similarly with or without patterned visual experience (Wiesel and Hubel, 1965; Crair et al., 1998; Crowley and Katz, 1999). Thus while retinal input is not required for initial topography, sensory-evoked activity is required to strengthen and maintain responses and selectivity (Crair et al., 1998).

To mimic this deprivation model for the auditory system while keeping it reversible for future auditory response analysis, animals would need to be reared in a completely sound-free environment, which even in sound-attenuated chambers is virtually impossible given the persistence of self-made vocalizations and movement-related noises. Studies attempting to induce transient hearing loss used bilateral earplugs in gerbils and assessed auditory neuronal properties following earplug removal before and after CP closure (in gerbil, P18) (Kotak et al., 2008; Sanes and Kotak, 2011; Caras and Sanes, 2015; Mowery et al., 2015). However, challenges with this method prevail given that earplugs frequently need to be adjusted and replaced, particularly in development when the inner ear is growing. Furthermore, earplugs elevate auditory thresholds by ~28 dB (Mowery et al., 2015), or 15-49 dB (Caras and Sanes, 2015), which creates a "blurred" environmental input paradigm rather than full sensory deprivation. An alternative method to induce brief hearing loss is via injection of a thermoreversible poloxamer hydrogel into the ear cavity, which can elevate auditory thresholds by 10-40 dB for several days before spontaneously dissolving and returning to normal levels (Polley et al., 2013). A study using this

procedure was able to show two distinct time windows for binaural integration in mice – brief hearing loss before P16 disrupts interaural frequency tuning, whereas hearing loss after P16 affects processing of interaural level differences (Polley et al., 2013). While informative for studies evaluating specific short-term windows during the critical period, this method cannot be used to assess the effect of acoustic input during longer time periods. A strategy to bypass these complications is to use moderate-intensity white noise to mask all other spectrotemporal patterned input, and thus mice can be raised in an environment devoid of salient auditory cues and without any behavioral significance. As such, noise-rearing (NR) might be more similar to full uni-modal sensory deprivation such as dark rearing and full whisker trimming studies.

Rats reared in continuous white noise during development exhibit auditory neurons with broader, nonselective spectral selectivity and a degraded tonotopic organization (Chang and Merzenich, 2003). However, rather than directly producing these changes, the authors proposed that noise rearing (NR) indefinitely prolongs the critical period by delaying refinement, and tested their hypothesis by exposing adult NR rats to pulsed tonal stimuli. They found a consistent overrepresentation to the exposed frequency in adult NR rats that does not exist in age-matched normally reared rats, suggesting that NR rats retain the propensity to reorganize. Similar effects are observed in V1 for dark reared animals, including poorly differentiated spatial receptive fields and orientation selectivity, and CP prolongation (Wiesel and Hubel, 1965; Timney et al., 1980; Mower, 1991; Fagiolini et al., 1994). Therefore, as in V1, the normal development and maturation of auditory cortex organization and single-

cell attributes requires exposure to patterned acoustic input, but sensory modalities might possess compensatory mechanisms to prevent premature termination of plasticity if insufficient inputs are present during this time period.

In contrast, pulsed white noise in development was found to have different effects than continuous white noise. While both deprivation models resulted in distorted topography and broader receptive fields, the patterned temporal structure of pulsed noise was sufficient to induce CP closure, and caused permanent consolidation of the degraded tonotopic organization (Zhang et al., 2002). It is thought that the temporally correlated input induced by modulated noise still drives synchronous correlated activity between neurons, initiates synaptic strengthening and weakening via Hebbian processes, and results in dysfunctional ACX maturation that prevents future exposure-induced reorganization as is possible with the continuous noise exposure model (Zhang et al., 2002). A further study using spectrally band-limited noise found that specific auditory areas could be preferentially held in a critical period immature state while surrounding areas not engaged by the band-limited noise matured normally (de Villers-Sidani et al., 2008). Thus, while behaviorally irrelevant patterned input is enough to terminate CP plasticity, acoustic complexity and environmental relevance is required for proper functional maturation and can differentially affect different areas of the tonotopic field.

Although passive exposure to altered auditory environments during the critical period has the power to restructure tuning organization in development, this simple paradigm does not have the same effect on the mature brain, in which both a stabilized extracellular matrix and persisting established connectivity impose

20

restraints on new neurite growth and synaptogenesis (Keuroghlian and Knudsen, 2007; McRae and Porter, 2012). Tone (Bao et al., 2001; Zhang et al., 2001) or noise (Zhang et al., 2002; Chang and Merzenich, 2003) exposure in adult rats did not induce changes in receptive field structure or cortical tonotopic maps. In adult animals, experience-dependent cortical plasticity requires behavioral context and involvement of neuromodulatory systems engaged through learning, attention, and reward/punishment paradigms.

Despite extensive studies probing the intricacies of the auditory cortex in adults and during development, the predominant methodology has involved measuring cortical responses with microelectrode penetrations – which, while excellent at mapping coarse topology, are limited in their ability to probe fine-scale organization and have a high selection bias. There is a shortcoming of studies investigating how the mesoscale functional maturation of ACX organization develops across layers during hearing acquisition, and what role sensory experience has in microcircuit assembly. While macroscale studies characterize activity in functionally distinct cortical areas or full systems with millimeter resolution, and single-cell studies detail the cellular electrical activity and receptive field structure of individual cells, intermediate-level mesoscale studies can bridge the gap between single neurons and large brain areas. Here we define mesoscale as the spatial resolution that allows visualization of large populations of individual neurons (within hundreds of microns) and inference of their local and medium-range connections (Oh et al., 2014). Mesoscale investigations are important due to the fact that sensory stimuli are not encoded by single neurons but rather by populations of neurons, and the network

activity patterns as well as activity correlations between neurons can contribute to information encoding. Given previous studies on a single-cell and macroscale level and the laminar differences in cortical circuitry in the adult, sensory experience might differentially influence the mesoscale network organization of L4 and L2/3.

Many questions remain in our understanding of ACX development, including, how does the dichotomy of topographic organization observed in adults – global tonotopy with local disorder – manifest during development (**Fig. 1.2**)? Secondly, how critical is sensory exposure for proper mesoscale assembly? How are the critical
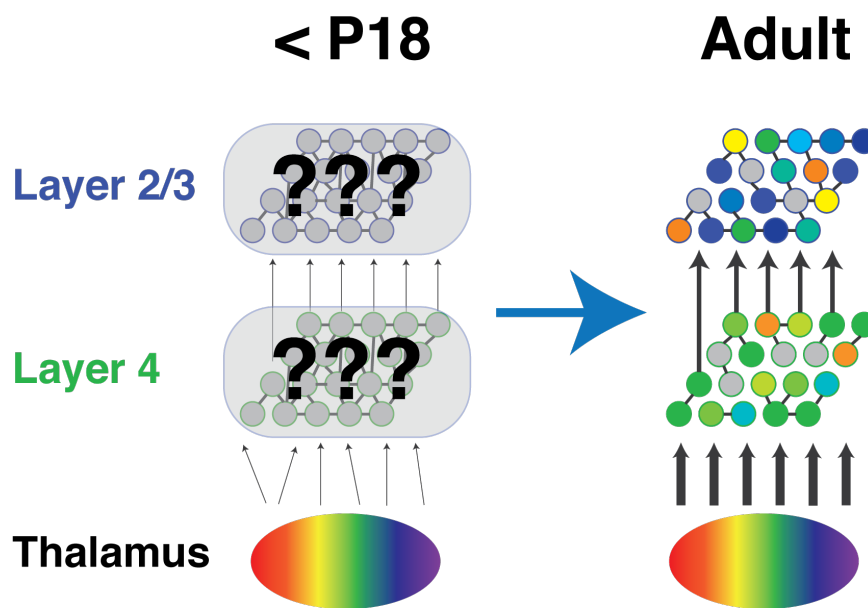


**Figure 1.2. What circuitry changes occur in L2/3 and L4 over development**? In the adult, strong columnar feedforward thalamocortical input to L4, ascending input to L2/3, and intralaminar connections combine to generate global tonotopy with local heterogeneous tuning, but it is unknown how this population activity emerges over the course of postnatal development and what role sensory experience has on this process.

circuitry changes involving subplate during early postnatal ages represented in the next two processing stages – within thalamorecipient L4 and supragranular L2/3? And finally, how are feed-forward thalamocortical strengthening and intracortical synaptic remodeling during critical period plasticity reflected in the emergence of neuronal population responses to sound stimuli and tuning maturation, and what role does auditory experience play in this process? Answering these crucial questions will provide insight into the maturational processes of ACX thalamocortical and intracortical connectivity as well as into the relationship between sensory input and mesoscale cortical organization.

## Plasticity in Adulthood

While a hallmark of sensory cortices is their ability to rewire during the critical period in response to environmental input, the capacity for plasticity is not fully extinguished in adulthood, and can be reactivated in response to specific environmental events such as learning, motherhood, and cross-modal compensation for the loss of another sensory modality. Studies have shown that in order to successfully induce plasticity in adult auditory circuits, the mature brain must be convinced of the behavioral relevance of a stimulus. This can be accomplished either by training an animal to attend to a stimulus via positive or negative reinforcement (Edeline et al., 1993; Fritz et al., 2003; Fritz et al., 2005; Rutkowski and Weinberger, 2005; Polley et al., 2006), or by pairing a stimulus with electrical stimulation applied to a neuromodulatory circuit, such as the cholinergic nucleus basalis (Kilgard and Merzenich, 1998; Bao et al., 2003) or the dopaminergic ventral tegmental area (Bao

et al., 2001; Keuroghlian and Knudsen, 2007). Animals actively attending to auditory tasks can rapidly and transiently change the tuning of individual auditory neurons (Edeline et al., 1993; Fritz et al., 2003), which likely depends on the strengthening or weakening of specific inputs and may be regulated by top-down processing circuits such as from the prefrontal cortex (Fritz et al., 2010).

An additional environmental event that plays a big role in engaging cortical plasticity in adults is motherhood. Mothers must learn to recognize and respond to pup needs, such as hunger and low body temperature, and calls, particularly low-frequency wriggling calls and high-frequency ultrasonic vocalizations (USVs) (Elyada and Mizrahi, 2015). In new mothers, single neuron response properties and cortical representations of pup-vocalization frequency bands were unchanged between virgins and mothers, but this unique life event was found to result in an increase in noise correlations between pairs of auditory neurons (Rothschild et al., 2013; Elyada and Mizrahi, 2015). These changes, which are indicative of an increase in functional connectivity, are predicted to be a result of a combination of factors: the enriched sensory environments that mothers face, the learning process of becoming a mother, as well as the neuromodulatory circuits engaged during pregnancy and parturition (Rothschild et al., 2013). Motherhood is also characterized by a variety of multisensory, cross-modal cortical reorganizations, including an increase in ACX responses to pup vocalizations in L2/3 when exposed to pup odors, and an enhanced response of ACX neurons to USVs with whisker contact of pups (Elyada and Mizrahi, 2015).

Most recently, cross-modal plasticity in adults has been investigated by examining the effect of visual deprivation on ACX neurons. Humans experiencing vision loss from birth exhibit cross-modal perceptual enhancement of hearing, including improved sound localization abilities (Lessard et al., 1998; Voss et al., 2004), frequency discrimination performance (Gougoux et al., 2004), and auditory spatial tuning (Roder et al., 1999). A compensatory reorganization of the brain offsets the loss of vision and makes blind individuals more adept at mapping their external auditory environments (Lessard et al., 1998), and even brief periods of visual deprivation in humans can transiently improve auditory perception by enhancing sound source segregation (Page et al., 2016). Cats binocularly deprived from birth and ferrets with binocular eye suture in adulthood both show a significant compensatory enhancement in auditory spatial acuity, particularly with peripheral sound localization (Rauschecker and Kniepert, 1994; King and Parsons, 1999).

Further microscale studies attempting to characterize the cross-modal changes induced on a synaptic level found that visual deprivation in juveniles (P28) results in a global reduction in the strength of excitatory synaptic transmission (via miniature excitatory postsynaptic currents; mEPSCs) in L2/3 of ACX (Goel et al., 2006), while increasing the amplitude of evoked EPSCs in L4 of both juvenile and adult (P90) neurons (Petrus et al., 2014). The decrease in L2/3 mEPSCs was proposed to reflect a change in local intralaminar inputs, which comprise the main excitatory input to these neurons, whereas the increase in L4 mEPSCs involves a potentiation of feed-forward thalamocortical transmission in this layer (Petrus et al., 2015). Local intralaminar connectivity within L4 is also potentiated by visual deprivation, which could serve to

25

amplify inputs from the MGN via recurrent excitatory transmission, and this amplified signal within L4 is thought to contribute to the potentiation of feed-forward synaptic input from L4 to L2/3 (Petrus et al., 2015).

Studies using laser-scanning photostimulation and glutamate uncaging identified robust changes in functional connectivity following dark exposure. Cross-modal plasticity induced refinement of both intracortical synaptic connections within L2/3 and inter-laminar ascending input from L4 to L2/3, evidenced by a reduction in the total cortical area providing input to supragranular layers (Meng et al., 2015). Furthermore, visual deprivation also refined inhibitory connectivity from L4-L2/3 and within L2/3 in A1 without altering the balance of excitation and inhibition (Meng et al., 2015). These connectivity changes are paralleled by functionally distinct cross-modal alterations in inhibitory synaptic transmission in both layers. Specifically, while dark exposure potentiates inhibitory synaptic function within L4 by increasing amplitude of parvalbumin ($PV^+$)-evoked inhibitory postsynaptic currents (eIPSCs), only frequency of spontaneous miniature IPSCs (mIPSCs) is increased in L2/3 without any amplitude change (Petrus et al., 2015). It is not known whether feedforward and lateral connectivity within L4 is also refined. These synaptic and connectivity changes resulting from cross-modal sensory deprivation had profound functional consequences on auditory neuronal responses when measured by electrode recordings, including sharpened frequency selectivity, lower activation thresholds, and increased neuronal excitability in L4, and may be responsible for hearing enhancement following vision loss (Petrus et al., 2014). These studies show that adults retain a strong capacity for plasticity, particularly when recruited across

sensory modalities. It remains to be investigated, however, how these laminar-specific cross-modal synaptic and connectivity changes are reflected in neuronal population responses and tuning organization of ACX *in vivo*.

## *Conclusion*

Cortical circuits exhibit profound plasticity during critical periods of development, and rely on sensory experience throughout life to assemble and maintain connectivity patterns that are most suited to their environment. Within the auditory cortex, neurons that are not properly engaged early in development by relevant auditory stimuli will not have a chance to learn how to "understand" sound (Sharma et al., 2007) and thus untreated hearing impairments early in life result in irreversible, abnormal organization of ACX and lead to permanent speech and language disabilities.

The goal of this dissertation is to understand how the mesoscale functional organization in ACX develops across cortical layers and how circuits reorganize in response to uni-modal and cross-modal sensory deprivation. In Chapter 2, I first describe the detailed methods undertaken throughout the course of these studies, which consist of multi-scale imaging (wide-field and two-photon $Ca^{2+}$ imaging) and computational analysis methods. Two-photon calcium imaging allows simultaneous measurement of hundreds of neurons with single-cell resolution, thus at a much greater spatial resolution than possible with electrophysiological experiments. Studies conducted on the mesoscale have the potential to bridge the knowledge acquired from

single-scale studies of receptive field properties (which may be biased toward strong cells) and macroscale studies (which might not account for the full repertoire of distinct cellular and laminar changes), and fill crucial gaps in our understanding of circuit development, plasticity, and reliance on environmental stimuli.

In Chapter 3, I describe the emergence of neuronal responses to sound and organization of primary ACX from just before ear opening and into the mature adult. I further examine the effect of continuous noise exposure in early development on the proper formation of ACX microcircuit architecture. In Chapter 4, I investigate how cross-modal sensory deprivation in adulthood has the power to reorganize network circuitry and population dynamics in the spared sensory area. Based on our understanding of the canonical functional circuitry within sensory cortices and the interplay between feedforward and intracortical synaptic input I hypothesized that sensory experience during critical period plasticity (Chapter 3) and in certain cases in adulthood (Chapter 4) will alter network cortical organization in specific ways across laminae. In Chapter 3 I test the hypothesis that maturation of cortical circuitry to achieve adult receptive field structure and heterogeneous spatial representation of frequencies relies on the refinement of thalamocortical and intracortical circuits through experience-dependent processes. This hypothesis predicts that auditory deprivation via noise rearing during early development will cause significant changes in the assembly of neuronal networks across cortical laminae. In Chapter 4 I test the hypothesis that in addition to the single-cell effects and connectivity refinement observed in A1 with visual deprivation, local organization of frequency tuning and

pairwise correlations between neurons will likewise be dramatically affected as a result of feedforward and intracortical synaptic restructuring.

In Chapter 5, I summarize these comprehensive findings and discuss possible circuit mechanisms underlying the observed changes in spatial tuning organization. Lastly in Chapter 6, I relate these findings to relevant human hearing disorders. The experiments conducted in the following chapters offer support for my hypotheses and show how spatial frequency representation is reorganized in response to the sensory environment during early postnatal life and with later experience, and overall provide a greater understanding of the complexity and plasticity of ACX during development and adulthood.

# Chapter 2: General Methods

To study the development and cross-modal plasticity of ACX circuits I use *in vivo* two-photon calcium (Ca$^{2+}$) imaging of in-house bred C57BL/6 wild-type and transgenic mice, selected based on their use as the background strain for many genetic manipulations and as models of auditory communication disorders (Shnerson and Pujol, 1983; Steel et al., 1983). All animal procedures are approved by the University of Maryland's Animal Care and Use Committee, protocols R13-02 and R-15-95.

## Two-photon Calcium Imaging Overview

Two-photon calcium imaging is a powerful technique for investigating the activity of populations of neurons at single cell resolution. Much of our understanding of the auditory cortex and tonotopic organization has been acquired from studies using intra- and extracellular electrode recordings, in which microelectrodes are inserted into the middle layers of the brain to measure currents produced by neuronal activity in response to acoustic stimuli. However, extracellular recordings have a selection bias towards strongly responsive neurons with high firing rates, and inflict damage to neuronal tissue through electrode insertion (Harris et al., 2016). Given the sparse representation of sound-evoked responses in the auditory cortex and low neuronal firing rates (Hromadka et al., 2008), studies focusing on electrode recordings are likely to miss out on the breadth of tuning capable of auditory cortical neurons given their focus on solely V-shaped neurons, and underestimate the vastness

of neuronal response heterogeneity that might be required for complex stimulus processing. I use two-photon imaging in an attempt to interrogate a more diverse auditory neuronal population, include non-"V-shaped" auditory neurons in my investigations, and can image hundreds of neurons with single-cell resolution. Thereby, this method allows me to acquire a more thorough portrayal of how network activity patterns contribute to stimulus information encoding. Though it has many advantages, this method likewise has several disadvantages, predominantly stemming from the fact that calcium imaging *infers* neuronal spiking activity through the fluorescence activity of calcium sensitive dyes and proteins, which have a slower time resolution than spikes and a nonlinear relationship with actual action potentials, rather than directly electrically measuring spike output. These challenges will be discussed in more detail at the end of this chapter. Regardless, two-photon calcium imaging has already begun to reveal a far greater complexity of cortical population activity than has previously been appreciated.

**Calcium indicator methods**

In the initial stages of this study, several approaches to monitoring calcium dynamics were attempted: (1) via bolus-loading of calcium indicator synthetic dye Fluo-4 AM ester (Winkowski and Kanold, 2013), (2) cortical viral injection of AAV-GCaMP6 in P21-P30 adult mice, (3) intracerebroventricular AAV-GCaMP6 injection in P0-P1 pups, and (4) multiple genetically engineered lines of mice expressing GCaMP6. Each method presented its own set of advantages and disadvantages, described below.

(1) Calcium Indicator dyes Fluo-4 and OGB-1

Bulk-loading of $Ca^{2+}$ indicator fluorescent dye Fluo-4 has previously been used successfully to infer neuronal activity from fluorescent calcium signals (Bandyopadhyay et al., 2010; Winkowski and Kanold, 2013). In this loading procedure, the dye solution is prepared by dissolving 50 μg of Fluo-4 acetoxymethyl ester (Fluo-4 AM, Invitrogen) in 4 μl of 20% pluronic acid in DMSO (Invitrogen) and diluting it with artificial cerebrospinal fluid (ACSF) (Stosiek et al., 2003; Sato et al., 2007). Sulforhodamine-101 (SR-101) is also added to the dye solution for visualization of astrocytes and to distinguish them from neuronal cells (Nimmerjahn and Helmchen, 2012), although this dye has recently been shown to induce cortical seizure-like activity at concentrations typically used (Rasmussen et al., 2016). Immediately following the standard craniotomy and cranial window procedure (described below), a pipette with a 2-4 μm tip diameter is filled with the dye solution and introduced into the cortex at a 30° angle (to prevent damage to the immediate imaging site). The pipette is advanced to a depth of 300-600 μm, and dye is slowly pressure-injected (**Fig. 2.1a**). This method allows for imaging of loaded neurons 45-60 minutes after injection, at an excitation wavelength of 800 nm (**Fig. 2.1b**).

Small molecule dyes such as Fluo-4 have the advantage of labeling all neurons in the vicinity of the injection and surpass many protein-based indicators in sensitivity and speed (Chen et al., 2013). However, they are limited in that they can be difficult to introduce into neurons *in vivo*, can cause acute inflammation and
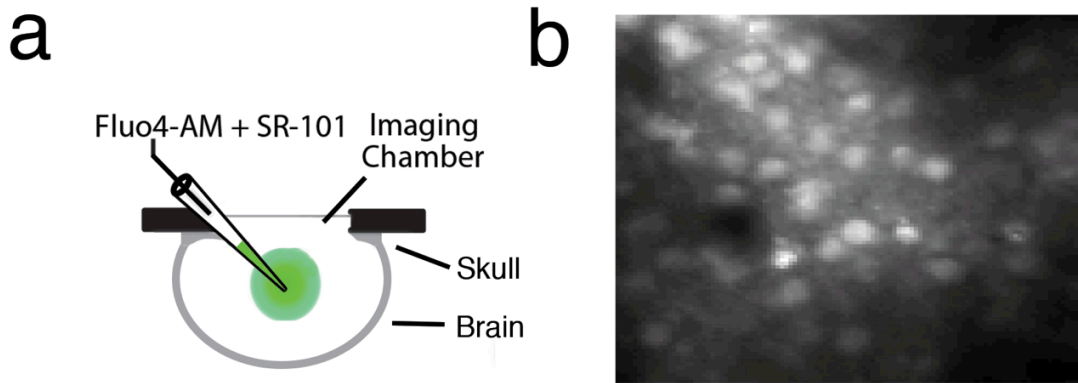
**Figure 2.1. Synthetic calcium indicator dye Fluo-4.** (**a**) Schematic of bolus cortical injection of Fluo-4 (adapted from Winkowski and Kanold, 2013). (**b**) *In vivo* two-photon image of a single optical plane in ACX that has been injected with Fluo-4 AM

bleeding at the site of injection, are extruded from cytoplasm in hours, and cannot target specific cell types or populations (Stosiek et al., 2003; Sato et al., 2007; Hires et al., 2008; Bandyopadhyay et al., 2010; Looger and Griesbeck, 2012).

## (2) Adult transfection with AAV-GCaMP6 via cortical injection

Another method of calcium detection utilizes cortical viral injection of genetically engineered calcium indicators (GECI's), such as the recently developed ultrasensitive protein calcium sensor GCaMP6 (Chen et al., 2013). Adeno-associated virus (AAV) expressing GCaMP variants can be used to infect cortical cells to promote long-term, stable GCaMP6 expression, which can rapidly detect single action potentials. Multiple variants of this GECI exist, with slow, medium, or fast kinetics (6s, 6m, and 6f, respectively), with speed inversely related to sensitivity (ie. 6s has the slowest kinetics but is the most sensitive) (Chen et al., 2013). Furthermore,

GCaMP can be expressed under different promoters, such as the neuron-specific promoter synapsin-1 (SYN), or a cre-inducible version (CAG), which can be used to target GCaMP6 to specific cell populations or layers by selective cross-breeding.

We obtained AAV1.Syn.GCaMP6s.WPRE.SV40 (UPenn Vector Core) for use in our injections. The virus is directly injected into the auditory cortex of 3-4 week old mice using a Nanoject, and shows stable expression of GCaMP6 in cells after about two weeks (Chen et al., 2013; Packer et al., 2015). When evaluated in mouse V1, GCaMP6s-transfected neurons had a fluorescence rise to peak time of 179 $\pm$ 23 ms for a single action potential, a decay half time of 550 $\pm$ 52 ms, and a fluorescence change ($\mathbf{\Delta F/F_0}$) of 23 $\pm$ 3.2% (Chen et al., 2013).

For this procedure, mice are anesthetized with 4% inhaled isoflurane in an isolation chamber, and then transferred to a bite bar for complete head stability (Mouse Gas Anesthesia Head Holder, Model 1923-B, Kopf Instruments), while isoflurane is reduced to 2%. Depth of anesthesia is monitored by toe pinch reflex and by observing the respiratory pattern of the animal. Body temperature is maintained at 37°C using a homeothermic blanket system (Harvard Apparatus) and a flexible probe to monitor internal temperature. The skin over the injection site is shaved, and a rostrocaudal incision is made over the left temporal lobe. Three small craniotomies are made less than 0.5 mm in diameter over the auditory cortex, using a Foredom Micromotor drill and burrs from Fine Science Tools. Each mouse was injected using a Nanoject II (Drummond Scientific) with 30-40 nl per craniotomy (4.6 nl/injection at a rate of 23 nl/sec) for a total of 80-110 nl per animal. The skin was then sutured and animals were returned to the colony and allowed to recover for a two week period to

give time for full and stable transfection of neuronal populations in the auditory cortex. Sections immunostained for NeuN and GFAP cortex-injected AAV-GCaMP6s confirm only neurons and not glial cells were GCaMP6-positive (**Fig. 2.2**).
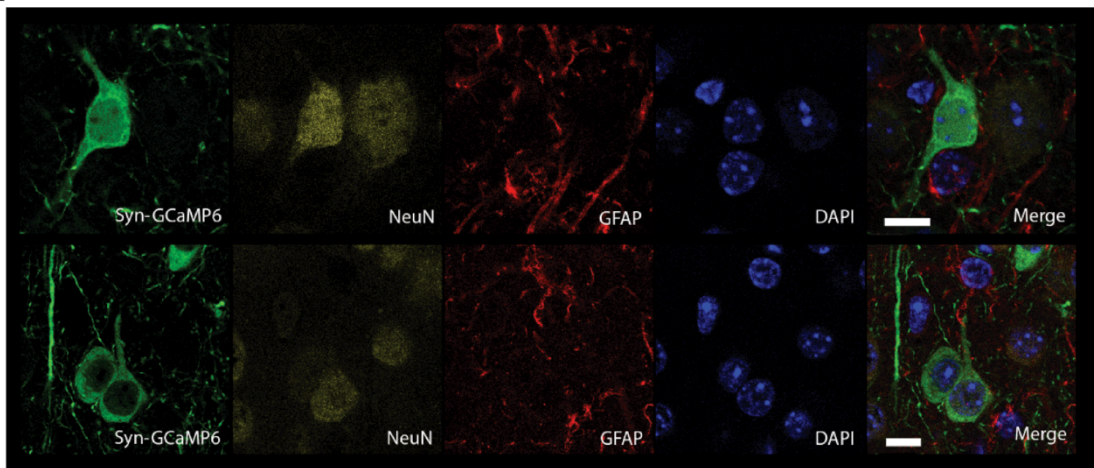


**Figure 2.2. Immunohistochemistry of mice following cortical injection of AAV1.Syn.GCaMP6s.** Sections stained with GFP (to enhance GCaMP6 signal), NeuN (for neuronal cell bodies), GFAP (for astrocytes), and DAPI (for all cell nuclei). Merged images are in the farthest right column (scale bar = 10 µm). Images confirm that GCaMP6 is selectively expressed in auditory cortex neurons and not glial cells.

Compared to fluorescent dyes, this method shows more consistent fluorescent labeling, more sensitive fluorescent responses, and allows for longer imaging sessions. However, the fact that this technique requires a physical injection introduces an element of unreliability between mice since it is difficult to guarantee routine precision in injection volumes. Additionally, the need to subject mice to a survival surgery that inherently causes mild to moderate damage to the area that will be

imaged is another disadvantage, and increases the difficulty of performing craniotomies for imaging without any bleeding or inflammation. Complete prevention of acute cortical trauma is a prerequisite for imaging activity-dependent changes in GCaMP fluorescence, as any damage usually eliminates all responses (Issa et al., 2014) – and thus lowers the success rate of imaging experiments. AAV-injection is also limiting in the extent of the area accessible for imaging, since the virus in my experiments has shown low diffusion and only local GCaMP6-expression. On a cellular level, long-term and/or high levels of expression using viral infection has been shown to cause neurotoxicity of cells, as evidenced by accumulation of GC6 in the nucleus (sign of cytomorbidity) and neuronal dysfunction in these nuclear-filled cells (loss of tuned responses) (Chen et al., 2013; Packer et al., 2015). Filled cells were not selected for further analysis.

(3) Intracerebroventricular (ICV) injection of AAV-GCaMP6

Given that cortical injection of AAV-GCaMP6 requires two weeks for viral incorporation and stable expression in cells, this calcium indicator method is not suitable for early developmental research. I experimented with injecting AAV-GCaMP6 directly into the left ventricle of P0-1 pups, and preliminary data proved that this method could be successful in targeting a wide area of auditory cortex neurons as early as 8 days after injection (**Fig. 2.3**), albeit with slightly sparser transfection than direct cortical injections. This method relies on the ability of the virus to move freely from the cerebral ventricles into the brain while the ependymal lining is still immature and permeable (Glascock et al., 2011; Kim et al., 2014).
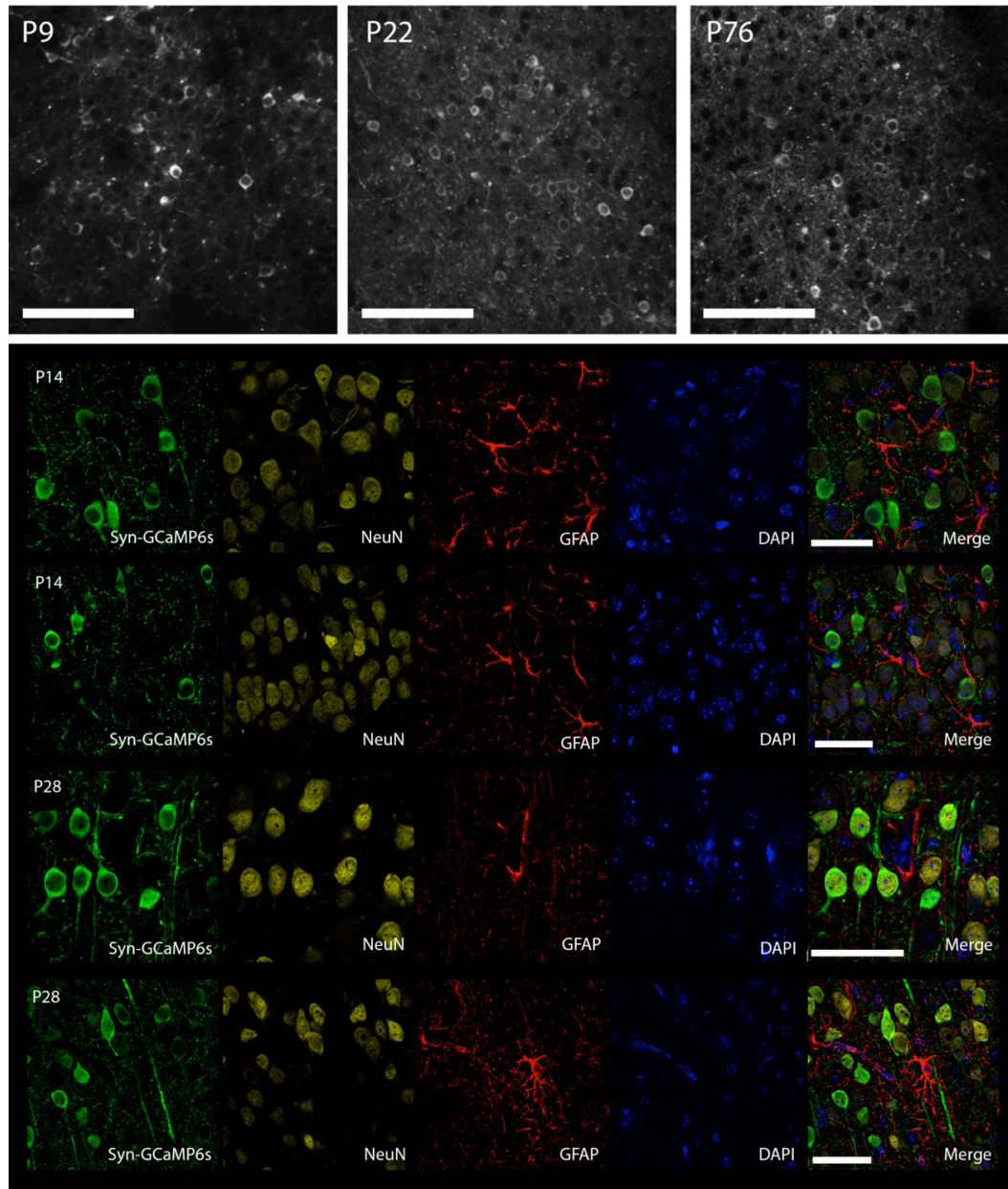
**Figure 2.3. IHC of mice following intracerebroventricular (ICV) injection of AAV-GCaMP6s.** Top row shows three *in vivo* two-photon images of single optical planes in the ACX of mice that have been transfected with AAV-GCaMP6 within 24 hours after parturition, imaged 8, 21, and 76 days after injection (scale bar = 100 μm). Bottom portion of figure shows immunostained images from ICV-injected mice stained with GFP, GFAP, and DAPI. Merged images are in the farthest right column (scale bar = 50 μm).

For ventricle injections (Glascock et al., 2011; Kim et al., 2014), pups are placed in a beaker in an ice bath to induce hypothermia anesthesia. After 3-5 minutes, full anesthesia is confirmed by gently squeezing a paw or the tail and monitoring for no movement. Individual pups are then placed on a Wee Sight Transilluminator and are freely held by hand during the injection. Glass pipettes back-filled with oil and attached to a syringe are used to inject 2 μl of AAV-GCaMP6s mixed with fast blue dye 2 mm through the olfactory bulb and into the left ventricle of the pup. Proper injection site is immediately confirmed by visualization of the fast blue dye spreading to fill the ventricle (usually both lateral ventricles are seen to be filled). An injection typically lasts 1-2 minutes, after which the pup is placed on a warming pad until its body temperature and skin color return to normal, and the pup begins to move freely. Prior to returning pups to their home cage with their mother, they are wiped down with 70% alcohol.

When ACX was imaged at 8 and 21 days post-injection (at P9 and P22, respectively), fluorescent cytoplasmic rings were already visible (**Fig. 2.3**). Sections immunostained for NeuN and GFAP in P14 and P28 mice (injected at P1) showed that only neurons and not glial cells were transfected with GCaMP6 (**Fig. 2.3**). Furthermore, while direct cortical injection of AAV-GCaMP6 has a high potential of neurotoxicity over time, likely given the high concentrations of virus used, a ventricle-injected mouse imaged three months after injection (at P76) still showed active neurons with fluorescent cytoplasmic rings (**Fig. 2.3**). Therefore, the advantages of this method include: (1) no direct damage to ACX since injections are performed through the olfactory bulb, (2) much quicker injection time (2-3 minutes

per mouse, versus 45-60 minutes for Fluo-4 or cortical AAV-GCaMP6 injection), and most significantly, (3) the ability to image GCaMP6s infected cells at younger ages.

Nevertheless, several disadvantages persist with the ICV viral injection technique of AAV-GCaMP6 delivery. Like cortical injections, it is difficult to guarantee routine precision in injection volumes, and the physical act of injection can cause damage to cortical areas (even though not necessarily specific to the future imaging location). Other limitations include the narrow window permissible for surgery (within 24 hours after birth), and a slightly sparser percentage of labeled cells.

(4) GECI-expressing transgenic lines

Recently, transgenic versions of the optimized indicator GCaMP6 have become available under the control of the *Thy-1* promoter (Dana et al., 2014) as well as in a Cre-inducible version (Chen et al., 2013), which potentially overcome many of these limitations. Transgenic GCaMP6 mouse lines were obtained (from Jackson Labs; **Table 2.1**), and breeding colonies were established within the University of Maryland's animal facility to maintain active colonies. All genetic strains showed reliably fluorescent cells with two-photon imaging (**Fig. 2.4**).

**Table 2.1 | Transgenic GCaMP6 Strains**

| Strain | JAX No. | References |
|---|---|---|
| CAG-GCaMP6f | 024105 | [2]Chen et al. (2013) |
| CAG-GCaMP6s | 024106 | [2]Chen et al. (2013) |
| Thy1-GCaMP6f | 024276 | [3]Dana et al. (2014) |
| Thy1-GCaMP6s | 024275 | [3]Dana et al. (2014) |
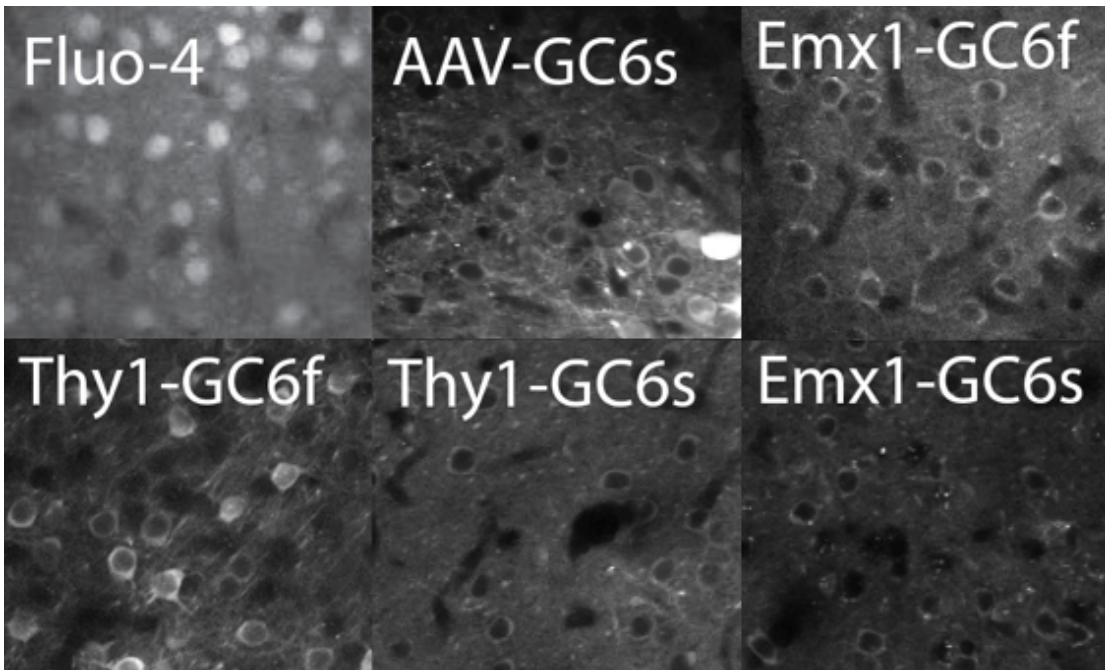
**Figure 2.4.** *In vivo* two-photon images of ACX neurons acquired from different calcium indicator methods evaluated.

Transgenic mice allow stable GCaMP6 incorporation into more global (or selectively specific) cortical areas/layers, guarantee reliability in expression and concentration between mice, have stable long-term expression without neuronal toxicity (remain excluded from the nucleus), and have the potential to be used in younger mice without any need for injections. Imaging of Thy1-GCaMP6s (GP4.3) mice shows reliable GCaMP6 expression as early as P8 (**Fig. 2.5**) and persists in adults. Sections immunostained for NeuN and GFAP in P10 and P14 Thy1-GCaMP6s mice show that only neurons and not glial cells are GCaMP6-positive, and that neurons in both L2/3 and L4 are labeled (**Fig. 2.5**). This technique seems an ideal

Ca$^{2+}$ tracking method that could mitigate problems associated with the previously discussed calcium indicator methods.
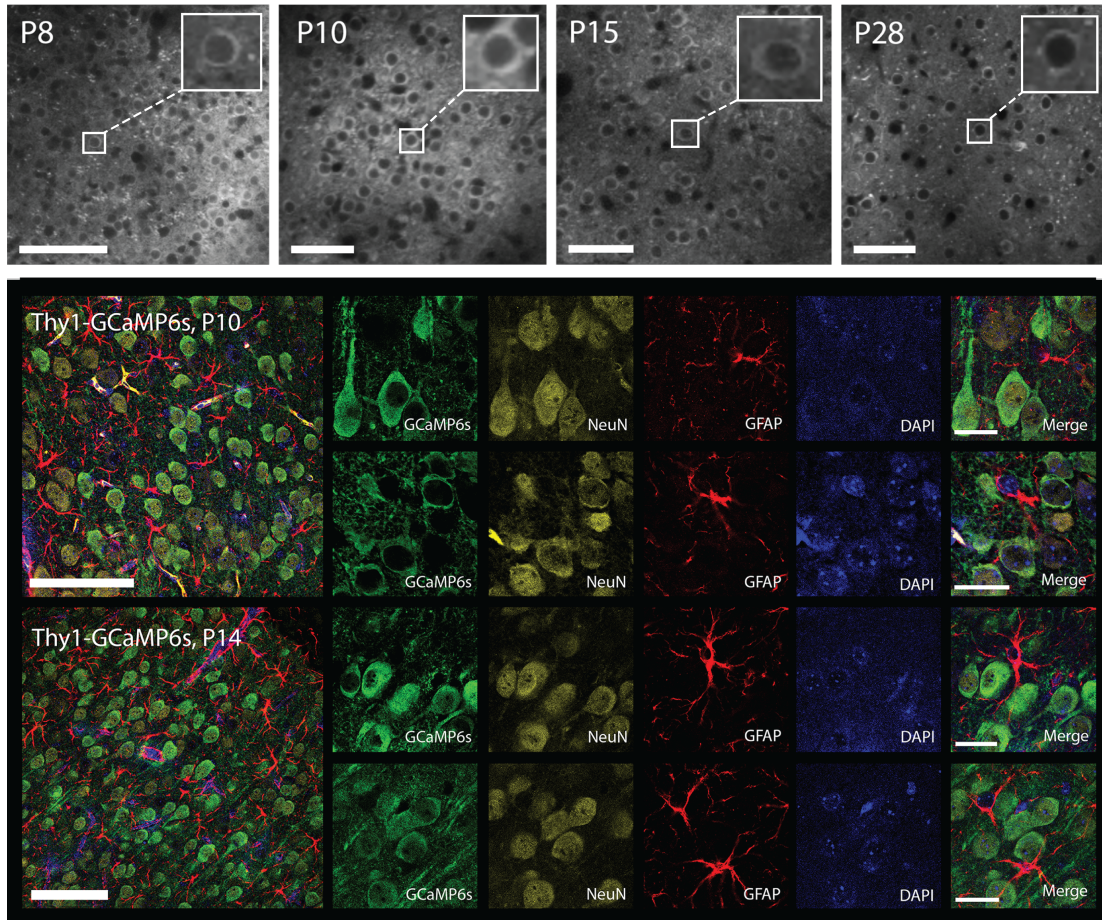


**Figure 2.5. Immunohistochemistry of Thy1-GCaMP6s mice.** Top panel reveals that mice begin expressing GCaMP6s under the *Thy1* promoter as early as 8 days post parturition, and remain stably expressing GCaMP6s until adulthood (examined as late as P69, not shown; scale bar = 50 µm). In lower panel, sections were stained with GFP, NeuN, GFAP, and DAPI. Merged images are in the farthest right column (scale bar = 25 µm). Merged images in the left column are from a wider-field view (scale bar = 100 µm). IHC confirms that GCaMP6 is selectively expressed in neurons and not glia.

## Detailed Methods

<u>Acute cranial window surgery</u>

Mice were initially anesthetized with 4% inhaled isoflurane (Fluriso, VetOne) using a calibrated vaporizer (Matrx VIP 3000), which was reduced to 2-2.5% for the craniotomy procedure in order to maintain stable anesthesia. Anesthetic state was monitored throughout using the toe-pinch reflex test. Body temperature was maintained near 37°C with a heating block. Tissue overlying the left auditory cortex was exposed and the skull was affixed to a custom titanium headplate (UMD Mechanical Development Group) using cyanoacrylate adhesive (Loctite Prism 454). A small circular craniotomy (2-4 mm diameter) was then performed by drilling into the skull using a Foredom micromotor drill and removing the bone to expose the surface of ACX, as determined by skull and vascular landmarks (**Fig. 2.6b**) (Stiebler et al., 1997; Dorr et al., 2007). A circular glass coverslip (5 mm, #0 thickness, Warner Instruments) was fixed to the surface of the craniotomy with 1.5-2% warm agarose (Sigma-Aldrich) to dampen pulsations, and was secured with glue on the outer edges to the headplate.

The mouse was then transferred to a custom built imaging stage (Thorlabs parts), with the head rotated ~45° around the coronal axis to bring the surface of the left auditory cortex perpendicular to the microscope objective. Body temperature was again maintained at 37°C, now using a homeothermic blanket system (Harvard Apparatus) and a flexible probe to monitor internal temperature. For mice younger
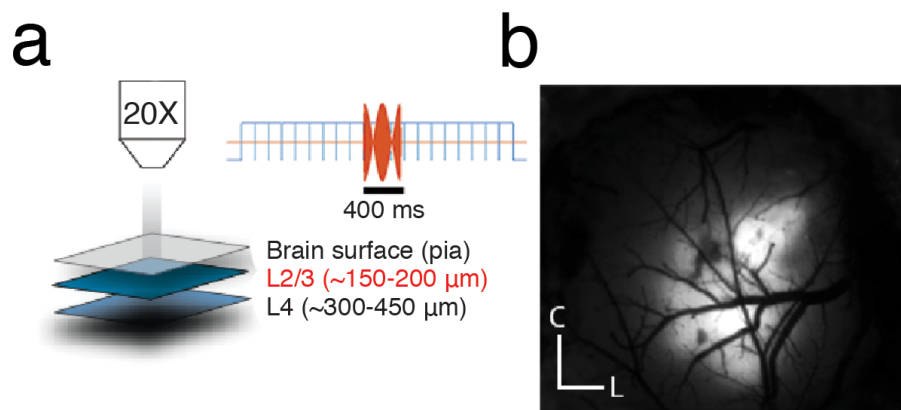
**Figure 2.6. Two-photon imaging setup.** (**a**) Schematic of experimental imaging setup and depth below pia for imaging L2/3 and L4. Top right inset shows a SAM tone 400 ms in duration, presented half-way during frame acquisition. (**b**) Image of craniotomy with typical location of blood vessels (C= caudal; L= lateral).

than P20, the flexible probe was secured externally to the ventral surface of the animal. Isoflurane was reduced to 1-1.5% for the duration of the imaging session. To prevent cortical cooling and avoid network cortical dysregulation, a constant perfusion of warmed saline (35-37 °C, Warner Instruments Inline heater) was allowed to flow over the coverslipped surface of the craniotomy (Kalmbach and Waters, 2012). For this to work, the custom headplate was created with grooved edges to allow for objective immersion and saline perfusion.

Wide-field calcium imaging

Cortical images of wide-field GCaMP6s fluorescence in blue light were acquired at a depth of 500 μm from the surface using StreamPix software (NorPix) with either a CoolSNAP HQ2 or a CoolSNAP MYO CCD Camera (Photometrics), and with

either a tandem-lens combination setup (Ratzlaff and Grinvald, 1991) or a 2x objective (Nikon). Sound stimuli consisted of 1000 ms duration, sinusoidally amplitude-modulated tones at frequencies 4, 8, 16, 32, and 64 kHz. Each frequency was randomly repeated 5 times at three sound levels: 40, 60, and 80 dB SPL for a total of 75 iterations. Wide-field imaging of tone-evoked GCaMP6s fluorescence activity is one of the methods we use to identify auditory areas and confirm imaging location in A1 via the typical rostrocaudal decreasing frequency gradient (**Fig. 2.7**).
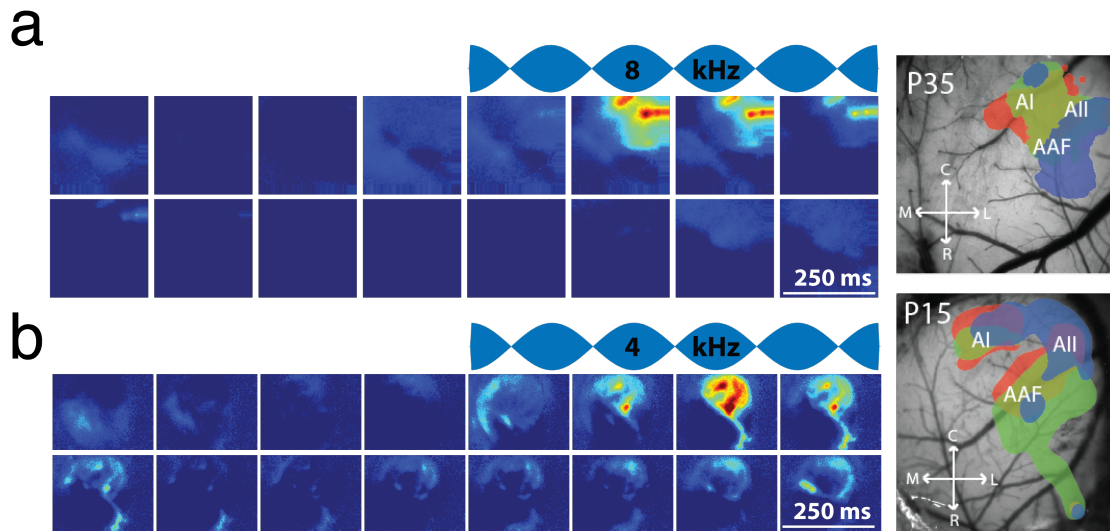


**Figure 2.7. Wide-field imaging of auditory cortex.** Time-lapse sequences (every 250 ms) of tone-evoked responses from a *Thy1*-GCaMP6s P35 (**a**) mouse responding to an 8 kHz stimulus, and a P15 (**b**) mouse responding to a 4 kHz stimulus. Panels to right show bright field images of craniotomies from the respective mice with typical location of blood vessels, with overlapped frequency-specific evoked responses (red = 16 kHz, green = 8 kHz, blue = 4 kHz). Primary auditory cortex (A1), anterior auditory field (AAF), and secondary auditory cortex (AII) are also labeled.

Two-photon calcium imaging

Imaging of sound-evoked calcium transients was performed using a two-photon microscope (Ultima, Prairie Technologies) and a MaiTai DeepSee laser (SpectraPhysics), equipped with a high sensitivity GaAsP photo detector module (Hamamatsu) and galvanometer and resonant scanning mirrors. Excitation was set at 900 nm focused at 150-200 μm beneath the pia for supragranular layers 2/3 and 300-450 μm for thalamorecipient layer 4 imaging (**Fig. 2.6a**). Regions within ACX were either galvanometer scanned at 3-8 Hz (~200 μm$^2$) or resonant scanned at 30 Hz (300 μm$^2$) through a 20x, 0.95 NA water-immersion objective (Olympus), with image resolution at 0.58-1.16 microns/pixel.

For galvo-scanned image sequences dwell time was set to 2-6 μs. For each stimulus iteration, a total of 20 images were acquired, with ten frames preceding sound onset, and ten frames during and after the sound stimulus. Frame triggering was used to initiate sound onset at exactly the 10$^{th}$ frame.

For resonant-scanned image sequences, about 50 frames preceded the stimulus, and about 50 frames followed, with the onset of the stimulus time-locked to 1.5 seconds after trial initiation. The high speed imaging that resonant scanners allow offer a tremendous advantage for capturing neuronal dynamics that occur on a much faster time scale than galvanometer scan mirrors are able to acquire.

Auditory stimulation

Sound stimuli were generated in MATLAB using custom software, presented, and attenuated using Tucker-Davis Technologies RX6, ED1 (Electrostatic Speaker

Driver), and PA5 (Programmable Attenuator), and delivered either with a TDT EC1 speaker coupled to a tube positioned next to the ear canal or a free field TDT ES1 speaker placed close to the contralateral (right) ear. Sound intensity was calibrated to 90 dB, performed with a microphone (Brüel & Kjær 4944-A) placed where the animal's right ear would be during an experiment. Unless measuring FRA's, sounds were played at 30 dB attenuation, which corresponds to 60 dB (about 20-30 dB above mouse hearing threshold in adult). Auditory stimuli consisted of 400 ms-long sinusoidal amplitude-modulated (SAM) tones (5 Hz modulation, cosine phase), ranging from 4-64 kHz at quarter octave spacing (thus covering 4 octaves). Each of these 15-17 stimuli was repeated 10 times with a 6-10 second interstimulus interval, for a total of 150-170 iterations. For sound threshold determination and FRAs, sounds were played at 3-6 different dB levels (from 30 to 80 dB) at 10-20 dB spacing.

Data Analysis

*Wide field data analysis*: Image sequences were analyzed using custom routines in Matlab (Mathworks). Images were parsed into trial-based epochs in which each frame sequence represented a single trial consisting of the presentation of a single sound frequency-intensity combination. For each trial, response amplitude (dF/F) as a function of time for each pixel was determined using the following formula, $(F - F_0)/ F_0$), where F corresponds to the time varying fluorescence at a given pixel, $F_0$ was estimated by finding the $10^{th}$ percentile of these fluorescence values for a given trial and pixel. For construction activation maps, the amplitude of the dF/F pixel response during the 1sec (i.e., ~4 frames) after stimulus onset was

46

averaged across time and repetitions, yielding an average response magnitude that was assigned to each pixel. To determine total responsive area for each animal, the average activation map for each sound frequency-intensity combination was binarized according to a threshold (mean + 2STD of baseline activity). Binarized activation maps were then summed across sounds and total area determined using the *regionprops* function in Matlab, which can be used to return measurements of contiguous and discontiguous image regions. These are then converted to real measurements ($mm^2$) based on the spatial calibration of the optical system. The values of total area were grouped either according to age or rearing condition and compared. To estimate baseline activity, the variability (standard deviation) of dF/F values of baseline (pre-stimulus) frames across all stimulus presentation trials was determined for each pixel, then averaged. This yielded a single value of baseline dF/F variability for each animal. The values of baseline variability were grouped either according to age or rearing condition and compared.

*Two-photon data analysis:* Image sequences were first loaded in to ImageJ (NIH) to visually examine if fluorescent responses were present and if there were any movement artifacts. When minimal and only in x-y, movement artifacts were corrected with the ImageJ Turboreg plug-in. Image sequences with a high amount of motion unable to be corrected were discarded and not analyzed. Raw fluorescence signals (*F*) of auditory neurons were directly used to calculate frequency time course traces. Cells were manually selected as circle regions of interest (ROIs) or rings (without including the nucleus, which does not express GCaMP6s), and pixel intensity within each ROI were averaged to generate fluorescence over time. Neuropil

correction was performed by selecting a circular region of the same area near the cell, with no other cells present, or by taking a ring-shaped area around the selected cell at a width that generates an equal area over which pixel intensity will be averaged. The average fluorescence of this area (background fluorescence, $F_B$) was then subtracted from the cell's fluorescence. Changes in fluorescence $(\Delta F/F)$ were calculated with the following equation (Chen et al., 2012): $[(F - F_B) - (F_0 - F_B)] / (F_0 - F_B)$, where $F_0$ is the average fluorescence signal during the baseline frames preceding stimulus onset. A responsive cell is defined as a cell that responds to at least one of the presented stimuli significantly (at a 99% confidence interval). Remaining analysis is performed only on significantly responding cells.

Mean time course traces were generated by averaging fluorescence traces over ten repeats, and frequency-tuning curves were determined by taking the maximum $(\Delta F/F)$ from the mean time course trace, across the frames following sound onset. Best frequency (BF) was then defined as the peak of the frequency-tuning curve (the tone which elicits the maximum $\Delta F/F$ at 60 dB). As a measure of a cell's response reliability, the number of responding trials (out of a total of 10) were summed for each neuron's BF. A response was considered to be significant if the $\Delta F/F$ of the baseline frames differed from the $\Delta F/F$ of the stimulus period with a 95% confidence interval.

Frequency preference variability was calculated for each neuron in a field by calculating the interquartile range (IQR, difference between the first and third quartiles) of BFs (in octaves) within a 100 μm radius for a cell (Winkowski and Kanold, 2013). To further understand how auditory information is represented in

neuronal networks, signal correlations (stimulus-related cross correlations) and noise correlations (trial to trial response variability) of cells were computed using custom MATLAB analytical computations, as previously described (Rothschild et al., 2010; Winkowski and Kanold, 2013) but with minor changes described in more detail in Chapter 3. Signal correlations were determined by computing the cross-correlation between the mean calcium responses over time during each sound stimulus presentation, for each unique cell pair in a field of view. Noise correlations were calculated by taking the individual fluorescence traces during each repeat of a sound stimulus, subtracting out the mean response, and measuring the covariance of the remaining fluorescence fluctuations. High signal correlations suggest neurons are driven by shared inputs, whereas high noise correlations indicate cortical interconnectivity.

Cell-attached recordings of action potentials *in vitro*

Cell-attached patch clamp recordings were performed *in vitro* in voltage clamp to simultaneously measure spiking activity and $\Delta F/F$ (Goncalves et al., 2013). Thalamocortical slices containing primary auditory cortex (A1) were prepared as previously described (Zhao et al., 2009; Meng et al., 2015). The extracellular recording solution consisted of artificial cerebral spinal fluid (ACSF) containing: 130 NaCl, 3 KCl, 1.25 $KH_2PO_4$, 20 $NaHCO_3$, 10 glucose, 1.3 $MgSO_4$, 2.5 $CaCl_2$ (pH 7.35-7.4, in 95% $O_2$ − 5% $CO_2$. Action potentials were recorded extracellularly in loose-seal cell-attached configuration (seal resistance typically 20-30 MOhm) in voltage clamp mode. Borosilicate glass patch pipettes were filled with normal ACSF

49

diluted 10%, and had a tip resistance of ~3-5 MOhm in the bath. Data were acquired with a Multiclamp 700B patch clamp amplifier (Molecular Devices), low-pass filtered at 3-6 kHz, and digitized at 10 kHz using the MATLAB-based Ephus software (Suter et al., 2010). Action potentials were stimulated either by 1) a bipolar electrode placed in L1 or L2/3 to stimulate the apical dendrites of pyramidal cells (pulse duration 1-5 ms) or 2) by gradually increasing the extracellular $K^+$ concentration (up to ~8 mM) until spontaneous action potentials began to occur. Data were analyzed offline using MATLAB.

Histology

For a subset of mice following imaging (AAV-GCaMP6), or instead of imaging (for transgenic lines), mice were euthanized and the brains were removed and drop-fixed in freshly prepared 4% paraformaldehyde (Electron Microscopy Sciences) and stored at 4°C. The fixed brains were then dehydrated in 30% sucrose and sectioned in the coronal plane at a thickness of 50 microns using a freezing microtome. Slices were then rinsed in 1X Phosphate buffered saline (PBS tablets, Sigma-Aldrich) for 15 minutes, blocked with normal goat serum (Kirkegaard & Perry Laboratories) and Triton X-100 (Sigma-Aldrich) for one hour on a shaker, and incubated overnight at room temperature on a shaker with primary antibodies against GFP (pChicken; 1:500; Aves Labs) to enhance GCaMP6 cytosolic signal, GFAP (pRabbit, 1:1000; Life Technologies) for astrocytes, and NeuN (mMouse; 1:50; EMD Millipore) to stain neuronal cytoplasms. After rinsing three times in 1X PBS, sections were further incubated for 2 hours at room temperature with corresponding secondary

antibodies raised in goat: Alexa Fluor 488 (anti-chicken, 1:200, Life Technologies), Dylight 594 (anti-rabbit, 1:100, Vector Laboratories), and Alexa Fluor 546 (anti-mouse, 1:200, Life Technologies). Sections were mounted on superfrost glass slides using Fluoromount-G (SouthernBiotech) with DAPI to stain all cell nuclei and compare neuronal (NeuN) to non-neuronal cells. Images of immunostained sections were acquired with a Leica SP5 X Confocal Microscope courtesy of the Imaging Core Facility at UMD (see **Fig. 2.2, 2.3, 2.5**).

For an additional subset of mice, a crystal of the fluorescent lipophilic tracer 1,1'-dioctadecyl-3,3,3',3'-tetramethylindocarbocyanine perchlorate (Di-I; Invitrogen) was injected into the imaging site following an imaging session, and the mice were then euthanized and brains drop-fixed in 4% paraformaldehyde. These fixed brains
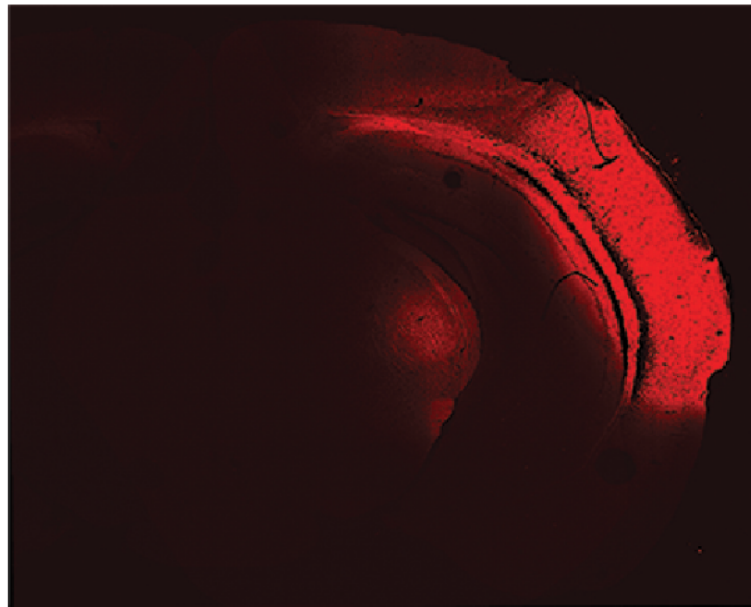


**Figure 2.8. Di-I Injection to confirm imaging location in ACX.** Recording location shown by Di-I lipophilic tracer injection into ACX and retrograde tracing of thalamocortical fiber pathways back to MGN.

were then incubated at 37°C to permit Di-I diffusion. The brains were subsequently sectioned to fifty-micron-thick sections with a freezing microtome in the coronal plane, and mounted and coverslipped with Fluoromount-G. This retrograde and anterograde tracer is used to examine the thalamocortical fiber pathways in the previously imaged ACX to confirm that the imaging location was in fact auditory cortex, by identifying Di-I labeling of the medial geniculate (**Fig 2.8**) (Cruikshank et al., 2002).

## Methodological Considerations

*Calcium indicators infer spiking activity*

Calcium imaging is used to infer action potential activity through the increase in intracellular calcium that occurs during depolarization. However, it is not a direct measure of spiking such as obtained from electrical recordings, and is limited in its ability to precisely infer spikes due to the nonlinearities of calcium indicators (Rose et al., 2014; Harris et al., 2016). Synthetic calcium dyes such as Fluo-4 and OGB-1 are more linear indicators that can resolve spikes relatively well for low firing rates, but reach saturation levels quickly (Rose et al., 2014). This makes it particularly challenging to resolve activity resulting from fast sequential stimuli if the intracellular calcium levels do not have sufficient time to return to baseline. Genetically-engineered calcium indicators (GECIs) have shown an improved ability to reach the faster rise times for single action potentials that dyes have (Fluo-4 and OGB: 10 ms;

GCaMP6f: 45 ms; GCaMP6s 180 ms) but show non-linear responsive curves due to the four cooperative calcium-binding sites of calmodulin (Chen et al., 2013; Rose et al., 2014). For the studies in Chapter 3 and 4, I performed cell-attached patch clamp recordings to assess if the observed fluorescence changes were due to changes in cellular $Ca^{2+}$ dynamics (see **Fig 3.5** and **Fig 4.2**).

*Calcium indicators are differentially selective to neuronal types*

Earlier imaging studies using Fluo-4 and OGB-1 non-selectively targeted excitatory and inhibitory cell populations. Likewise, the AAV-Syn-GCaMP6s construct targets the promoter synapsin-1, which is found in excitatory and inhibitory neurons. While inhibitory neurons represent a small fraction (10-20%) of the total cortical neuronal population (Nathanson et al., 2009; Hu et al., 2014), the differences in response patterns and selectivity could bias analysis of results. For example, parvalbumin-positive (PV+) interneurons in L2/3 have higher spontaneous firing rates and higher pairwise correlated activity than pyramidal neurons (Maor et al., 2016), and can be broadly (Wu et al., 2008; Li et al., 2014) or narrowly tuned (Chang et al., 2005; Moore and Wehr, 2013). On the other hand, the *Thy1*-targeted GCaMP6s expression used for the development studies presented here specifically targets excitatory neurons.

*Anesthesia affects spiking patterns*

It is important to note that the studies to follow were all conducted in isoflurane-anesthetized animals. Anesthetized animals have been suggested to be a

"reduced model" since cortical activity is altered (Wu et al., 2011). Specific studies have found that acoustic stimuli in animals anesthetized with ketamine or barbiturates result in only transiently-evoked responses consisting of a few spikes, whereas awake animals show continuous responses to longer stimuli (Wang, 2007; Willmore and King, 2009). This prevents analysis of ongoing activity patterns during sustained stimuli, although prolonged, complex activity has been reported in the auditory cortex of halothane-anesthetized cats (Moshitch et al., 2006) and ketamine-anesthetized ferrets (Campbell et al., 2010). It is worth noting that some studies have observed severely diminished or absent cortical activity with isoflurane anesthesia (Issa et al., 2014), particularly within the first postnatal week of development (Adelsberger et al., 2005; Sitdikova et al., 2014). However, frequency tuning and tonotopic organization of frequency preference is preserved with anesthesia in most studies (Wu et al., 2011; Guo et al., 2012a), with variability likely attributed to differences not just in anesthetic used but also depth of anesthesia maintained during experiments. Thus, the short duration (400 ms) tonal stimuli I use in these studies should efficiently resolve neuronal activity from fluorescent responses. This, combined with the difficulty in suppressing movement-artifacts in young mice with soft skulls, led me to pursue anesthetized imaging, which is still a valuable method of characterizing functional organization (Wu et al., 2011).

# Chapter 3: Differential influence of the acoustic environment on the functional laminar mesoscale organization of primary auditory cortex

## Abstract

Sensory experience shapes the functional organization of the brain. In the primary auditory cortex (A1), the spatial representation of sound frequency (tonotopy) is transformed between thalamocortical layer 4 (L4) and L2/3, and tonotopy becomes locally heterogeneous. To probe the influence of the acoustic environment on the laminar organization of A1, we combined *in vivo* wide-field and two-photon $Ca^{2+}$ imaging in L4 and L2/3 of mouse A1. We found that neighboring neurons in both layers showed the highest similarity in frequency preference and maximal activity correlations during the critical period. Early exposure to noise stimuli reduced the frequency selectivity of single neurons in both layers, but differentially altered the network organization. Neighboring L4 cells in noise-reared mice showed increased similarity in frequency selectivity and increased pairwise correlation compared with normally-reared mice, whereas neighboring L2/3 cells showed the opposite. Thus, the heterogeneous spatial representation of sound frequency is shaped by sensory experience, and experience-dependent network changes vary between cortical layers.

## Introduction

Exposure to sensory stimuli during the postnatal critical period shapes the organization of sensory cortices (Hensch, 2005; Feldman, 2009; Schreiner and Polley, 2014). In adult mice raised in normal acoustic environments, studies investigating the transformation of sound representation between thalamorecipient layer 4 (L4) and supragranular layers 2/3 (L2/3) in primary auditory cortex (A1) have revealed that while the spatial frequency organization (tonotopy) in L4 is relatively homogeneous, local tuning in L2/3 is heterogeneous (Bandyopadhyay et al., 2010; Rothschild et al., 2010; Chen et al., 2011; Hackett et al., 2011; Guo et al., 2012a; Winkowski and Kanold, 2013). The difference in the degree of tonotopy between layers is likely due to differences in the underlying microcircuitry – while L4 receives tonotopically-organized thalamic input, L2/3 integrates both intra-columnar ascending input from L4 as well as diverse cross-columnar and cross-hemispheric intracortical inputs (Schreiner and Winer, 2007; Atencio et al., 2009; Atencio and Schreiner, 2010; Chen et al., 2011; Guo et al., 2012a). Although much work has been done to investigate laminar A1 circuitry in adult mice, the timepoint during development at which heterogeneous frequency representation in L2/3 emerges, and if this process is dependent on auditory experience, is not known.

Microelectrode recordings from mid-cortical layers of A1 have shown that the tonotopic map of frequency preference, as well as frequency tuning properties of single neurons, can be altered by manipulating acoustic environments during hearing development (Zhang et al., 2001, 2002; Chang and Merzenich, 2003; de Villers-

56

Sidani et al., 2007; Insanally et al., 2009; Barkat et al., 2011; Polley et al., 2013). Rearing animals in the presence of continuous moderate-intensity noise, which masks salient environmental sounds, reduces the frequency selectivity of single neurons and disrupts macroscale tonotopy (Zhang et al., 2002; Chang and Merzenich, 2003). While macroscale studies characterize activity in functionally distinct cortical areas or full systems with millimeter resolution, studies on a mesoscale spatial resolution allow us to investigate the network activity of large populations of individual neurons (within hundreds of microns) and their local and long-range connections. Given the findings on a single-cell and macroscale level and the laminar differences in the underlying circuitry, sensory experience might influence the mesoscale network organization of L4 and L2/3 differently.

We thus investigated how mesoscale organization emerges in L4 and L2/3 in A1, and if noise rearing has distinct effects on network properties. We performed multi-scale *in vivo* wide-field and two-photon $Ca^{2+}$-imaging in mice from neurons in both L4 and L2/3 from before ear opening (P9-11) to adulthood (>P28). Using wide-field imaging to investigate macroscale development, we find that spontaneous activity is most pronounced before ear opening (P9-11). Tonal stimuli evoke responses at all ages studied, and activate the largest cortical area in late critical period (P18-20). Using two-photon $Ca^{2+}$ imaging to probe mesoscale development, we find that tonal responses are present at P9 and that during the early critical period (P15-16), individual neurons are least frequency selective and neighboring neurons show the highest degree of similarity in their frequency preference and activity correlation. The spatial heterogeneity of frequency preference in L2/3 emerges after

57

the critical period, paralleled by a decrease in pairwise activity correlations between neurons. This gradual emergence of heterogeneous L2/3 tonotopy suggests that experience might sculpt this process.

Early exposure to ambient noise from before ear opening to P20 had a similar effect on single-cell properties in both layers, specifically a decrease in the frequency selectivity of individual cells. In contrast, the mesoscale properties within each layer were differentially affected by noise exposure. In L4, noise rearing increased the homogeneity of the local spatial representation of frequency preference and increased the pairwise activity correlations between cells. However in L2/3, the local spatial representation of frequency preference became more heterogeneous and correlated activity between cells was reduced. Our findings reveal a laminar-specific effect of sensory experience on functional cortical organization. Thus, experience can shape single-cell and network properties independently, and might produce distinct effects on thalamocortical versus inter- and intra-laminar circuits.

## Methods

Experiments were performed in male and female *Thy1*-GCaMP6s (GP4.3) transgenic mice (JAX strain 02475; (Dana et al., 2014)), bred in house. All animal procedures were approved by the University of Maryland's Animal Care and Use Committee.

Noise rearing: *Thy1*-GCaMP6s mice were reared in continuous moderate-intensity white noise (75 dB sound pressure level) beginning at P5-6. This moderate noise intensity was delivered via a speaker placed 20 cm above the new litters and

commenced well before ear opening. This sound level is expected to mask salient structured acoustic inputs but is not enough to cause hearing damage via acoustic trauma to the cochlea. Normal-reared control mice were raised in our main mouse colony with ambient room noise at 48-52 dB.

*In vivo imaging*

Imaging was performed during postnatal days (P)9-59, which encompasses a period of time before ear opening (P9-11; n=4), ear opening and hearing onset (P12-14; n=7), the critical period for rapid auditory spectral tuning, which we split into an early window (P15-16; n=4) and a late window (P18-20; n=9), and through to the mature adult (P28-59; n=9). Acute cranial windows were surgically implanted using methods described previously (Chapter 2). For mice <P12-13 in which the ear canal was still naturally closed, a small surgical incision was made to open the ear and allow sound to enter without additional impedance. Wide-field and two-photon calcium imaging were performed as described previously (Chapter 2; also see Winkowski and Kanold, 2013). Sound stimuli for wide-field imaging consisted of 1000 ms-long sinusoidally-amplitude modulated (SAM) tones at 5 frequencies from 4-64 kHz at one octave spacing, repeated 5 times at three sound levels: 40, 60, and 80 dB SPL. For two-photon imaging, 400 ms long SAM tones consisting of the same frequencies but with quarter-octave spacing, and at a single sound level of 60 dB were used. For each stimulus iteration, a sequence of 100 images were acquired for a duration of 3.3 seconds, with sound onset at 1.5 seconds (or at about the 45th frame). To generate frequency response areas (FRAs), sounds were played either at 4

different dB levels (30, 45, 60, and 75 dB SPL) or at 6 different dB levels (30, 40, 50, 60, 70, 80 dB SPL), with each stimulus repeated 5 times.

*Data analysis*

Cells were manually selected as ring-like regions of interest (ROIs) that cover soma but exclude cell nuclei, and pixel intensity within each ROI was averaged to generate fluorescence over time. Neuropil correction was performed by selecting a circular region with a radius of 20 μm around the cell, excluding all pixels that are contained within other ROIs. For each neuropil mask, the brightest 20% of pixels were also excluded as they might be neural processes from adjacent cells that are also tonally tuned, which otherwise will bias cell response to a smaller value or introduce irregularities in response patterns (Peron et al., 2015). The average fluorescence of this area (background fluorescence, $F_B$) was then subtracted from the cell's fluorescence at each time point. Changes in fluorescence *($\Delta F/F$)* were calculated with the following equation (Kerlin et al., 2010; Chen et al., 2012): $[(F - r*F_B) - (F_0 - r*F_B)] / (F_0 - r*F_B)$, where $F_0$ is estimated by taking the $5^{th}$-percentile value of the entire subtracted fluorescence trace (for some cells $10^{th}$-percentile value is chosen to avoid negative $F_0$), and r is the contamination ratio 0.7. A responsive cell was defined as a cell that responds to at least one of the presented stimuli significantly ($p<0.001$). Remaining analysis was performed only on significantly responding cells, and is detailed in Chapter 2.

For each trial within each cell, response amplitude is calculated first by identifying the frame where maximum change in $\Delta F/F$ occurs, and then a window of

5 frames is centered around that frame, where the average $\Delta F/F$ within the window, with baseline $\Delta F/F$ subtracted, serves as response amplitude. Signal correlations (stimulus-related cross correlations) were determined by computing the cross-correlation between the mean calcium responses over time during each sound stimulus presentation, for each unique cell pair in a field of view. When trial number is small for each stimulus signal correlations can be strongly biased by noise correlations (Rothschild et al., 2010; Rothschild et al., 2013), and thus to overcome this bias, terms contributing to noise correlations are omitted from the sum in the equation for signal correlation (Rothschild et al., 2010; Winkowski and Kanold, 2013). Noise correlations (trial to trial response variability) were calculated by taking the individual response to each repeat of a sound stimulus, subtracting out the mean response to that particular stimulus, and measuring the covariance of the concatenated responses from every single trial of different stimuli (Rothschild et al., 2010; Winkowski et al., 2013). High signal correlations indicate neurons are driven by shared inputs, whereas high noise correlations indicate cortical interconnectivity.

## Results

To investigate how network organization changes over development in A1, we used wide-field and two-photon $Ca^{2+}$-imaging in *Thy1*-GCaMP6s (GP4.3) mice (JAX strain 02475 (Dana et al., 2014)). Immunostaining for GFP (to enhance cytosolic GCaMP6 signal), NeuN (neuronal cell bodies), and GFAP (astrocytes) showed that the GFP expression overlapped with the NeuN but not GFAP signal, indicating that GCaMP6 is selectively expressed in neurons and not glial cells (**Fig.**

**2.5**). We performed *in vivo* imaging during postnatal days (P) P9-P59, which encompasses a period of time before ear opening (P9-11), ear opening and onset of hearing (P12-14 (Shnerson and Pujol, 1983)), the critical period (CP) for auditory spectral tuning (Willott and Shnerson, 1978; Barkat et al., 2011), and through to the mature adult (P28-59; **Table 3.1**). To delineate more precisely events within the CP, we further subdivided this age group into an early (P15-16) and late CP (P18-20). The closed ear canals in early development attenuate sounds, thus to ensure comparable acoustic stimulation, we surgically opened the ear canals in the youngest age group.

**Table 3.1 | Animals, fields, and cell numbers imaged**

| Layer | Age | Animals | Fields | Mean depth | # Cells |
|-------|-----|---------|--------|------------|---------|
| **L2/3** | P9-11 | 4 | 12 | $186 \pm 7.4$ µm | 508 |
| | P12-14 | 7 | 12 | $188 \pm 6.4$ µm | 699 |
| | P15-16 | 4 | 10 | $189 \pm 4.8$ µm | 1301 |
| | P18-20 | 9 | 22 | $190 \pm 3.4$ µm | 2210 |
| | P28-59 | 8 | 15 | $189 \pm 4.1$ µm | 989 |
| **L4** | P9-11 | 3 | 6 | $348 \pm 29.3$ µm | 217 |
| | P12-14 | 6 | 7 | $345 \pm 18.8$ µm | 497 |
| | P15-16 | 4 | 13 | $347 \pm 7.7$ µm | 1039 |
| | P18-20 | 8 | 21 | $348 \pm 14.6$ µm | 1264 |
| | P28-59 | 9 | 14 | $370 \pm 10.9$ µm | 846 |

*Auditory cortical area changes over the course of hearing development*

To delineate the developmental changes in the macroscale organization of ACX, we performed wide-field imaging ($\sim$3x3 mm$^2$) of global GCaMP6s signal with tone presentation of various frequencies and sound levels (**Fig. 3.1a**). We defined
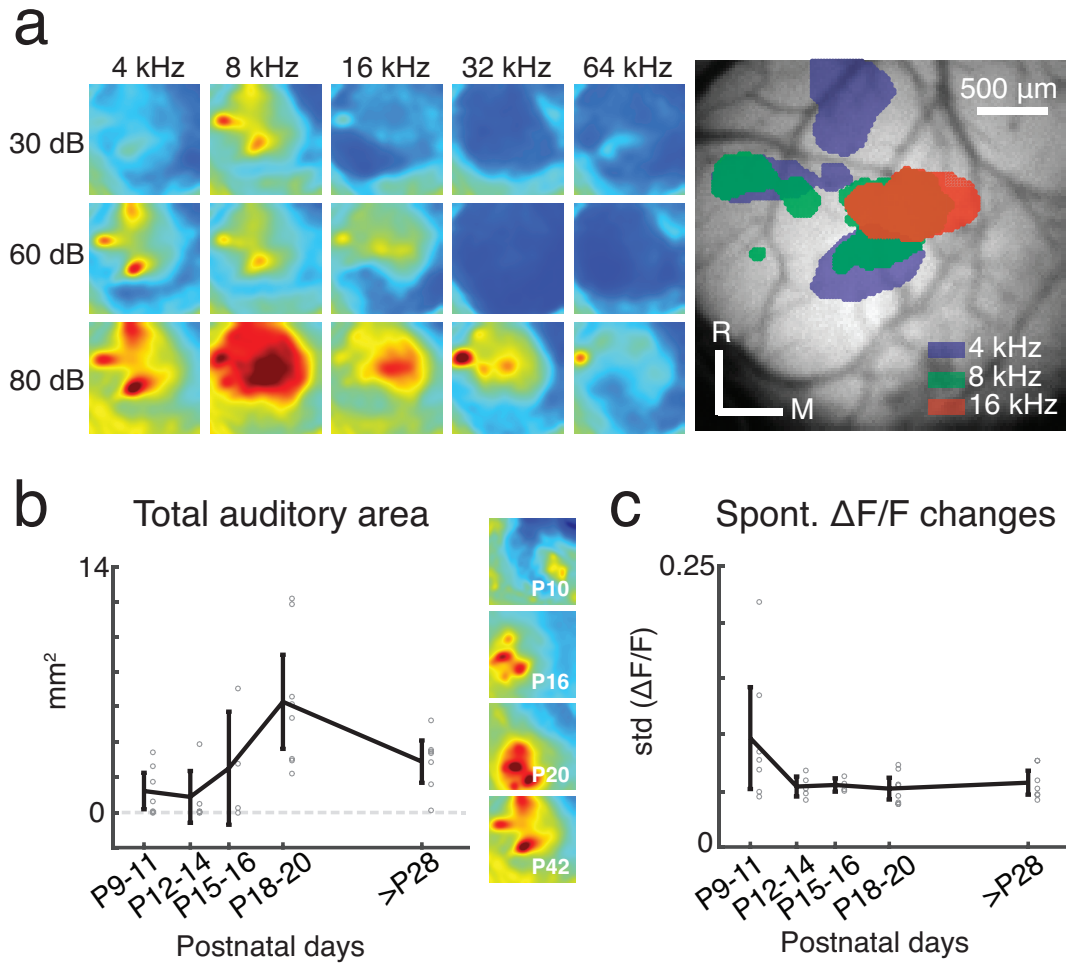
**Figure 3.1. Wide-field imaging reveals changes in tone-evoked auditory area and spontaneous activity with age.** (**a**) Sound-evoked wide-field fluorescence changes in an adult *Thy1*-GCaMP6s mouse in response to various frequencies and sound levels. Panel to the right shows an image of a craniotomy with typical location of blood vessels, with overlapped frequency-specific evoked responses. (**b**) Total auditory area (measured as mm$^2$) changes over development, with the greatest auditory area seen in late-CP. Panels to right depict representative auditory response areas at P10, P6, P20, and at P42. (**c**) Spontaneous activity, as measured by baseline variance in ΔF/F, was greatest in P9-11 mice before natural ear opening (~P12).

ACX as the cortical area showing sound-evoked changes in fluorescence. The ACX area expands over development and peaks in the CP (P15-P20), consistent with prior microelectrode studies (Zhang et al., 2001) (**Fig. 3.1b**). A1 is defined as the central thalamorecipient tonotopic area of ACX. Auditory evoked responses were present as early as P9, but in P9-14 mice, a clear tonotopic gradient could not be detected and we therefore identified A1 based on fluorescence responses and vasculature pattern. We could observe rostrocaudally-oriented tonotopic gradients as early as P15 and thus could identify A1, AAF, and A2 based on the observed gradients. Moreover, in the youngest cohort (P9-11), we also regularly observed large fluorescence transients that preceded tone presentation and thus represented spontaneous activity driven either by spontaneous cochlear activity (Wang and Bergles, 2015) or intrinsic cortical activity (Adelsberger et al., 2005). To quantify the amount of spontaneous activity, we calculated the variance in $\Delta F/F$ signal for each pixel across all stimulus presentation trials during a time window prior to the stimulus onset (**Fig. 3.1c**). We found that, prior to ear opening (P9-11), mice exhibit greater baseline variance in $\Delta F/F$, indicating higher levels of spontaneous activity before ear opening (~P12).

*A1 neurons in L4 and L2/3 show auditory responses from P9 onwards*

Having observed widespread auditory-evoked ACX activation as early as P9, we next characterized the response properties of single A1 neurons to tonal stimuli over development by *in vivo* two-photon $Ca^{2+}$ imaging of a 300x300 $\mu m^2$ region in either L2/3 or L4 (150-200 $\mu m$ or 300-450 $\mu m$ depth; **Table 3.1**). We used a sound level of 60 dB across all developmental ages to identify how networks process an

identical acoustic stimulus in their environment. Tone presentation could cause fluorescence increases ($\Delta F/F$) in neurons as early as P9 (before natural ear opening) (**Fig. 3.2-3.3**), but the fraction of responding cells was low at P9-14. The numbers of responding cells increased during the early-CP (P15-16), especially in L2/3 (**Fig. 3.4a**), then decreased by the late-CP (P18-20) and remained stable until adulthood (**Fig. 3.4a**). The fraction of cells responding to tones, and reliability responding to repeated presentations, was higher in L4 than in L2/3 (**Fig. 3.4a,b**). Since cell-attached patch recordings *in vitro* showed that a single action potential evokes fluorescence changes ($\Delta F/F$) at each age, with changes being larger at P10 than in
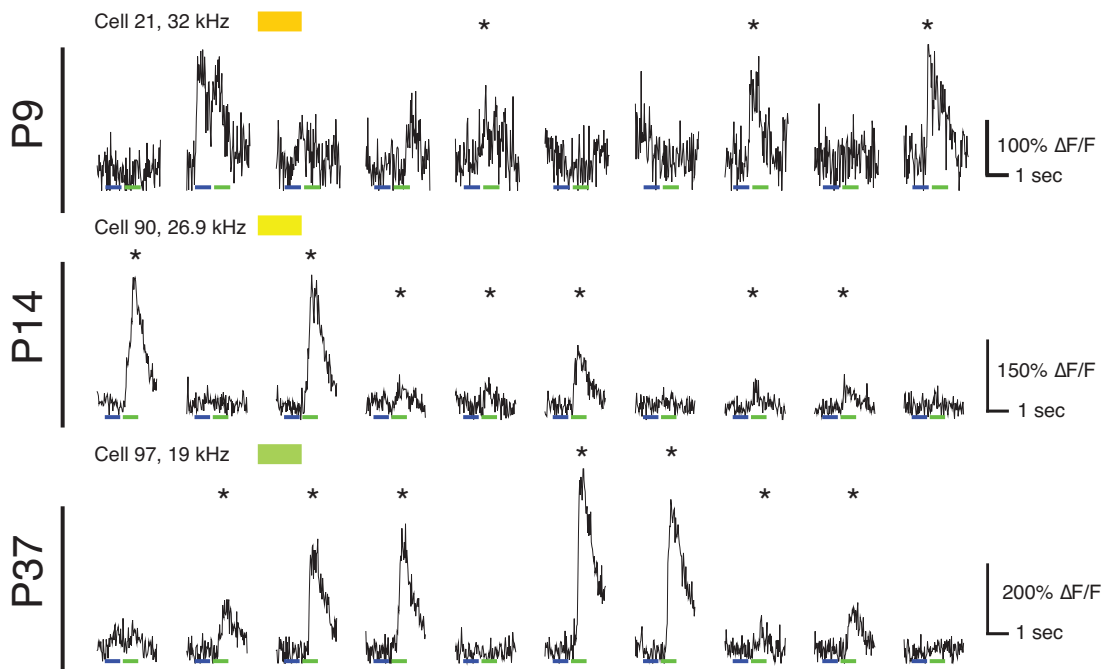


**Figure 3.2.** Individual time course traces from each BF stimulus repeat for the P9, P14, and P37 sample cells shown in Figure 2. Asterisks (*) indicate the responses that passed our significance criteria ($p < 0.01$).
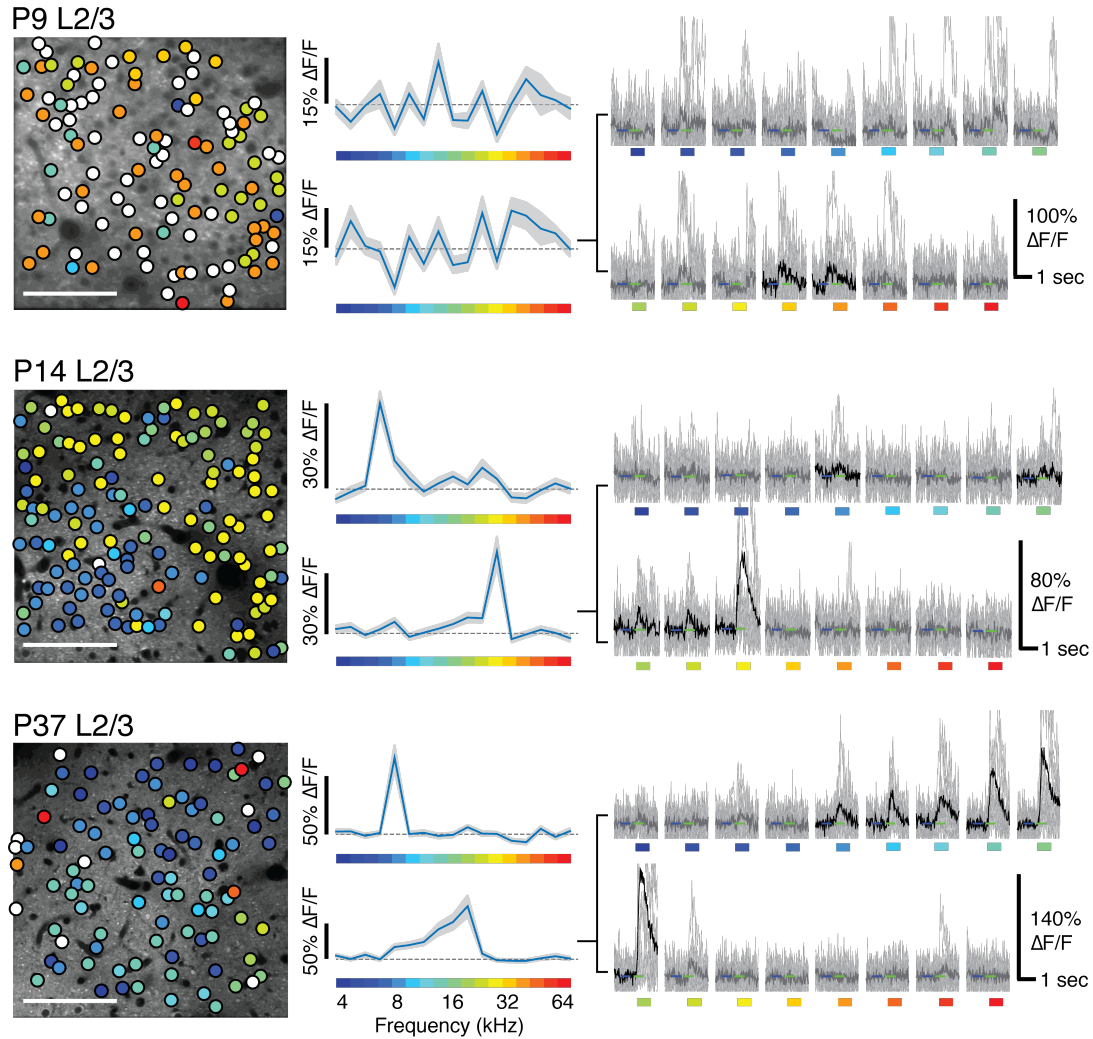
**Figure 3.3. A1 fluorescence response traces with two-photon Ca²⁺ imaging.** (*Left column*) *In vivo* two-photon images of single optical planes in A1 L2/3 of P9, P14, and P37 mice (scale bar = 100 µm), overlaid with a spatial color map of best frequencies (BFs) for all imaged neurons in the field (color indicates BF and white circles indicate unresponsive cells). (*middle column*) Sample tuning curves for two representative neurons from each field (mean ± SEM). (*right column*) Time course traces for one cell from each field responding to all frequencies presented (black lines indicate mean of significant responses (p < 0.001), gray lines are individual repetitions from each trace).
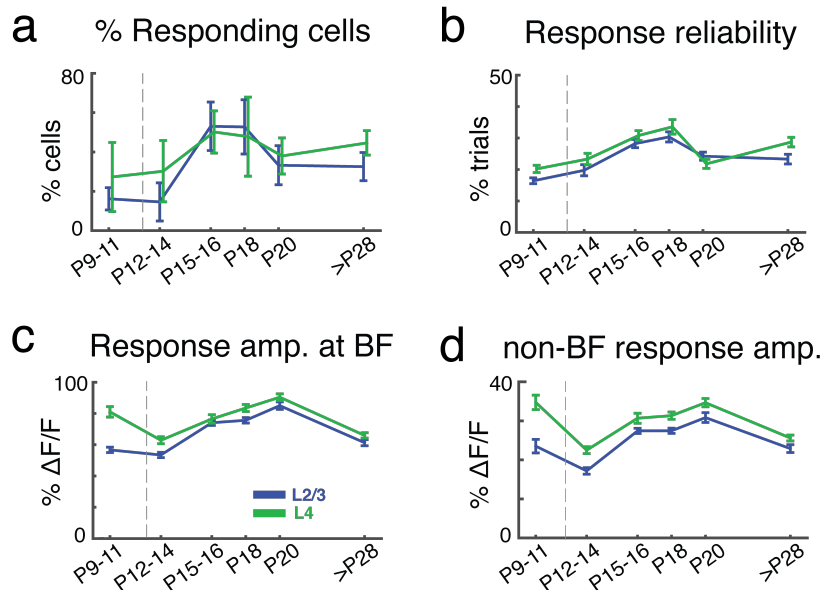
**Figure 3.4. A1 single-cell response properties.** (**a**) Fraction of responding cells was low at P9-11 and P12-14 but increases during the early-CP (P15-16) especially in L2/3 (Wilcoxon rank-sum test for medians, p<0.001). The numbers of responding cells decreased by the late-CP (P18-20) and remained stable until adulthood (Adult L4 = 44.6% tone-responsive cells, Adult L2/3 = 32.5% tone-responsive cells). (**b**) The reliability to repeated presentations of BF-stimuli increased over early development, peaked in the CP, and showed a slight decrease to adulthood. BF (**c**) as well as non-BF (**d**) response amplitudes were lowest at ear opening, rose during early-CP (P15-16), peaked in late-CP (P18-20), decreased and reached steady-state in adulthood.

adult (**Fig. 3.5**), the change in the fraction of responsive cells and reliability is due to changing neural selectivity and not changing $Ca^{2+}$ dynamics. To characterize the magnitude of sound-evoked responses, we varied the sound frequency and
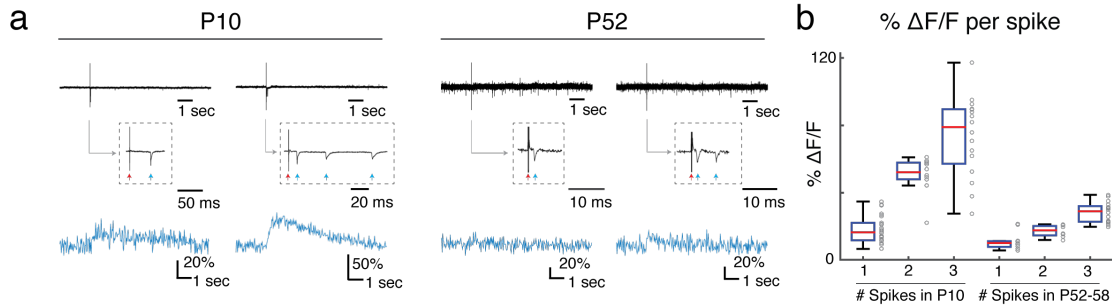
**Figure 3.5. Cell-attached patch recordings *in vitro* from neurons at P10 and P52-58.**
(**a**) Sample traces from a P10 and P52 mouse evoked by a single action potential or 2-3 consecutive spikes. Dashed boxes show zoomed in traces with red arrow pointing to the stimulus artifact and blue arrows identifying individual spikes. (**b**) Boxplot shows median and interquartile range of fluorescent-evoked responses to 1-3 spike in these two age groups. A single action potential evokes a fluorescence change ($\Delta F/F$) at each age but changes were larger at P10 than in adult ($\Delta F/F$ per spike: P10= 16.5 ± 10.4%, P52-58 = 10.2 ± 3.45%; median ± iqr; Wilcoxon rank-sum test for medians, p=0.0018). A greater variability of fluorescence amplitudes is observed in P10 from a single spike, but within individual cells of P10 and adult mice 1-3 spikes result in additive fluorescence changes.

determined the frequency that evoked the largest response (best frequency, BF) for every cell. BF as well as non-BF response amplitudes were lowest at ear opening, increased during early-CP (P15-16), peaked in late-CP (P18-20), then decreased and stabilized in adulthood (**Fig. 3.4c,d**). Response amplitudes to BF and non-BF stimuli were higher in L4 than in L2/3 at all ages (**Fig. 3.4c,d**), consistent with prior imaging results (Winkowski and Kanold, 2013). Together, these data show that A1 neurons exhibit sound-evoked responses as early as P9 and that the fraction of responding

cells and the tone-evoked response amplitude is transiently increased during the critical period.

*A1 neurons are least frequency-selective during the critical period*

While surgical opening of ear canals allows sounds to reach the inner ear similarly over the ages studied, neural thresholds of individual A1 neurons might change over development. We thus presented tones at various sound levels (in 10-20 dB steps) to determine the lowest sound level that reliably evoked a response. Neural thresholds varied widely between cells, but over the population were constant between P9-P18, fluctuated slightly in the late-CP (P20), and then decreased to adult levels (**Fig. 3.6a**). Because of imaging time limitations, we did not use sound level increments smaller than 10 dB. This limiting factor, as well as the stringent criteria we used to determine significance of a response, and the lack of electrode bias, likely resulted in higher threshold levels than previously reported with microelectrodes ($39.4 \pm 12.4$ dB in L4 (Petrus et al., 2014)). Regardless, our results show that, on average, most A1 cells could respond to 60 dB tones at all ages examined. The threshold shifts we observed in late-CP and >P28 likely could contribute to the observed response amplitude changes. However, the decreased threshold in adults compared to P9 mice is counterbalanced by the larger fluorescence transients evoked by single action potentials in P10 mice (**Fig. 3.5**). Moreover, we observe decreased response amplitudes in adults while neural thresholds are lowest then, consistent with gradual maturation of inhibitory inputs to A1 cells (Oswald and Reyes, 2011).

**a** **Threshold**

**b** **Spontaneous activity**

**c**

**d**

**e** 75% cutoff

**f** 60% cutoff

70
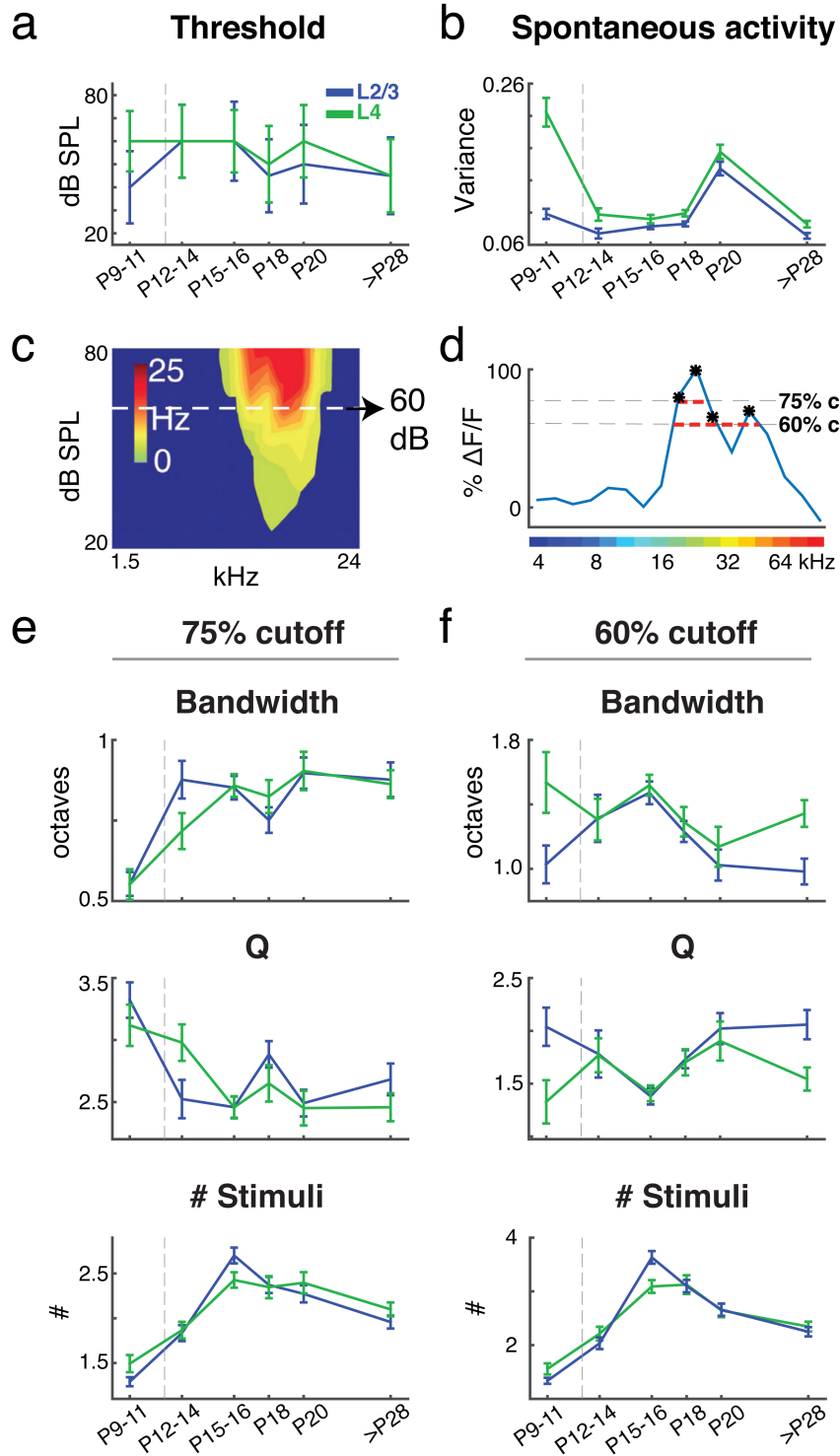
**Figure 3.6. A1 neuronal frequency selectivity decreases during the CP.** (**a**) Neural thresholds varied widely between cells but over the population were constant between P9-P18 (P9-11 L4: 60 ± 20 dB; P12-14 L4: 60 ± 30 dB; P15-16 L4: 60 ± 15 dB; P18 L4: 50 ± 30 dB, median ± iqr; one-way ANOVA, not signif.), fluctuated slightly in the late-CP (P20 L4: 60 ± 25 dB; P18 to P20 one-way ANOVA p=0.0012), and then decreased to adult levels (>P28 L4= 45 ± 30 dB, p<0.001 for all ANOVA comparisons except for P18). (**b**) Spontaneous activity, as measured by baseline variance in ΔF/F traces, was greatest in L4 in P9-11 mice before natural ear opening (~P12). In both layers, we observed a secondary peak in baseline variance in late-CP (P20). (**c**) Sample frequency response area (FRA) illustrating the fixed stimulus intensity (60 dB) used in this study (adapted from Petrus et al. 2014). (**d**) Neuronal selectivity was quantified at two separate peak-related thresholds (75% and 60% of peak) using three measures: normalized bandwidth in octaves, quality factor (Q=BF/bandwidth), and number of stimuli that evoked a response. Sample trace with 75% and 60% cutoffs are illustrated. (**e**) The central frequency region (75% cutoff) of L2/3 and L4 neuronal tuning curves broadens throughout development. (**f**) Selectivity outside the central frequency region (60% cutoff) emerges during the early-CP, then narrows and reaches more selective adult-like values in late-CP.

Tuning curves (frequency-response areas, FRA) in many auditory structures are "V-shaped," with frequency selectivity decreasing as sound level increases. However, adult A1 also contains neurons with "I-shaped" FRAs, indicating minimal level dependence of frequency selectivity (Schreiner et al., 2000). Microelectrode studies of rodent A1 draw contradicting conclusions about the development of frequency selectivity – A1 cells either become more (Zhang et al., 2001; Chang and

Merzenich, 2003) or less (de Villers-Sidani et al., 2007) frequency-selective over development. We measured the normalized bandwidth of the central response area at two separate peak-related thresholds (60% and 75% of peak) and calculated the Quality factor (Q=BF/bandwidth; **Fig. 3.6c-f**). The two threshold criteria examine different parts of the traditional FRA: The 75% threshold measures the central preferred-peak region of a neuron's FRA, while the 60% threshold criterion evaluates selectivity outside the central frequency region (**Fig. 3.6d**).

For the 60% criterion, the Q factor of L2/3 neurons decreases between P9 and P15, yet increases beyond P15, indicating an increase in frequency selectivity from the critical period to adulthood. In L4, frequency selectivity increased after P9, briefly decreases at the early-CP, and increases again in late-CP (**Fig. 3.6f**). In contrast, for the 75% criterion (**Fig. 3.6e**), the Q factor of both L2/3 and L4 neurons decreases from P9 to the critical period and remains low into adulthood, indicating a gradual decrease in frequency selectivity throughout development. This indicates that different parts of neuronal tuning curves mature at different developmental stages. Specifically, selectivity outside the central frequency region (60% cutoff) emerges during the early-CP, then narrows and reaches more selective adult-like values in late-CP, whereas the central frequency region (75% cutoff) is narrowest before ear opening, and then broadens, reaching adult values by early-CP (P15-16). The similarity of our 60% criterion results with prior microelectrode studies (Zhang et al., 2001; Chang and Merzenich, 2003) and the differences to the results at the 75% criterion (consistent with other microelectrode studies (de Villers-Sidani et al., 2007)), suggest that receptive fields become less "V-shaped" and more "I-shaped"

during the CP, possibly by strengthening of columnar input from thalamus to L4 and from L4-L2/3, a refinement in horizontal spectral integration (Katz and Shatz, 1996; Douglas and Martin, 2007; Oswald and Reyes, 2008; Butts and Kanold, 2010; Ko et al., 2013), or increased inhibition (Oswald and Reyes, 2011).

Since A1 neurons can show non-"V-shaped", or multi-peaked frequency selectivity curves (Schreiner et al., 2000; Winkowski and Kanold, 2013), our bandwidth measure ignores responses outside the central frequency selectivity region. Thus, as an additional measure, we calculated the number of frequencies to which a given neuron responded (**Fig. 3.6e,f**). A1 neurons in both layers responded to more frequencies from P9 to P16, thus showing decreased frequency selectivity until early-CP, followed by an increase in frequency selectivity. These changes were similar for both criteria and for both layers investigated, suggesting that during the early-CP, A1 neurons in L2/3 and L4 respond to more sound frequencies outside their central frequency region.

*The heterogeneous spatial representation of frequency preference emerges during development*

While global topographic maps of stimulus preference are characterized by a smooth frequency gradient, neighboring neurons in adult A1 can prefer sound stimuli of very different frequencies, particularly in L2/3 (Bandyopadhyay et al., 2010; Rothschild et al., 2013; Winkowski and Kanold, 2013). The question then becomes: does the heterogeneous spatial representation of sound frequency emerge from an initially ordered, or an initially *dis*ordered, sound representation? To discriminate

between these two alternative scenarios, we measured the local spatial order of frequency preference by calculating the interquartile range (IQR) of BFs in a local area (<100 μm) (**Fig. 3.7**). This measure is zero if neurons within 100 μm have the same BF. We find that $IQR_{BF100}$ is highest at the youngest ages in both L4 and L2/3 (**Fig. 3.7b**), indicating that, while individual neurons could selectively respond to certain tones, local populations preferred very different frequencies. This finding is consistent with poor tonotopic organization in younger mice (**Fig. 3.1**). Immediately after ear opening (P12-14), L4 $IQR_{BF100}$ decreases whereas L2/3 $IQR_{BF100}$ remains stable, which suggests that thalamocortical ascending input to L4 refines prior to sensory-evoked changes within L2/3. $IQR_{BF}100$ in both layers decreases to a minimum at P15-16, suggesting that feedforward refinement from thalamus to L4 and from L4 to L2/3 is driving peak-response similarity between neighboring neurons, although at this age these neurons are also responding to the most frequencies outside of their preferred peak region (**Fig. 3.6e,f**). $IQR_{BF100}$ in both layers increased by P20 and into adulthood, indicating wider sampling of inputs of L2/3 neurons from L4 and from other L2/3 cells (Bandyopadhyay et al., 2010; Chen et al., 2011; Hackett et al., 2011; Winkowski and Kanold, 2013). $IQR_{BF100}$ in adult L2/3 is larger than in L4 (**Fig. 3.7b**), consistent with prior studies (Winkowski and Kanold, 2013). This wider sampling and integration of diverse synaptic inputs likely occurs due to the refinement of intracolumnar and intercolumnar horizontal connectivity in L2/3, which also results in broadening of receptive fields (**Fig. 3.6e,f**) (Douglas and Martin, 2007; Oswald and Reyes, 2008; Atencio et al., 2009; Atencio and Schreiner, 2010).
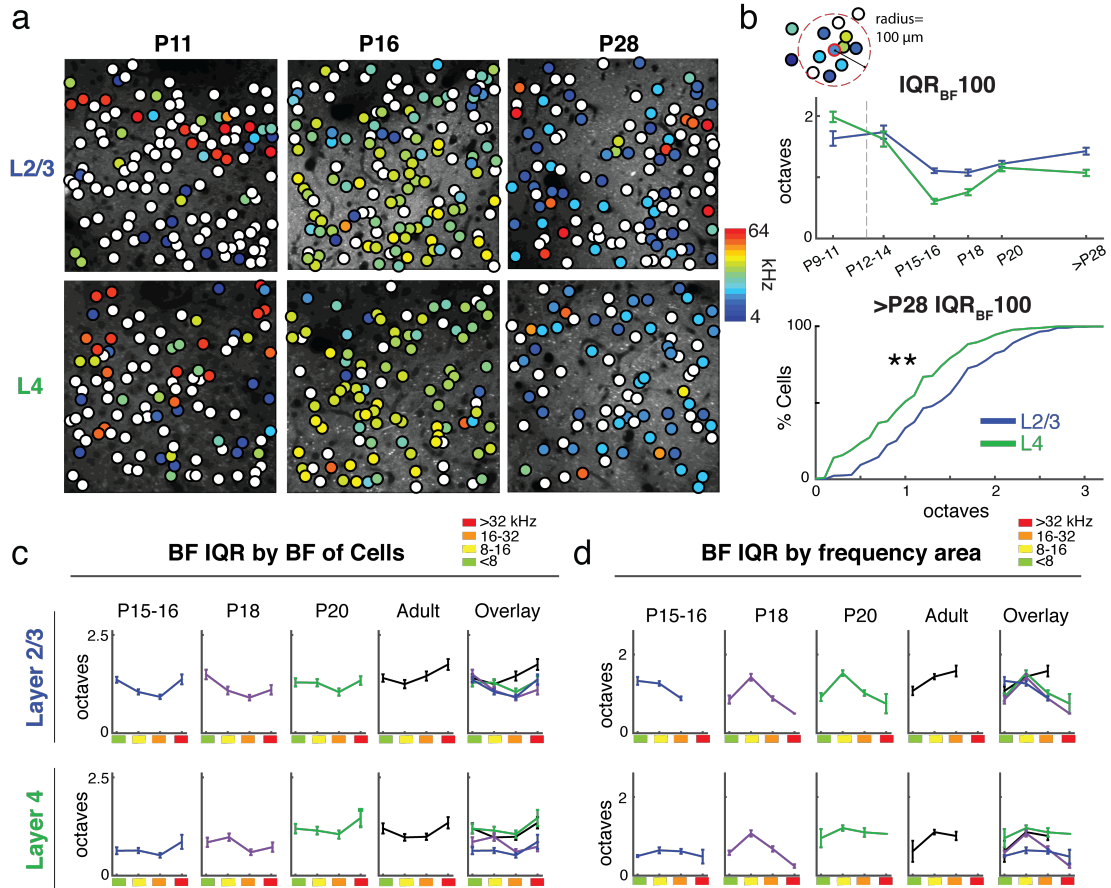
**Figure 3.7. The heterogeneous spatial representation of frequency preference emerges during development.** (**a**) Paired L2/3 and L4 imaging fields from mice at P11, P16, and P28, overlaid with a spatial color map of best frequencies (BFs) for all neurons in the field. (**b**) To quantify the spatial representation of frequencies over development we calculate $IQR_{BF100}$ for each neuron. $IQR_{BF100}$ is highest at P9-11 (P9-11 IQR L4= 1.99 ± 0.044, L2/3= 1.63 ± 0.061), decreases at P12-14 in L4 (1.62 ± 0.062, p<0.001), but does not change in L2/3 (1.74 ± 0.055, p=0.20). $IQR_{BF}100$ in both layers decreases to a minimum at P15-16 (L2/3= 1.11 ± 0.020, L4= 0.61 ± 0.021), then increases at P20 and into adulthood. $IQR_{BF100}$ in adult L2/3 (1.43 ± 0.030) is larger than in L4 (1.07 ± 0.027). To isolate changes in BF variability across the tonotopic axis we measured $IQR_{BF100}$ based on either individual cell BF (**c**) or local average frequency preference (**d**), dividing into four frequency groups.

To identify if A1 contains different organizational features across its tonotopic axis, we examined if cells with different BFs (**Fig. 3.7c**), or cells within different tonotopic regions (as identified by the mean BF of a local <100 mm region, **Fig. 3.7d**) have different $IQR_{BF100}$ (Winkowski and Kanold, 2013). We split $IQR_{BF100}$ into four groups based on either individual cell BF or local average frequency preference (4-8 kHz, 8-16 kHz, 16-32 kHz, 32-64 kHz). When grouping $IQR_{BF100}$ by cell BF, we find that, in general, neurons with BF's <8 or >32 kHz have the highest local heterogeneity, whereas cells tuned to middle frequencies are more likely to be surrounded by cells with similar tuning preference. However, when grouping cells by local frequency preference, we find that cells in middle frequency areas of the tonotopic map display the most local heterogeneity compared to low-frequency regions (<8 kHz). This suggests that central areas of A1 are in a prime location to promote widespread sampling of laminar inputs to generate more complex receptive fields. Furthermore, these results indicate that cells in different tonotopic areas mature at different ages.

Together, we find that there is a developmental remodeling of the spatial representation of sound frequency during early hearing development. The high amount of BF homogeneity at P15-18, together with the low frequency selectivity during this time, suggests that sensory manipulation during this epoch would have the largest effect since it would impact the most neurons, thus defining the critical period. Furthermore, our data suggests that the spatial heterogeneity of frequency tuning is a developing feature of A1 and implies that the transition from local BF homogeneity

to heterogeneity, particularly in L2/3, could be dependent on exposure to salient auditory cues.

*Correlated activity between neurons changes over development*

The developmental re-emergence of heterogeneous frequency spatial organization suggests that cortical connections are remodeled. To gain insight into the changing networks, we calculated both neuronal pairwise noise correlations (NC), which reflect stimulus-independent, trial-to-trial covariance, and signal correlations (SC), which represent stimulus-driven correlated activity (corrected for noise correlations) (Averbeck et al., 2006; Rothschild et al., 2010; Winkowski and Kanold, 2013). To examine age differences, we averaged the correlations between cells in a local area (within 50-100 μm of each cell; **Fig. 3.8a,b**).

NCs are highest in both L4 and L2/3 prior to ear opening (P9-11), and are greater than SCs in both cortical layers. This implies that neurons at this age receive weak feedforward (presumably thalamic) input (Barkat et al., 2011) and are most strongly driven by existing horizontal connectivity, consistent with gap-junction coupling of neighboring excitatory neurons in early development (Yao et al., 2016) without preferential functional connectivity (Ko et al., 2013). After ear opening (P12-14), NCs decrease while L4 SCs begin to increase, consistent with increased thalamic input to L4 (Barkat et al., 2011) causing nearby neurons to receive more shared stimulus-driven inputs. The decrease in NC and increase in SCs is consistent with the loss of electrical synapses and formation of chemical synapses between neurons
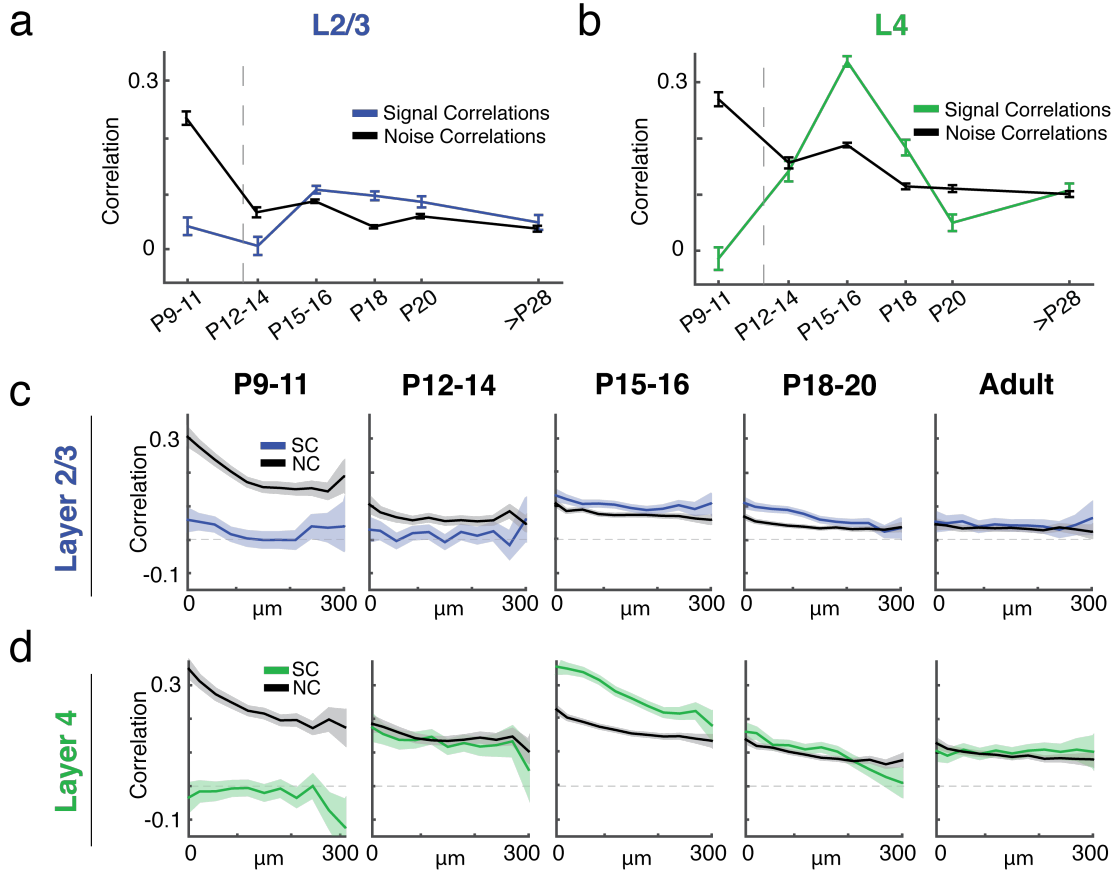
**Figure 3.8. Correlated activity between neurons changes over development.** (**a**) L2/3 and (**b**) L4 signal and noise correlations within 50-100 μm are plotted over development (means ± sem). NCs are highest prior to ear opening (P9-11 L2/3 NC= 0.24 ± 0.006, L4 NC= 0.27 ± 0.006), and are greater than SCs in both cortical layers (L2/3 SC= 0.041± 0.008, L4 SC= -0.014 ± 0.010). After ear opening (P12-14), NCs decrease (L4 NC= 0.16 ± 0.005, L2/3 NC= 0.066 ± 0.005) while L4 SCs begin to increase (L4 SC= 0.142 ± 0.009). SCs in L2/3 and L4 are highest during the early-CP (P15-16 L2/3 SC= 0.106 ± 0.004, L4 SC= 0.337 ± 0.005; L2/3 NC= 0.086 ± 0.002, L4 NC= 0.190 ± 0.002). SCs and NCs decline in the late-CP to the final mature state (Adult L2/3 NC= 0.037 ± 0.003, L4 NC= 0.102 ± 0.003; Adult L2/3 SC= 0.047 ± 0.007, L4 SC= 0.108 ± 0.006). (**c, d**) Correlations as a function of distance between cell pairs in L2/3 (**c**) and L4 (**d**).

responding to similar sensory features (Ko et al., 2013). SCs in L2/3 and L4 are highest during the early-CP, with L4 SCs more than three times that of L2/3 SCs at this age. The increased SCs and NCs during early-CP implicate over-connectivity within feedforward thalamocortical circuits to L4 and L4-L2/3 circuits as well as L2/3-L2/3 circuits. The heightened correlations we observe during this stage combined with the maximal responsiveness to a variety of external auditory stimuli suggest that sensory manipulation during this window could have a large effect. SCs and NCs decline in the late-CP, likely due to experience-dependent refinement, to the final mature state.

Pairwise correlations can be reflective of underlying neuronal circuits and can thus depend on the spatial relationships between neurons (Levy and Reyes, 2012; Ko et al., 2013; Winkowski and Kanold, 2013). We thus analyzed these correlations as a function of the distance between cell pairs (Winkowski and Kanold, 2013) (**Fig. 3.8c,d**). At P9, SCs in L4 are independent of intracortical distance up until ~240 μm (**Fig. 3.8d**), after which SCs sharply decline, which suggests a reduced probability of receiving shared ascending input at greater distances. In contrast, pairwise NCs in L2/3 and L4 in P9-11 mice are highest between cells in close proximity (**Fig. 3.8c,d**), which is consistent with neighboring cells being connected via chemical or electrical synapses (Peinado et al., 1993; Katz and Shatz, 1996; Ohki et al., 2005; Ko et al., 2013; Yao et al., 2016). Distance dependency of SCs emerges in L4 at P12, which indicates that neurons at greater distances are less likely to share common input. This

**P9-11**
*Before ear opening,
intracortical spont. act.*

**P12-14**
*Ear opening,
sensory innervation*

**P15-16**
*Early CP,
connectivity over-growth*

**P18-20**
*Late CP,
TC and IC refinement*

**Adult**
*Mature,
consolidation*

Layer 2/3

Layer 4

Thalamus
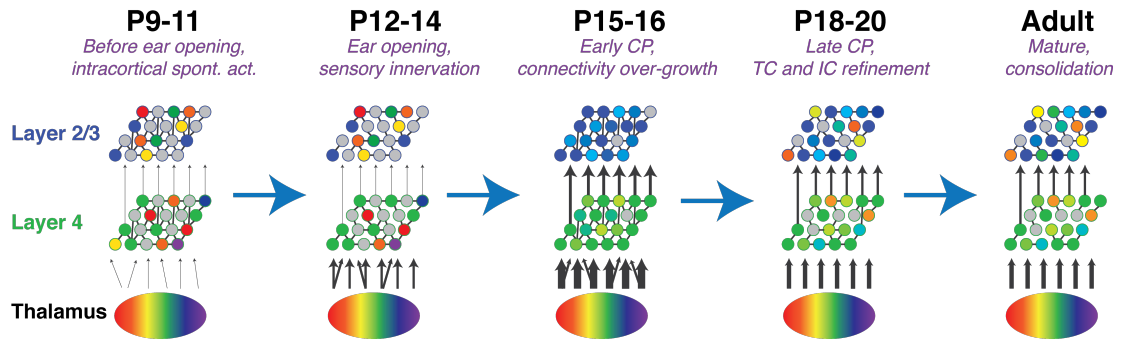
**Figure 3.9. A representation of circuitry changes in L2/3 and L4 over development**. At P9-11, the presence of selective but unreliable responses in L2/3, coupled with high NCs, suggests that immature L4 input is established before ear opening along with exuberant connections between nearby L2/3 neurons, possibly mediated via gap junctions, which results in spontaneous activity patterns. At ear opening ~P12, L4 SCs increase consistent with thalamocortical strengthening, while NCs decrease in both layers suggesting the start of intralaminar reorganization and potentially loss of electrical connectivity between neighboring cells. The early-CP at P15-16 is characterized by the highest pairwise SCs and greatest local response homogeneity, suggesting a period of ascending over-connectivity. During this time, neurons respond robustly to many stimuli. The serial relay of patterned sensory information from L4 to L2/3 drives the refinement of L2/3-L2/3 connections at P18-20 and through to adult via selective strengthening of connections between neurons responding to similar stimulus features and elimination of non-responsive or uncorrelated horizontal connections.

distance dependency within L4 peaks at P15-16 and is no longer evident at ages older than P20. In L2/3, SCs at P9 show a dual-peaked spatial dependence, and are highest among cells within 60 μm or >240 μm apart, while in both P15-16 and P20 age

80

groups, SCs between cells in L2/3 exhibit a secondary peak at ~240 μm. Secondary

peaks are also evident in the NC distributions in P9-11 L2/3 (at 300 μm) and at P12-

14 L2/3 (at 270 μm). These NC peaks are consistent with the patchy connectivity of

intracortical circuits (Watkins et al., 2014; Kratz and Manis, 2015).


*Sensory experience differentially alters laminar network organization in A1*

Given the differences in the functional organization between layers and the

developmental changes we observed, we speculated that altered sensory experience

such as noise rearing could have a large laminar-dependent effect on mesoscale

network organization. We raised mice (n=5) in the presence of moderate-intensity 75

dB white noise beginning at P5/P6 (Zhang et al., 2001, 2002; Chang and Merzenich,

2003). Thus, mice are reared in an environment devoid of sounds with any

spectrotemporal structure (Chang and Merzenich, 2003). Since most organizational

properties in A1 stabilized by P20, and since synaptic inputs to L2/3 are stable at P19-

P29(Oswald and Reyes, 2008), we investigated the cortical organization in L2/3 and

L4 of noise-reared mice (NR) at P20 and compared them to P20 control mice (CTL)

(**Table 3.2**) (Oswald and Reyes, 2008).


**Table 3.2 | Noise-reared vs. control animals imaged**

|  | Layer | Animals | Fields | Mean depth | # Cells |
|---|---|---|---|---|---|
| **P20 CTL** | L2/3 | 6 | 14 | 190 ± 3.9 μm | 1243 |
|  | L4 | 5 | 12 | 349 ± 18.8 μm | 717 |
| **P20 NR** | L2/3 | 4 | 12 | 191 ± 3.7 μm | 1524 |
|  | L4 | 5 | 11 | 366 ± 15.2 μm | 1244 |

We first investigated whether the noise-rearing paradigm affected overall hearing thresholds by measuring response thresholds in both groups (Chang and Merzenich, 2003). Thresholds in L2/3 NR neurons were unchanged (**Fig. 3.10a**), whereas L4 neurons showed decreased thresholds. Wide-field imaging revealed no
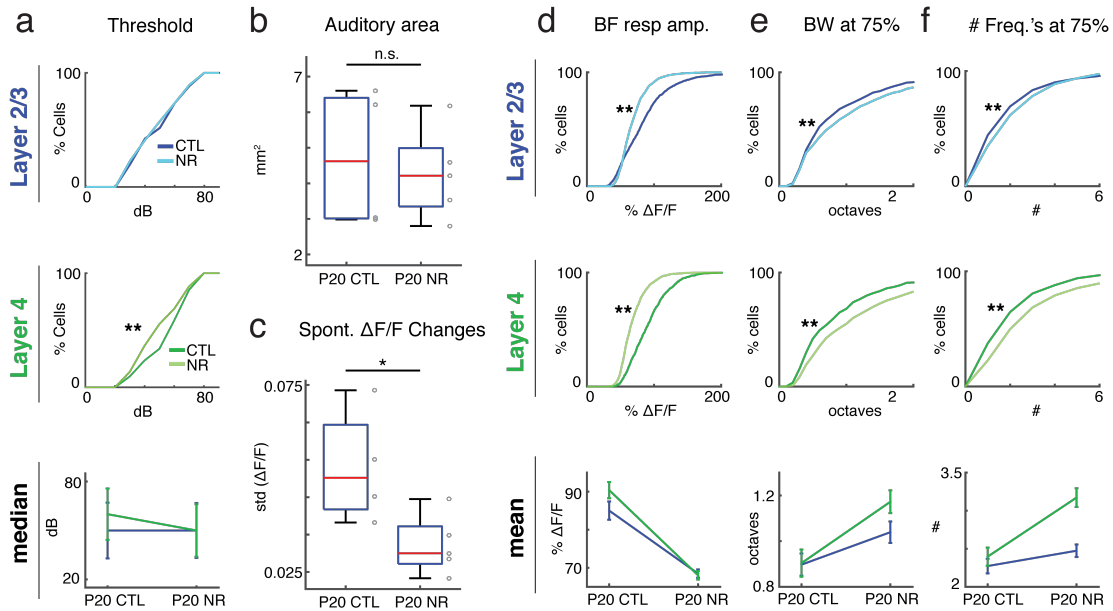


**Figure 3.10. Sensory experience has a similar effect on single cell properties in L4 and L2/3.** (**a**) Noise-rearing did not affect thresholds of L2/3 neurons (L2/3 P20 CTL median threshold ± iqr = 50 ± 30 dB, P20 NR= 50 ± 30 dB; Wilcoxon rank-sum test, p= 0.16), whereas L4 neurons had decreased thresholds (L4 P20 CTL= 60 ± 25 dB, P20 NR= 50 ± 30 dB; $p<10^{-5}$). (**b**) Wide-field imaging revealed no changes in total ACX area with NR. (**c**) Baseline fluorescence variability is reduced in NR mice (ANOVA p=0.033). (**d**) Amplitude of single-cell responses to BF stimuli in both layers after NR was reduced compared to CTL (mean ± 1.96*SEM) (**e-f**) A1 neurons in L4 and L2/3 showed decreased frequency selectivity (at the 75% cutoff) after noise rearing (mean ± 1.96*SEM).

changes in total ACX area after noise-rearing (**Fig. 3.10b**). However, baseline

fluorescence variability was reduced after noise-rearing, indicating decreased

spontaneous activity (**Fig. 3.10c**). A1 neurons in both L4 and L2/3 of NR mice

showed decreased frequency selectivity (**Fig. 3.10e,f**), and reduced amplitude
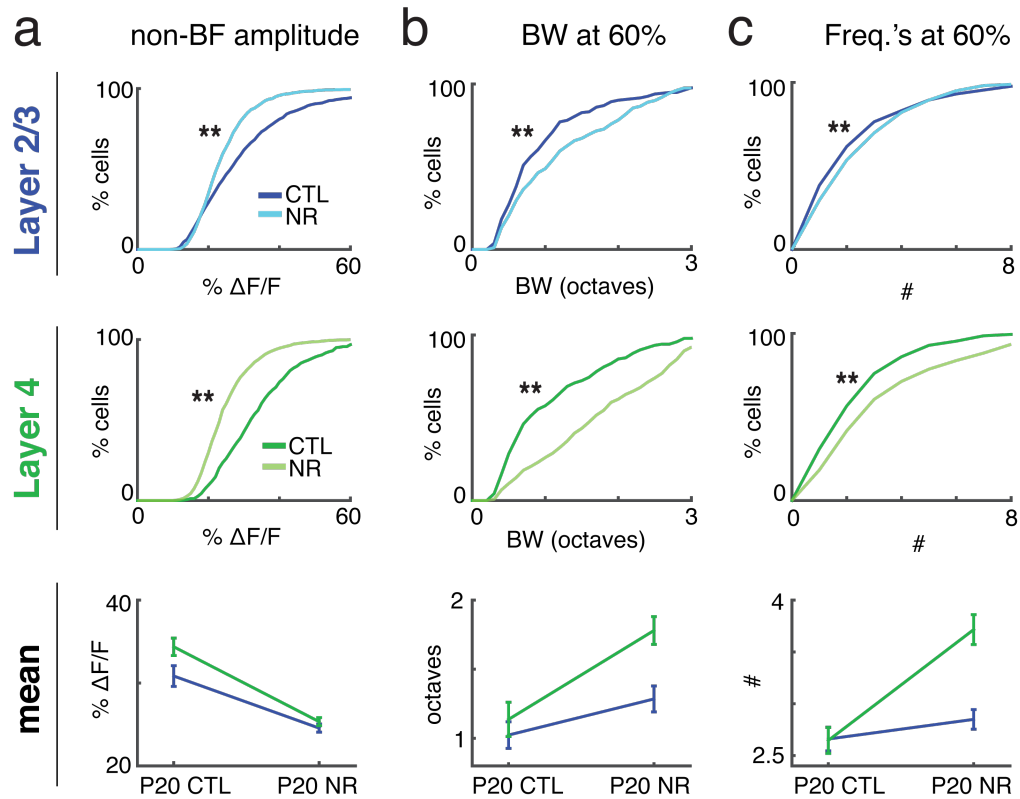


**Figure 3.11. Sensory experience has a similar effect on single cell properties in L4 and L2/3**. (**a**) The amplitude of single-cell responses to non-BF stimuli in both layers after NR was reduced compared to CTL (mean ± 1.96*SEM), consistent with the amplitude change observed to BF stimuli. (**b-c**) NR-induced frequency selectivity decrease at the 60% tuning curve cutoff is also consistent with the broadening observed at the peak of the tuning curve (75% cutoff; **Fig. 3.10**).

responses to both BF and non-BF stimuli compared to CTL (**Fig. 3.10d**; also see **Fig. 3.11**). Our findings are consistent with prior microelectrode results (Zhang et al., 2002; Chang and Merzenich, 2003), while our imaging data reveals additional laminar differences in the influence of sensory experience.

We next investigated the effect of noise rearing on network properties of neuronal populations. A decrease in frequency selectivity of single neurons would be expected to increase the similarity in frequency tuning of neighboring neurons. Indeed in L4 we observe a decrease in $IQR_{BF100}$ following NR (**Fig. 3.12a**), thus nearby L4 neurons are *more* likely to share BFs. In contrast, in L2/3 after NR we observed an increase in frequency tuning heterogeneity. Thus, despite the widening of tuning curves in both L4 and L2/3, nearby cells in L2/3 are even *less* likely to share BFs after NR. Together, these results show opposite changes in local organization of L2/3 and L4 in response to an altered sensory environment.

To identify if different tonotopic regions show differential changes in local tuning variability, we tested if cells with different BFs or with different local BF means (<100 μm) have different $IQR_{BF100}$s (**Fig. 3.13**). We find that the NR-induced increase in L2/3 response heterogeneity is isolated to the 16-32 kHz region of the tonotopic map, whereas the L4 increase in homogeneity occurs in the 8-16 kHz region. This suggests that different areas of A1 are preferentially affected by our NR paradigm.

To gain insight into the potential circuitry changes underlying the observed opposing shifts in IQR after NR, we next investigated the influence of NR on the
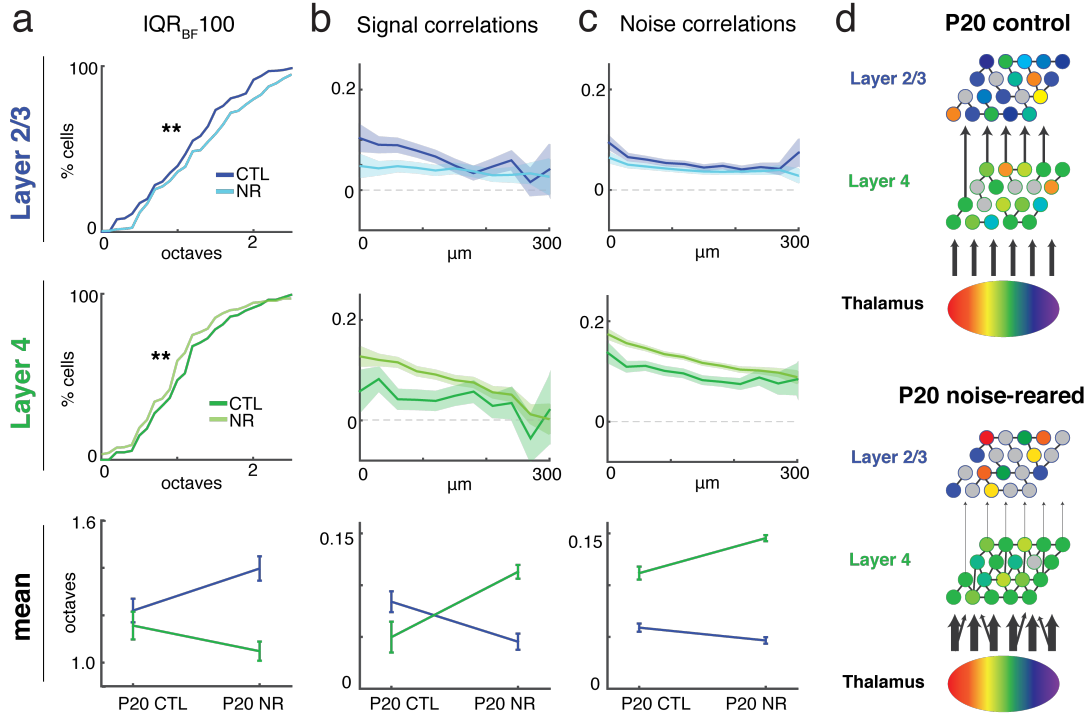
**Figure 3.12. Sensory experience differentially alters laminar network organization in A1. (a)** NR increases the frequency tuning similarity of neighboring neurons in L4 (IQR$_{BF100}$ P20 L4 CTL IQR$_{BF100}$ median = 1.13 octaves; P20 L4 NR = 1.00 octave; Wilcoxon rank-sum test, $p < 10^{-3}$), while nearby neurons in L2/3 are *less* likely to share BFs (IQR$_{BF100}$ P20 L2/3 CTL IQR$_{BF100}$ median = 1.25 octaves; P20 L2/3 NR = 1.38 octaves; $p < 10^{-4}$). Lower row averages show mean ± 95% confidence interval (1.96*SEM). Signal correlations (**b**) and noise correlations (**c**) are plotted as a function of distance between cell pairs (line=mean, shading= 95% confidence interval). **(d)** A schematic of circuitry differences within L2/3 and L4 of control and noise-reared mice. NR, and thus lack of experience-dependent activity, results in a prolonged critical period in which delayed refinement of thalamocortical projections to L4 result in depression of L4-L2/3 and L2/3-L2/3 horizontal connectivity.

pattern of pairwise correlations (**Fig. 3.12b,c**). In L4, both SCs and NCs increased after NR, comparable to the level of correlated activity observed in P12-14 mice. In contrast, in L2/3 both SCs and NCs decreased, suggesting decreased ascending input into L2/3 and decreased intralaminar connectivity within L2/3. In control mice, the degree of neuronal correlated activity depends on the distance between cell pairs (see **Fig. 3.8**). In L4, NR leads to increased SCs for cells <150μm apart and increased NCs for cells <200μm, with no difference in correlations between cells at further distances apart (**Fig. 3.12b,c**). In contrast, L2/3 shows *decreased* SCs and NCs between neurons <100 μm apart in NR compared to control P20 mice. Additionally, in
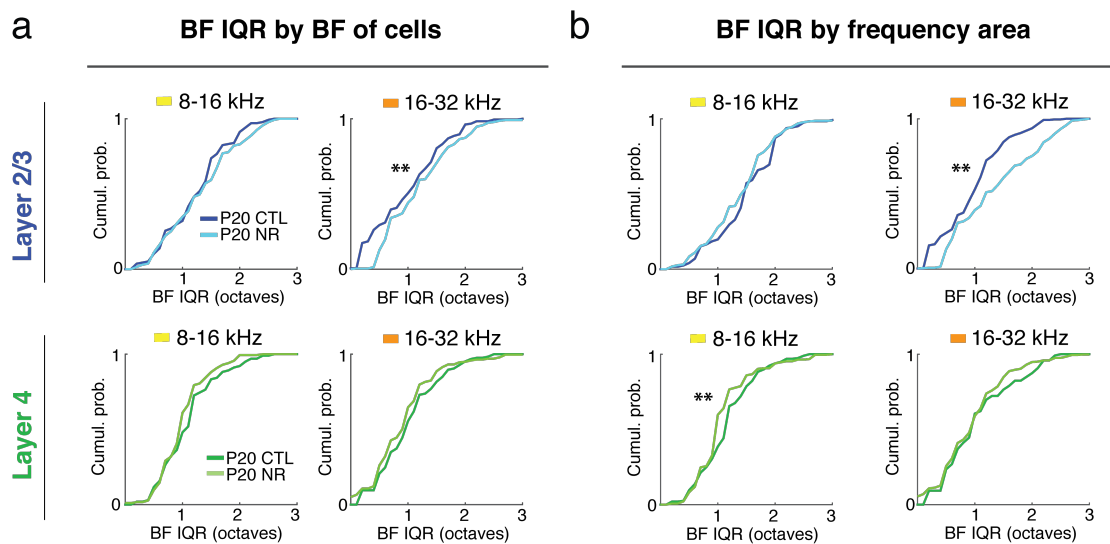


**Figure 3.13. Different regions of the A1 tonotopic map are differentially affected by noise-rearing.** Local tuning variability was assessed by grouping $IQR_{BF100}$'s by individual cell BF (**a**) and local BF means, <100 μm (**b**). NR-induced increases in L2/3 response heterogeneity are only significant in the 16-32 kHz region of the tonotopic map, whereas the L4 increase in homogeneity occurs in the 8-16 kHz region.

contrast to normal-reared P20 animals, we do not observe secondary peaks at ~240-300 μm (Watkins et al., 2014; Kratz and Manis, 2015) in P20 NR mice (Bandyopadhyay et al., 2010; Guo et al., 2012a) suggesting that patchy connectivity is due to early sensory experience.

Thus, while noise rearing has a similar effect on the tuning properties of single cells in L4 and L2/3, the spatial representation of preferred sound frequency as well as pairwise correlations between cells are altered in opposite directions in the two laminae, suggesting that laminar circuitry is differentially susceptible to sensory experience.

## Discussion

The development of sensory cortical circuitry is a complex, experience-dependent process. We here used multi-scale imaging in mice over the first three months of life to show that circuits in the different laminae of A1 are differentially susceptible to sensory input. Our results show that the spatial representation of BF in L2/3 and L4 is most homogeneous during the early-CP, and then becomes differentially heterogeneous across A1. Thus, BF heterogeneity is a feature of A1, consistent with the proposed role of A1 for encoding behaviorally-relevant sounds (Nelken, 2004; Kanold et al., 2014). The BF heterogeneity in adult mice confirms prior studies using synthetic indicators (Bandyopadhyay et al., 2010; Rothschild et al., 2013; Winkowski and Kanold, 2013) but is in contrast to reports emphasizing local frequency preference similarity (Issa et al., 2014). The differences are likely due us using a more sensitive $Ca^{2+}$ indicator (we use GCaMP6 vs. GCaMP3) and

analyzing cells with varied, not solely V-shaped, receptive fields allowing us to characterize a more inclusive representation of A1 neurons.

Sensory experience alters A1 on the single cell and mesoscale. Cells in L4 and L2/3 of NR mice respond to tones with weakened amplitudes and with decreased frequency selectivity, consistent with prior multielectrode studies (Zhang et al., 2002; Chang and Merzenich, 2003), and is also consistent with deprivation-induced changes in other sensory cortices, following binocular deprivation (Wiesel and Hubel, 1963) or whisker trimming (Shepherd et al., 2003). In contrast, noise-rearing altered the mesoscale organization in L2/3 and L4 in opposite ways. NR decreased pairwise correlations and BF homogeneity in L4 while both measures increased in L2/3. The differential laminar effects suggest that the circuit states are different in each layer.

The correlations and BF-homogeneity after NR in L4 resembles the early CP (P15-16) state while the increased local BF heterogeneity and decreased correlations within L2/3 are similar to ~P12-14 (pre-CP state). Thus, NR induces distinct changes in auditory processing within L2/3 and L4 reflective of different developmental stages, consistent with a serial progression of peripherally-driven refinement. We propose a model (**Fig. 3.12d**) in which L4 changes are evidence of a delayed maturation where the immature feedforward thalamocortical over-connectivity established via sensory-independent mechanisms is retained but is prevented from undergoing sensory-driven refinement. This is consistent with the increased correlations and local tuning homogeneity evident in L4 of NR mice. The L2/3 changes suggest an even more delayed maturation, in which the delayed refinement of L4 connectivity drives temporally uncorrelated synaptic activity in L2/3 neurons

and results in depression of L4-L2/3 and L2/3-L2/3 intralaminar connectivity. Our findings are also consistent with sensory deprivations having a greater effect on L2/3 than L4 (Fox, 1992; Trachtenberg et al., 2000; Shepherd et al., 2003; Foeller and Feldman, 2004).

NR induces sensory deprivation by rearing mice in an environment devoid of any auditory structural significance and spectrotemporal cues across the frequency spectrum (Chang and Merzenich, 2003). Thus, NR is similar to full uni-modal sensory deprivation paradigms such as binocular deprivation (Wiesel and Hubel, 1965; Kirkwood et al., 1995), or full-whisker trimming studies (Shepherd et al., 2003) and different from partial deprivation studies such as monocular deprivation and single-whisker trimming, which induce competitive plasticity mechanisms within a sensory system. While our results show that L2/3 and L4 respond to NR differently, such differences might also be present for other forms of deprivation.

The mesoscale changes allow us to delineate distinct laminar-dependent developmental periods. The high NCs in P9-P11 mice are consistent with responses driven by spontaneous peripheral and central activity patterns (Feller et al., 1996; Katz and Shatz, 1996; Butts, 2002; Adelsberger et al., 2005; Tritsch et al., 2007; Wang and Bergles, 2015). L4 SCs increase around P12, consistent with thalamocortical strengthening (Barkat et al., 2011), while NCs decrease in both layers suggesting the start of intralaminar reorganization (Ko et al., 2013). Typically, the CP is characterized by altering the period of sensory deprivation (Insanally et al., 2009; Barkat et al., 2011; Caras and Sanes, 2015; Mowery et al., 2015). We here identify the substrate of this time window as a period when neurons respond robustly to many

stimuli, when neighboring neurons share tuning properties, and when pairwise correlations are high.

Whereas L4 'inherits' frequency preference from thalamic input, L2/3 frequency preference is determined by ascending, intralaminar, and long-range connections (Atencio et al., 2009; Atencio and Schreiner, 2010). The presence of selective but unreliable responses in L2/3, coupled with high NCs, suggests that L4 input to L2/3 is established before ear opening, along with extensive connectivity between nearby L2/3 neurons, possibly mediated via gap junctions (Ko et al., 2013; Yao et al., 2016). The serial relay of patterned sensory information from L4 to L2/3 then likely drives the refinement of L2/3-L2/3 connections via selective strengthening of connections between neurons responding to similar stimulus features and elimination of non-responsive or uncorrelated horizontal connections (Douglas et al., 1995; Foeller and Feldman, 2004; Douglas and Martin, 2007; Ko et al., 2013). Without patterned sensory input, the immature feedforward L4-L2/3 projections drive deprivation-induced synaptic depression between L4-L2/3 and L2/3-L2/3 via STDP because uncorrelated pre- and post-synaptic signals likely predominate (Feldman, 2000; Bender et al., 2003; Celikel et al., 2004; Feldman, 2009).

Overall, we show that the laminar organization of A1 develops on multiple scales and that sensory experience modulates different aspects of this development. In particular, we reveal a dissociation of plasticity of single-cell, mesoscale, and macroscale network properties in the face of sensory manipulations.

# Chapter 4: Visual deprivation alters the functional organization of adult mouse auditory cortex

## Abstract

Although within-modality sensory plasticity is limited to early developmental periods, cross-modal plasticity can occur even in adult sensory cortices. Transient visual deprivation (dark exposure, DE) in adult mice improves the frequency selectivity and discrimination of single neurons in primary auditory cortex (A1). Since on the circuit level, visual deprivation strengthens thalamocortical synapses and causes a refinement of intracortical circuits, these changes might also result in mesoscale changes in the functional organization of A1. In animals reared under normal light conditions, the spatial representation of sound frequency in A1 differs between thalamorecipient layer 4 (L4) and layer 2/3 (L2/3), with nearby L2/3 neurons preferring different frequencies while neighboring L4 neurons prefer similar frequencies. We thus investigated if DE results in changes in A1 functional organization in mice using *in vivo* two-photon $Ca^{2+}$ imaging. We find that DE reduces the spatial heterogeneity of frequency preference of neurons in both L2/3 and L4 and increases pairwise correlations in neuronal activity. Thus, the spatial representation of sound frequency in L2/3 and L4 locally becomes more similar after DE. The observed changes were largest in frequency regions within the vocal spectrum of mice,

suggesting that animals adjust their auditory processing for behaviorally-relevant stimuli. These results show that cross-modal sensory experience has the power to alter network circuitry and population dynamics even into adulthood, and likely plays a role in the enhancement of one sensory modality (hearing) following the loss of another (vision).

## Introduction

Sensory cortices process diverse features of sensory stimuli, and within primary sensory areas, neuronal stimulus properties are represented in peripherally-organized topographic maps. In the primary auditory cortex (A1) sound frequency is represented as a gradient across the rostrocaudal cortical axis (Schreiner and Winer, 2007). *In vivo* imaging in mice revealed that while neighboring neurons in thalamorecipient layer 4 (L4) prefer similar frequencies, nearby supragranular layer 2/3 (L2/3) neurons are selective for very different frequencies (Bandyopadhyay et al., 2010; Rothschild et al., 2010; Winkowski and Kanold, 2013; Maor et al., 2016). Thus, the representation of sound frequency preference is more heterogeneous in L2/3 than L4, which suggests that this organization might support L2/3 neuronal network processing of complex behaviorally-relevant auditory stimuli (Nelken, 2004; Kanold et al., 2014).

A hallmark of sensory cortices is their ability to rewire in response to environmental input especially during specific critical periods of development (Wiesel and Hubel, 1963; Hubel and Wiesel, 1970; de Villers-Sidani et al., 2007; Sanes and Bao, 2009; Barkat et al., 2011). However, the capacity for plasticity is not

fully extinguished in adulthood. Within A1, plasticity can be reactivated in response to specific events such as learning or motherhood (Kilgard and Merzenich, 1998; Bao et al., 2001; Fritz et al., 2003; Fritz et al., 2005; Rutkowski and Weinberger, 2005; Polley et al., 2006; Keuroghlian and Knudsen, 2007; Rothschild et al., 2013; Elyada and Mizrahi, 2015). Furthermore, loss of a sensory modality can engage plasticity in the remaining senses. Humans experiencing vision loss from birth exhibit cross-modal perceptual enhancement of hearing, including improved sound localization abilities (Lessard et al., 1998; Voss et al., 2004), frequency discrimination performance (Gougoux et al., 2004), and auditory spatial tuning (Roder et al., 1999). In particular, even brief periods of visual deprivation in humans can transiently improve auditory perception by enhancing sound source segregation (Page et al., 2016). Cats binocularly deprived from birth and ferrets with binocular eye suture in adulthood both show a significant compensatory enhancement in auditory spatial acuity, particularly with peripheral sound localization (Rauschecker and Kniepert, 1994; King and Parsons, 1999), yet the circuit basis for these perceptual enhancements is unclear.

In rodents, brief periods of visual deprivation increase frequency selectivity, lower activation thresholds, and increase neuronal firing rates of single neurons in L4 of A1 (Petrus et al., 2014). These changes on the single cell level are consistent with DE-induced potentiation of thalamic input to L4 and strengthening of ascending intracortical connections from L4 to L2/3 neurons (Goel et al., 2006; Petrus et al., 2014; Petrus et al., 2015), and refinement of both intra-laminar excitatory and inhibitory connections within L2/3 as well as inter-laminar ascending connections

93

from L4 to L2/3 (Meng et al., 2015). However, sensory stimuli are not encoded by single neurons but by populations of neurons and the network activity patterns as well as activity correlations between neurons can contribute to information encoding (DeWeese et al., 2003; Hromadka et al., 2008). Thus, changes in synaptic function have to be coordinated across neurons to improve network function.

Here, we examined if dark exposure (DE) in adulthood can restructure the mesoscale organization and connectivity of A1 by using *in vivo* two-photon calcium ($Ca^{2+}$) imaging, which allows visualization of large populations of individual neurons (within hundreds of microns) and inference of their local and long-range connections (Bandyopadhyay et al., 2010; Rothschild et al., 2010; Winkowski and Kanold, 2013). We measured the sound evoked activity from L2/3 and L4 A1 neurons in adult mice (>P28) after one week DE that occurred after the critical period for spectral tuning. We then quantified how DE affects the spatial representation of auditory information by calculating the best frequency (BF) variability of neighboring neurons, and computed signal and noise correlations between simultaneously imaged cells.

We find that DE reduces local heterogeneity of sound frequency representation. DE also increases response correlations between pairs of L4 and L2/3 neurons, consistent with modifications of ascending and intra-laminar inputs. Moreover, we observe that changes in sound frequency representation were more prevalent in A1 areas responding to frequencies in the range of mouse vocalizations. These experiments reveal that besides altering the tuning of single neurons, DE can alter network activity and population dynamics in adulthood, long after the canonical critical period for auditory and visual plasticity has ended (Goel et al., 2006; Barkat et

al., 2011; Petrus et al., 2014; Meng et al., 2015; Petrus et al., 2015). Thus, cross-modal plasticity might be more powerful than within-modality plasticity in rewiring cortical circuits.

## Methods

To study the cross-modal plasticity of A1 we used *in vivo* two-photon calcium ($Ca^{2+}$) imaging in 26 male and female C57Bl/6J wild-type mice, bred in house. AAV1-Syn-GCaMP6s-WPRE-SV40 (UPenn Vector Core) (Chen et al., 2013; Packer et al., 2015) was injected into the ACX of these mice at ages P22-P45 (for detailed procedure see Chapter 2: General Methods), after which animals were returned to the colony and allowed to recover. After a minimum of 7 days recovery, mice were either placed in a dark room for 7-10 days (Dark-exposed, n=10 mice) or left in a normal 12-hour light/dark cycle (Control, n=16 mice). Visual deprivation was always performed after the critical period for auditory cortical plasticity. All mice had access to food and water *ad libitum*.

Mice were imaged at least 14 days after injection (P41-68), in order to allow for viral transfection and stable expression of GCaMP6s in cells. Acute cranial window surgery was performed (see Chapter 2 for more detail) immediately prior to imaging. Dark-exposed mice were kept in darkness for the duration of imaging by 1) using a light-sealed carrying container to transfer them from the colony to the surgery room, 2) inducing anesthesia with the lights off and minimal light penetration, and 3) sealing their eyes shut with glue and covering with dark tape for the rest of the

95

imaging session. For control mice, only this last step was performed, and all mice therefore had no visual input while recording sound-evoked responses.

Using two-photon $Ca^{2+}$ imaging, regions were scanned at 3-8 Hz at 150-200 μm beneath the pial surface for supragranular layers 2/3 and 300-450 μm for thalamorecipient layer 4. Auditory stimuli consisted of 4 to 64 kHz SAM tones repeated ten times at 60 dB for most analyses. To generate frequency response areas (FRAs), sounds were played at 4 different dB levels (30, 45, 60, and 75 dB), with each stimulus repeated 5 times.

*Data analysis*

Cells were manually selected as circle regions of interest (ROIs), and pixel intensity within each ROI was averaged to generate fluorescence over time. Neuropil correction was performed by selecting a circular region of the same area near the cell, with no other cells present. The average fluorescence of this area (background fluorescence, $F_B$) was then subtracted from the cell's fluorescence at each time point. Changes in fluorescence *(ΔF/F)* were calculated with the following equation (Kerlin et al., 2010; Chen et al., 2012): $[(F - r*F_B) - (F_0 - r*F_B)] / (F_0 - r*F_B)$, where $F_0$ is the average fluorescence signal during the baseline frames preceding stimulus onset, and r is the contamination ratio 0.5, estimated by calculating $F_{blood\_vessel}/F_{neuropil}$ for the 20x/0.95NA objective used. A responsive cell was defined as a cell that responds to at least one of the presented stimuli significantly (99% confidence interval), and remaining analysis was performed only on significantly responding cells.

Signal correlations (stimulus-related cross correlations) were determined by computing the cross-correlation between the mean $Ca^{2+}$ responses during each sound stimulus presentation, for each unique cell pair in a field of view. When trial number is small for each stimulus signal correlations can be strongly biased by noise correlations (Rothschild et al., 2010; Rothschild et al., 2013), and thus to overcome this bias, terms contributing to noise correlations are omitted from the sum in the equation for signal correlation (Rothschild et al., 2010; Winkowski and Kanold, 2013). Noise correlation (trial to trial response variability) was measured by taking the individual response to each repeat of a sound stimulus, subtracting out the mean response to that particular stimulus, and measuring the covariance of the concatenated responses from each trial.

## Results

To visualize the activity of A1 neurons we injected adeno-associated virus carrying the $Ca^{2+}$ indicator GCaMP6s (AAV1.Syn.GCaMP6s) into the auditory cortex of 26 mice (at P22+), after which mice were randomly split into dark-exposed (DE, n=10) or normal reared control (CTL, n=16; **Table 4.1**) groups. Mice were imaged at least 14 days after injection using two-photon $Ca^{2+}$ imaging (at ages P41-68). We recorded neuronal fluorescence signals from L2/3 neurons by imaging planes at 150-200 μm below the pial surface and from L4 neurons by imaging at 300-450

**Table 4.1 | Animals, fields, and cell numbers imaged**

| Group | Layer | Animals | Fields | Mean depth | Total Cells | Responding Cells | Reliable Cells |
|---|---|---|---|---|---|---|---|
| Control | L2/3 | 16 | 49 | 188 ± 20 μm | 1824 | 1419 | 713 |
| | L4 | 10 | 25 | 337 ± 22 μm | 997 | 818 | 536 |
| Dark-Exposed | L2/3 | 9 | 29 | 185 ± 12 μm | 1213 | 1088 | 592 |
| | L4 | 10 | 19 | 334 ± 41 μm | 825 | 743 | 494 |

μm below the pial surface (**Fig. 2.6**). This approach allowed us to measure responses from thousands of neurons (**Table 4.1**). In table 4.1, responding cells denote neurons from the total cell population that showed a significant tone-evoked response to at least one frequency (ANOVA across 10 repetitions, $p < 0.01$), and reliable cells are neurons that had a significant response to their BF-stimulus at least 4 out of 10 repetitions of that stimulus (ANOVA for individual repetitions, $p < 0.05$). In several mice, Di-I crystal retrograde labeling of the medial geniculate nucleus of the thalamus was used to confirm that imaging occurred in A1 (**Figure 2.8**). Immunostaining for GFP (to enhance cytosolic GCaMP6s signal), NeuN (neuronal cell bodies), and GFAP (astrocytes) showed that GCaMP6 expression from cortical injections is isolated to neurons, and does not transfect glial cells (**Fig. 2.2**).

*Dark-exposure increases the reliability of tone-evoked A1 neuronal responses*

To characterize the single-cell response properties of neurons in control and DE mice, we imaged ~150-200 x 150-200 $μm^2$ regions within L2/3 and L4 and

generated tuning curves for each cell in a field of view based on average time course traces (**Fig. 4.1a-d**). The preferred tuning for each cell was determined to be the frequency that evoked the maximum amplitude response (best frequency, BF). As expected, neurons in both thalamorecipient L4 and supragranular L2/3 of CTL and DE mice showed frequency selectivity (**Fig. 4.1a-d**).

The probability of a cell responding to its best frequency (BF) was 40.87% ± 0.31 when averaged across all groups (i.e. approximately 4/10 stimulus repetitions yielded significant responses at $p<0.05$, median ± IQR; CTL cells: 4/10 ± 2, n=2237; DE cells: 4/10 ± 3, n=1831). DE increased the reliability of cells in L2/3 (**Fig. 4.1e**) but did not change the reliability of cells in L4 (**Fig. 4.1f**). Since it is possible that a spontaneous fluorescence increase can occur during the stimulus period that is not sound-evoked, we excluded cells that responded 3 or fewer times to 10 repetitions. When only including reliably tone-responsive cells (those with ≥4/10 significant responses at $p<0.05$), the median reliability of L4 cells increased (CTL: 5/10 ± 2, n=536; DE: 6/10 ± 2, n=494; p=0.006), consistent with electrophysiological recordings (Petrus et al., 2014), with no change in L2/3 cells (CTL: 5/10 ± 2, n=713; DE: 5/10 ± 2, n=592; p=0.062). Compared to imaging with Fluo-4 and OGB-1 (Bandyopadhyay et al., 2010; Winkowski and Kanold, 2013), the lower response reliability observed here could be attributed to differences in the $Ca^{2+}$ indicators used, e.g the higher sensitivity of GCaMP6s (Tian et al., 2009; Chen et al., 2013) might allow us to capture the less reliably responding cells.

Moreover, AAV-GCaMP6s transfected neurons showed a higher level of
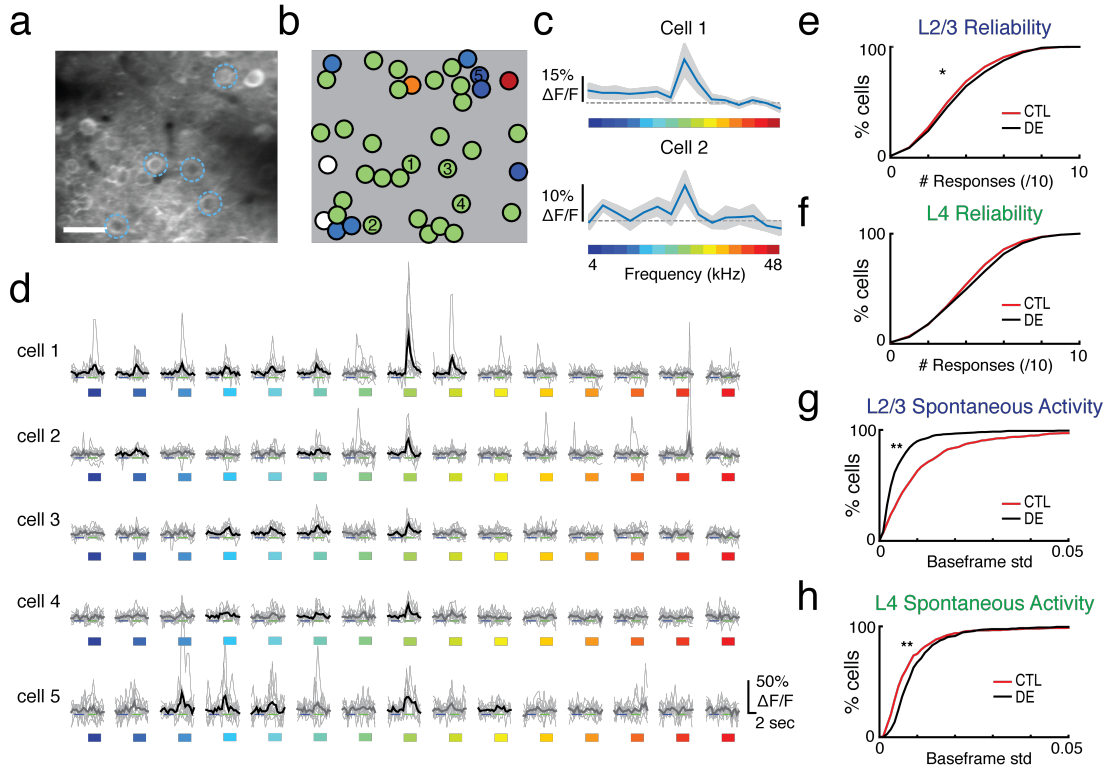
**Figure 4.1. Sound-evoked fluorescence changes in an adult AAV-GCaMP6-transfected mouse following DE.** (**a**) An *in vivo* two-photon image of a L2/3 region in A1 (scale bar = 20 μm). (**b**) Spatial map of BFs for all neurons in a field (color indicates BF, white circles indicate unresponsive cells). (**c**) Tuning curves for two sample neurons in the field (mean ± 1.96*SEM). (**d**) Time course traces of five sample cells responding to all frequencies presented (black lines indicate mean of responses that passed the significance criterion (ANOVA p < 0.01), gray lines are individual repetitions). (**e-f**) Response reliability to repeated presentations of BF-stimuli increased in L2/3 following DE (CTL median ± iqr: 4/10 ± 3; DE: 4/10 ± 2, Wilcoxon rank-sum test, p=0.01) and did not change in L4 (CTL: 4/10 ± 3; DE: 5/10 ± 3, p=0.086). (**g-h**) Spontaneous activity, as measured by baseline variance in ΔF/F traces, increased in L4 after DE (CTL median ± iqr L4: 0.0060 ± 0.006, DE L4: 0.0079 ± 0.007; p < $10^{-33}$), and decreases in L2/3 (CTL L2/3: 0.0078 ± 0.011, DE L2/3: 0.0036 ± 0.004, p < $10^{-9}$).

spontaneous activity relative to Fluo-4 and OGB-1, which was evidenced as fluorescence transients preceding the onset of the stimulus and during long-duration imaging without any stimulus presentation. The frequency of spontaneous transients increased in L4 after DE, as measured by variance during base frames preceding stimulus onset (**Fig. 4.1h**), consistent with *in vivo* recordings showing that L4 cells in DE animals have higher spontaneous firing rates (Petrus et al., 2014). However, L2/3 cells following DE were found to have a decreased frequency of spontaneous fluorescent transients (**Fig. 4.1g**).

Since $Ca^{2+}$ indirectly reports neuronal activity, we first excluded the possibility that the observed changes in reliability after DE were due to changes in cellular $Ca^{2+}$ dynamics by testing how observed fluorescence changes relate to spiking activity. We performed cell-attached patch clamp recordings *in vitro* (in voltage clamp) to simultaneously measure spiking activity and $\Delta F/F$ (Goncalves et al., 2013). The recordings show that a brief period of visual deprivation does not alter the amplitude of spike-induced fluorescence transients (**Fig. 4.2a,b**). Together with the fact that DE does not cause changes in intrinsic spiking properties of L2/3 cells (Meng et al., 2015), these data suggest that DE does not change the intrinsic properties and $Ca^{2+}$ dynamics of A1 neurons. Thus, the observed changes in BF response reliability are due to changes in the cortical circuits.


*Dark-exposure decreases neuronal thresholds in L2/3*

Microelectrode recordings show that DE decreases neuronal thresholds in L4
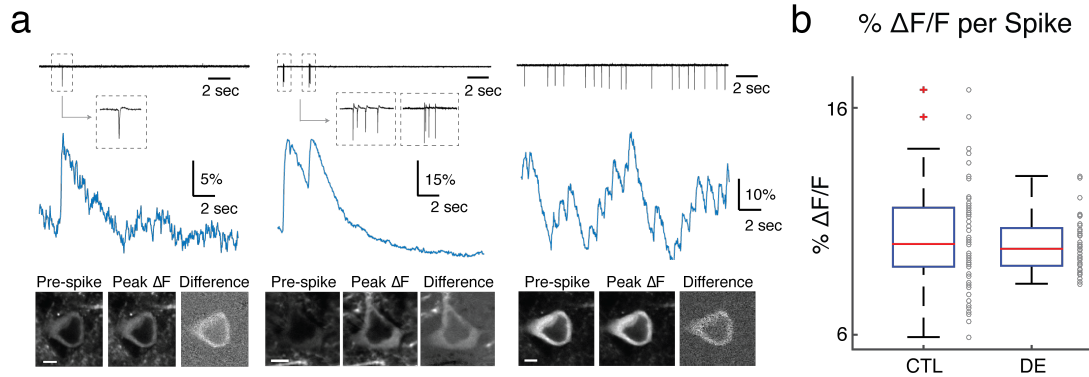
**Figure 4.2. Cell-attached patch recordings *in vitro* from AAV-GCaMP6S-transfected neurons.** (**a**) Simultaneous imaging and electrophysiological traces of spontaneous activity. Top row shows three representative examples of traces from two different patched neurons. Middle row shows the corresponding $Ca^{2+}$ rises (*ΔF/F*) in response to one or more action potentials – with insets showing magnified action potentials. Bottom row shows the corresponding two-photon images of GCaMP6s+ cells that were recorded: first image is of cell preceding spike, middle image is of cell at peak of fluorescent response, and third image shows the difference (scale bar = 5 μm). (**b**) Boxplot shows median and interquartile range of fluorescent-evoked responses to one spike in control and DE mice. DE does not alter the amplitude of spike-induced fluorescence transients (mean ΔF/F ± SEM per spike: CTL= 10.25% ± 0.29%, n=62 spikes; DE= 9.97% ± 0.20%, n=37 spikes; Two-sample Kolmogorov-Smirnov test, p= 0.16).

(Petrus et al., 2014). We thus tested whether DE also affects auditory response thresholds in L2/3. For these experiments, the same frequencies were presented at four different SPL levels: 30, 45, 60, and 75 dB. We find that in the adult mouse, L4 auditory neurons can respond to lower sound levels than L2/3 neurons (**Fig. 4.3**). DE decreases the threshold in L2/3 neurons (**Fig. 4.3**) and does not change L4 thresholds.

Since microelectrode recordings show that DE decreases threshold by only 4 dB (Petrus et al., 2014), the large dB increments used here (15 dB) might not be sufficient to detect these changes. Interestingly, even with the large dB step size there was a significant threshold decrease in L2/3 neurons following DE, which suggests that DE might result in larger effects on L2/3 than on L4 cells.
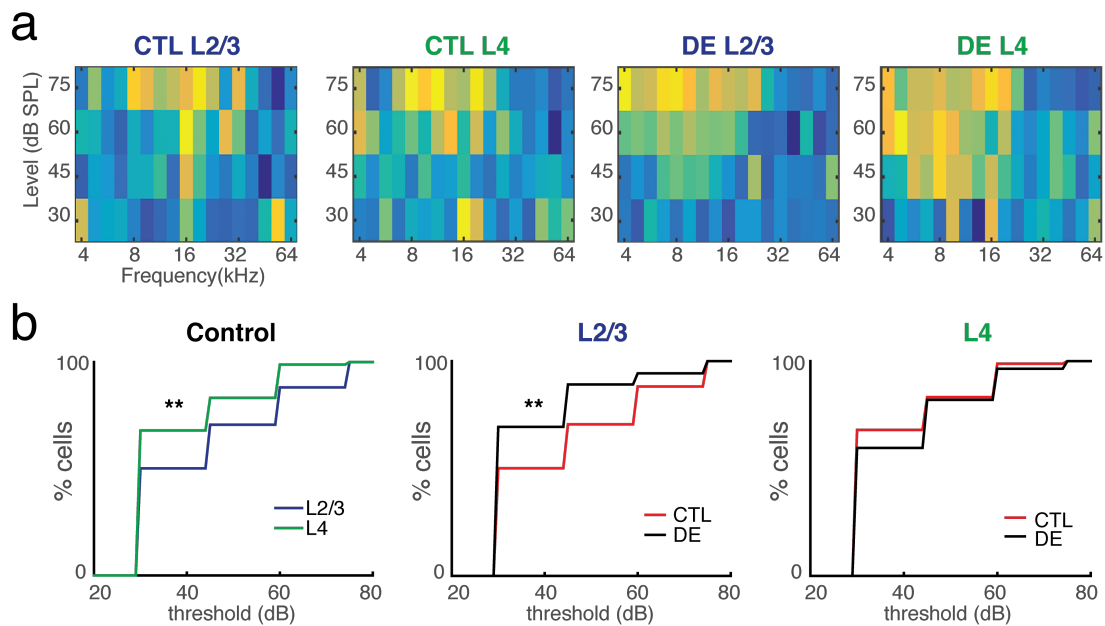


**Figure 4.3. Neural thresholds are differentially affected in L2/3 and L4 with DE. (a)** Sample frequency-response areas (FRAs) from L2/3 and L4 in CTL and DE mice suggest broadening of auditory receptive fields. (**b**) In control mice, L4 auditory neurons can respond to lower sound levels than in L2/3 (CTL mean ± std L2/3= 43.7 ± 16.0 dB SPL; L4= 37.5 ± 12.0 dB SPL; two-sample Kolmogorov-Smirnov test, p<$10^{-5}$). Dark exposure results in a decreased threshold in L2/3 neurons (DE L2/3= 37.08 ± 12.5 dB SPL, p<$10^{-10}$) and no change in L4 threshold (39.3 ± 12.9 dB SPL, p=0.15).

*Dark-exposure decreases frequency selectivity of neurons in L2/3 and L4*

Tuning curves (frequency-response areas, FRA) in many auditory structures are "V-shaped," with bandwidth increasing as sound intensity increases, but the adult auditory cortex also includes neurons with multi-peaked tuning curves (Schreiner et al., 2000; Kadia and Wang, 2003; Winkowski and Kanold, 2013). Previous studies using single-unit recordings and analyzing only "V-shaped" auditory neurons found than DE increases frequency selectivity, especially at sound levels close to threshold (10dB). These prior single-unit studies excluded neurons with more complex receptive fields (RFs). Since imaging can interrogate a more diverse auditory neuronal population, we wanted to assess whether we could reproduce the findings previously reported in L4, as well as whether the sharpening of tuning with DE could be extended to the next auditory processing stage, L2/3. In our imaging experiments, we used a fixed sound level of 60 dB to specifically assess how networks process an identical acoustic stimulus in the environment, and how this population response changes with visual deprivation. Thus given the average thresholds of L4 and L2/3 neurons these stimuli were ~20-30dB above threshold.

Since the tuning curves of imaged neurons showed either single frequency peaks or multiple peaks, we initially measured the number of frequencies to which each neuron had a significant fluorescent response (with significance determined by comparing the $\Delta F/F$ of the baseline frames to the $\Delta F/F$ of the stimulus period, one-way ANOVA p<0.01). We find that L2/3 and L4 cells respond to more frequencies following DE (**Fig. 4.4a**). We repeated this analysis by measuring only the number of
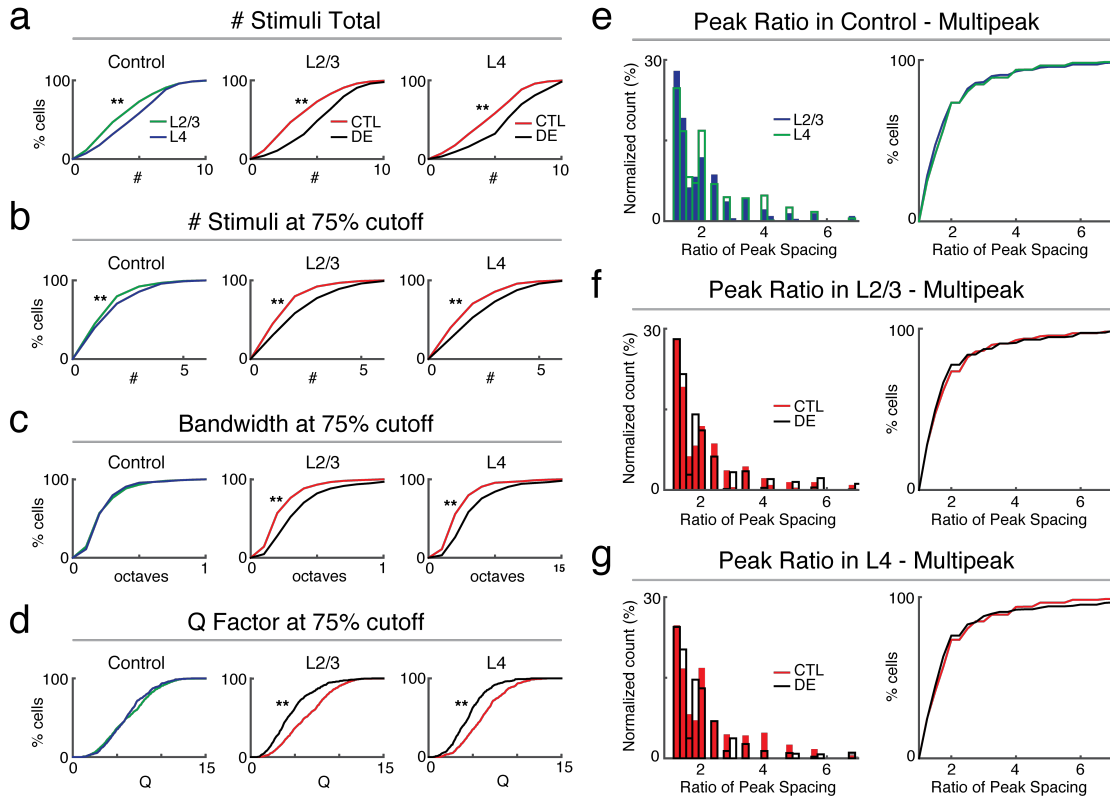
**Figure 4.4. DE decreases frequency selectivity of L2/3 and L4 neurons.** (**a**) L2/3 cells respond to more stimuli following DE (CTL mean ± std L2/3: 4.13 ± 2.28; DE: 5.58 ± 2.33; Wilcoxon rank-sum test for medians, $p < 10^{-54}$), as did L4 cells following DE (CTL L4: 4.85 ± 2.24; DE: 6.25 ± 2.44, $p < 10^{-36}$). (**b**) When only including stimuli that evoked a response exceeding 75% of the maximum amplitude, we found a consistent selectivity decrease after DE in both L2/3 and L4 (CTL L2/3: 1.87 ± 1.03; DE: 2.50 ± 1.44, $p < 10^{-30}$; CTL L4: 2.09 ± 1.18; DE: 2.65 ± 1.45, $p < 10^{-18}$). (**c-d**) Normalized bandwidth (in octaves) and Quality factor (Q= BF/bandwidth) at 75% of BF amplitude also showed DE-induced tuning curve broadening in both layers. (**e**) In control mice, auditory neurons had similar spectral spacing in both L2/3 and L4 (CTL IQR L2/3: 1.18; CTL L4: 0.96, Wilcoxon ranksum test: p= 0.26). (**f-g**) DE does not alter the spectral relationship between peaks in either L2/3 (DE IQR L2/3: 0.84, p= 0.58) or L4 (DE IQR L4: 0.62, p= 0.54).

frequency stimuli that evoked a response exceeding 75% of the maximum amplitude (at BF) and also find that cells in both L2/3 and L4 respond to more frequencies following brief DE (**Fig. 4.4b**). As a final measure of selectivity, we calculated normalized bandwidth (in octaves) at 75% of the cell's maximum amplitude response to BF. In agreement with measuring number of frequencies, we find that DE results in broadening of tuning curves in both layers (**Fig. 4.4c**).

While prior studies showed that DE results in sharper frequency tuning close to threshold (Petrus et al., 2014), our results indicate that refinement on a circuit level (Meng et al., 2015) does not necessarily lead to refined RFs at sound levels well above threshold. There are multiple differences between the current and the prior study. First, earlier studies used single-unit recordings to examine only single-peaked neurons with well-defined FRA's (Petrus et al., 2014). One limitation of electrophysiology is that the method targets a subset of strongly responsive cells, while two-photon imaging the sensitive GCaMP6s $Ca^{2+}$ indicator allows us to image a larger, more-inclusive population of auditory neurons, many with non-"V-shaped" tuning curves, which might respond differently to DE. Furthermore, we played tones at a single 60 dB sound level, thus our selectivity measures are ~20 dB above hearing threshold for CTL and DE L4 neurons (Petrus et al., 2014). Previous measurements conducted at 10 and 40 dB above threshold only indicated selectivity refinement at the 10 dB threshold cutoff and only in L4 (Petrus et al., 2014). This suggests that different parts of neuronal FRA's are differentially affected by DE, which could indicate that specific circuitry changes are occurring. DE could therefore narrow the peak of neuronal FRAs at BW10, make neurons more receptive to stimuli outside of

their preferred region at BW20, and have no effect on selectivity at BW40. Furthermore, the duration of tone presentation in the previous study (40 ms) was ten times shorter than our tone stimulus at 400 ms, which could potentially recruit different circuits and cell populations.

A final consideration is that the present study could have unintentionally sampled from discrete tonotopic regions and could thus be revealing changes specific to different spectral regions of A1. We thus separated BF bandwidths into three groups based on either the cell's BF or the average frequency preference (mean BF) of the area – low (4-8 kHz), middle (8-16 kHz), and high (16+ kHz; **Fig. 4.5**). In all spectral areas, DE was consistently found to increase bandwidth.

The multiple tuning peaks observed in auditory cortical neuron tuning curves (Schreiner et al., 2000; Kadia and Wang, 2003) are thought to aid in the extraction of spectral harmonics, such as those present in vocalizations. In all data sets, we observed a noticeable secondary peak near the peak ratio of two, corresponding to a one-octave spacing between peaks within a tuning curve (**Fig. 4.4e-g**). Furthermore, the median value for all distributions (1.68-1.70, or 0.75-0.77 octaves) is consistent with previous studies (Suter et al., 2010; Winkowski and Kanold, 2013). To determine if DE alters the spectral relationship between individual peaks in neurons, we calculated the ratio of all unique combinations of peaks within individual neuronal tuning curves. We found similar spectral spacing in both L2/3 and L4 (**Fig. 4.4e**), consistent with previous findings (Winkowski and Kanold, 2013). DE does not alter the spectral relationship between peaks in either L2/3 (**Fig. 4.4f**) or L4 (**Fig. 4.4g**).
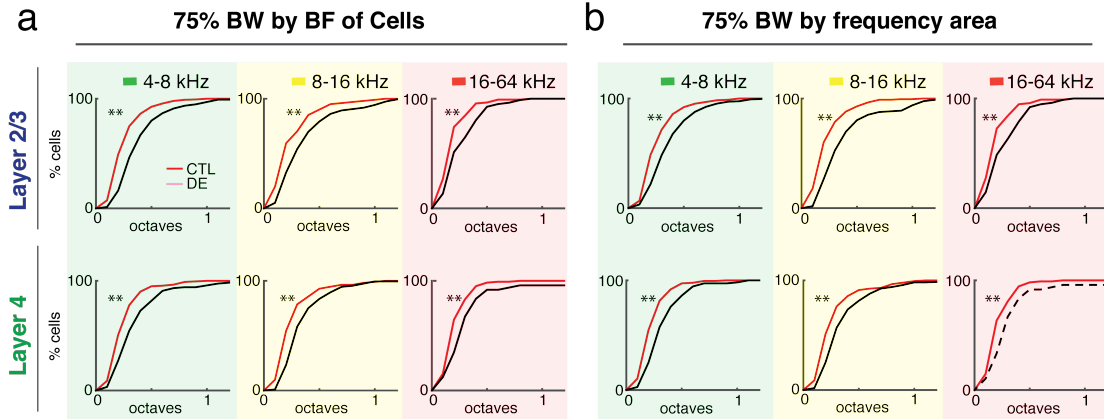
**Figure 4.5. DE increases bandwidth across the frequency axis.** (**a**) Bandwidths separated into three groups (low: 4-8 kHz, middle: 8-16 kHz, and high: 16+ kHz) based on BF of individual cells shows DE decreases selectivity in cells tuned to various BF's, and does not target any specifically tuned cells in both L2/3 (Low: CTL mean ± std in octaves= 0.30 ± 0.04, n=476; DE= 0.43 ± 0.06, n=348; Two-sample Kolmogorov-Smirnov test, $p < 10^{-12}$; Middle: CTL= 0.29 ± 0.05, n=105; DE= 0.41 ± 0.07, n=162; $p < 10^{-5}$; High: CTL= 0.23 ± 0.03, n=132; DE= 0.31 ± 0.04, n=82; p=0.002) and in L4 (Low: CTL= 0.29 ± 0.04, n=292; DE= 0.40 ± 0.06, n=241; $p < 10^{-4}$; Middle: CTL= 0.30 ± 0.05, n=115; DE= 0.38 ± 0.05, n=203; $p < 10^{-5}$; High: CTL= 0.24 ± 0.03, n=129; DE= 0.36 ± 0.08, n=50 $p < 10^{-3}$). (**b**) Bandwidths separated by tonotopic region (mean of local BF preference) also show that DE broadens tuning across the entire frequency spectrum, and different regions are not differentially affected by DE in L2/3 (Low: CTL= 0.31 ± 0.04, n=421; DE= 0.41 ± 0.05, n=344; $p < 10^{-7}$; Middle: CTL= 0.27 ± 0.04, n=184; DE= 0.43 ± 0.07, n=172; $p < 10^{-8}$; High: CTL= 0.23 ± 0.03 n=108; DE= 0.31 ± 0.04, n=76; p = 0.0011) and in L4 (Low: CTL= 0.27 ± 0.03 n=260; DE= 0.37 ± 0.05, n=210; $p < 10^{-5}$; Middle: CTL= 0.31 ± 0.05, n=163; DE= 0.40 ± 0.06, n=235; $p < 10^{-5}$; High: CTL= 0.25 ± 0.03, n=113; DE= 0.37 ± 0.08, n=49 $p < 10^{-3}$).

Thus, these results show that DE alters the frequency of single cells in all tonotopic regions of L4 and L2/3 in a similar manner.

*Frequency organization is more homogenous in L2/3 and L4 after dark-exposure*

Recent $Ca^{2+}$ imaging has revealed that while neural response properties within L2/3 are heterogeneous on a local scale (Bandyopadhyay et al., 2010; Rothschild et al., 2010; Winkowski and Kanold, 2013; Maor et al., 2016), responses in L4 are relatively homogenous, which is consistent with this layer being the first to receive tonotopically organized thalamic inputs (Winkowski and Kanold, 2013). This local heterogeneity of responses, particularly in supragranular layer 2/3, is thought to arise as a result of differing connectivity patterns across A1 layers within columnar microcircuits from L4-L2/3, which may have specific advantages in the hierarchical laminar transformation of auditory information integration (Atencio et al., 2009; Atencio and Schreiner, 2010). The more complex spectrotemporal receptive fields that are characteristic of L2/3 neurons could also arise from the abundance of local intralaminar connections, including input from spectrally distinct columns and long-distance cortico-cortical projections to this layer (Schreiner and Winer, 2007; Atencio et al., 2009; Atencio and Schreiner, 2010; Chen et al., 2011; Watkins et al., 2014). Since DE leads to a refinement of the ascending L4-L2/3 projection (Meng et al., 2015), the maps of frequency preference in L4 and L2/3 should be more similar after DE.

In order to determine if cross-modal plasticity affects the heterogeneity of frequency tuning of nearby neurons and thus provide insight into network

connectivity changes, we calculated the interquartile range of neurons' BFs ($IQR_{BF}$) within a 100 μm radius of each cell in each imaging plane (**Fig. 4.6a**). DE resulted in a reduction in the heterogeneity of local responses in L2/3 (**Fig. 4.6b**) as well as in L4 (**Fig. 4.6c**). Thus, a brief period of visual deprivation decreases the spatial BF variability in both the thalamorecipient layer and supragranular layers of A1.
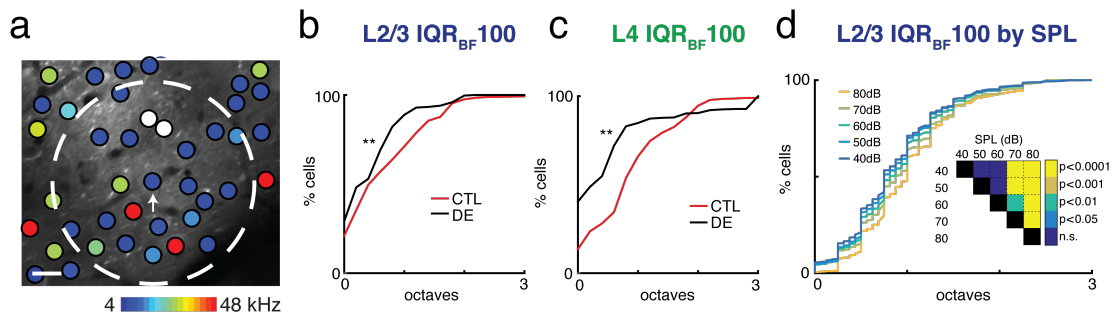


**Figure 4.6. The spatial representation of frequency preference is more homogeneous in L2/3 and L4 after DE.** (**a**) A sample *in vivo* two-photon image with a spatial color map of best frequencies (BFs) overlaid for all imaged neurons (color indicates BF and white circles are unresponsive cells). To quantify the BF spatial representation over development we calculate $IQR_{BF100}$ for each neuron (white dashed circle indicates the 100 μm radius for the cell identified by the white arrow). (**b-c**) Local frequency preference becomes more homogeneous after DE in L2/3 (CTL median ± iqr, in octaves 0.51 ± 1, n= 650; DE 0.38 ± 0.77, n= 565, Wilcoxon ranksum test p < $10^{-6}$), and in L4 (CTL: 0.77 ± 0.88, n=517; DE 0.38 ± 0.75, n=482 p < $10^{-26}$). (**d**) In L2/3 of *Thy1*-GCaMP6s mice, $IQR_{BF100}$ increases as a function of sound intensity (dB SPL; n cells at 40 dB: 512; 50 dB: 700; 60 dB: 802; 70 dB: 947; 80 dB: 1143; p values from one-way ANOVA).

Given that we observed a ~6 dB decrease in threshold for L2/3 neurons after DE and that previous studies reported a ~4 dB threshold decrease in L4, we questioned whether the increase in local response homogeneity we observed in both layers could be due to IQR dependence on sound level. We thus ran a separate analysis of BF variability in L2/3 of *Thy1*-GCaMP6s mice in response to tones at 5 different sound levels (40-80 dB SPL in 10 dB increments; **Fig. 4.6d**). We found that BF variability increases as a function of stimulus intensity, thus the decreased response thresholds in DE mice could not explain our findings that DE reduces the heterogeneity of local frequency tuning, which might instead depend on the potentiation of thalamic inputs to L4, and refinement of ascending L4-L2/3 projections.

To identify if A1 contains different organizational features across its tonotopic axis, we examined if cells within different tonotopic regions (as identified by the mean BF of the local <100 μm region; **Fig. 4.7a**), or cells with different BFs (**Fig. 4.7b**), show differential changes in local tuning variability. To investigate this, local $IQR_{BF}$ was first separated into three groups based on the average frequency selectivity (mean BF) within a 100 μm radius – low (4-8 kHz), middle (8-16 kHz), and high (16+ kHz; **Fig. 4.7a,b**). Few neurons were imaged in fields having a high average BF, which is likely due to the placement of our virus injections. In L4, we find that DE decreases the spatial BF variability in both low- and mid-frequency areas (**Fig. 4.7a**), but not in frequency areas over 16 kHz (**Fig. 4.7a**). In L2/3, we find no changes in low frequency areas due to DE, but a decrease in BF variability in mid-frequency

111

**a** $IQR_{BF}$ by frequency area

Layer 2/3 — % cells — 4-8 kHz / 8-16 kHz / 16-64 kHz (octaves 0 to 3)

Layer 4 — % cells — 4-8 kHz / 8-16 kHz / 16-64 kHz (octaves 0 to 3)

**b** $IQR_{BF}$ by BF of Cells

Layer 2/3 — % cells — 4-8 kHz / 8-16 kHz / 16-64 kHz (octaves 0 to 3)

Layer 4 — % cells — 4-8 kHz / 8-16 kHz / 16-64 kHz (octaves 0 to 3)
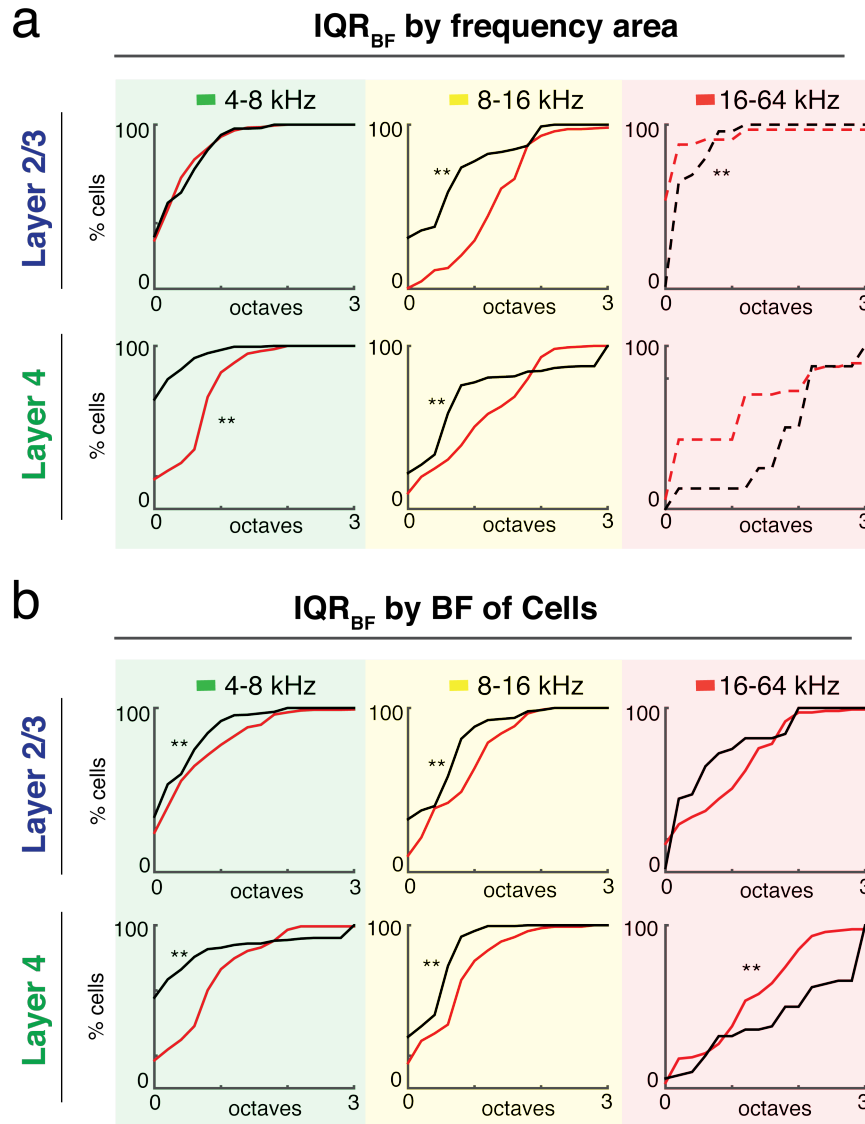
**Figure 4.7. DE effects in L2/3 are largest in mid-frequency regions.** (**a-b**) To isolate changes in BF variability across the frequency axis we measured $IQR_{BF100}$ based on either local average BF (mean BF within <100 μm region) (**a**) or individual cell BF (**b**), dividing into three frequency groups (low: 4-8 kHz, middle: 8-16 kHz, and high: 16+ kHz). (*a*) In L4, DE decreased the spatial BF variability in both low frequency areas (CTL L4 = 0.77 ± 0.59, n=252; DE = 0.00 ± 0.25, n= 201, p < $10^{-33}$) and middle frequency areas (CTL L4 = 1.063 ± 1.19, n=218; DE = 0.512 ± 0.64 n= 273, p < $10^{-6}$), with no change *(continued...)*

112

*(Fig. 4.7 continued…)* in high-frequency areas (CTL L4 = 1.19 ± 2, n=47; DE = 2.00 ± 0.5, n= 8, p= 0.093; dashed lines indicate fewer than 50 cells sampled). In L2/3, no change was observed in low-frequency areas after DE (CTL L2/3 = 0.320 ± 0.58, n=396; DE = 0.256 ± 0.77, n= 336, p= 0.86). BF variability in mid-frequency areas decreased after DE (CTL L2/3 = 1.50 ± 0.75, n=221; DE = 0.512 ± 1.02, n= 180, p < $10^{-19}$), while BF variability increased in L2/3 high-frequency areas (CTL = 0.063 ± 0.25, n= 33; DE = 0.256 ± 0.33, n= 49; p < $10^{-5}$). (**b**) For cells tuned to middle frequencies (8-16 kHz) we observed the same decrease in frequency heterogeneity evident in middle-frequency tonotopic areas for both L2/3 (CTL = 0.98 ± 0.87, n=90; DE 0.51 ± 0.77, n=149; p < $10^{-3}$) and L4 (CTL = 0.77 ± 0.77, n=110; DE = 0.512 ± 0.67, n=200; p < $10^{-7}$). L2/3 cells tuned to low frequencies had decreased frequency heterogeneity (CTL = 0.50 ± 0.87, n=450; DE = 0.26 ± 0.75, n=340; p < $10^{-4}$), with no change in high-frequency areas. Cells tuned to high frequencies in L4 had showed more tuning variability after DE (CTL = 1.25 ± 1.20, n=121; DE = 2.00 ± 2.50, n=50; p= 0.035).

areas (**Fig. 4.7a**). In contrast, in high-frequency areas of the tonotopic map, DE resulted in an increase in BF heterogeneity in L2/3, although like in the L4 results, we imaged few cells in these higher frequency-tuned areas.

Individual neuronal BF's can vary considerably from the tuning preference of the tonotopic region they reside in. Therefore, we also split neurons into three groups based on the individual cell frequency preference (**Fig. 4.7b**). For cells tuned to middle frequencies (8-16 kHz) we observed the same decrease in BF heterogeneity evident in middle-frequency tonotopic areas for both L2/3 and L4 (**Fig. 4.7b**). L2/3 cells tuned to low frequencies had decreased BF heterogeneity even though we saw

no changes in low-frequency areas, which suggests that cells that are tuned to low frequencies but reside in middle and high frequency areas could account for these changes. For cells tuned to higher frequencies, we observed no change in BF heterogeneity in L2/3 following DE and an increase in BF variability in L4. Together, our analysis shows that different areas along the A1 frequency axis are preferentially affected by DE, and that the effects of DE are laminar-specific. In particular, while changes in L4 are present in both low- and mid-frequency areas, changes in L2/3 are present only in the mid-frequency region of L2/3 but encompass neurons of all BFs.

*Dark-exposure alters correlated activity in L2/3 and L4*

To further understand how auditory information is represented in neuronal networks within L2/3 and L4, we calculated neuronal pairwise signal correlations (SC), which reflect stimulus-driven correlated activity, and noise correlations (NC), which represent stimulus-independent, trial-to-trial covariance (**Fig. 4.8**). Since signal correlations can be strongly biased by noise correlations, we corrected for this by subtracting NC from SC (Rothschild et al., 2010; Winkowski and Kanold, 2013). It has previously been demonstrated that measuring correlated activity in L4 reveals significant signal correlations between pairs of neurons owing to the predominance of stimulus-related input to these neurons from feed-forward thalamic projections (Winkowski and Kanold, 2013). We thus examined if DE alters the level of correlated activity between neurons in thalamorecipient L4. DE resulted in an increase in SC and NC between simultaneously imaged L4 cells (**Fig. 4.8b**). As such, neighboring
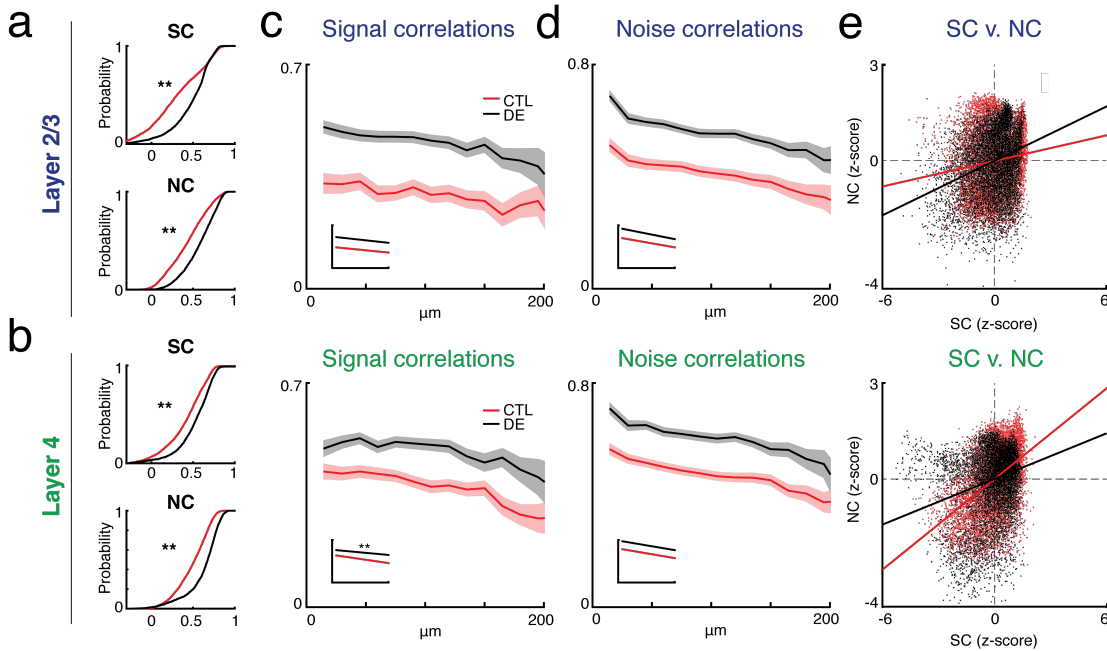
**Figure 4.8. Dark-exposure increases pairwise correlated activity between neurons in L2/3 and L4.** (**a**), In L2/3, DE increases SC (CTL median ± iqr = 0.31 ± 0.52; DE= 0.53 ± 0.29; Wilcoxon rank-sum test, $p < 10^{-85}$) and NC (CTL= 0.45 ± 0.37; DE= 0.60 ± 0.30; $p < 10^{-13}$) between cells within 50-100 μm. (**b**), Similarly in L4, DE increases SC (CTL= 0.45 ± 0.33; DE= 0.56 ± 0.27; $p < 10^{-70}$) and NC (CTL= 0.52 ± 0.29; DE= 0.68 ± 0.22; $p < 10^{-167}$) between simultaneously imaged cells. (**c-d**), Signal and noise correlations are plotted as a function of spatial distance between cell pairs. Insets show best linear fit. In control mice, SC decline with distance ($slope_{L2/3}$ = -0.00046, $R^2$ = 0.0043, $p < 10^{-8}$; $slope_{L4}$ = -0.00068, $R^2$ = 0.016, $p < 10^{-30}$) and NC decline with distance ($slope_{L2/3}$ = -0.00081, $R^2$ = 0.024, $p < 10^{-43}$; $slope_{L4}$ = -0.00080, $R^2$ = 0.034, $p < 10^{-16}$). Likewise after DE, SC decrease with distance ($slope_{L2/3}$ = -0.00050, $R^2$ = 0.0085, $p<10^{-8}$; $slope_{L4}$ = -0.00043, $R^2$ = 0.0059, $p<10^{-11}$) and NC decrease with distance ($slope_{L2/3}$ = -0.00092, $R^2$ = 0.042, $p<10^{-78}$; $slope_{L4}$ = -0.00079, $R^2$ = 0.028, $p<10^{-54}$). DE decreases the *(continued...)*

(*Fig. 4.8 continued...*) distance dependency of pairwise signal correlations in L4 compared to control (ANOCOVA p = 0.0026) but does not change slope of NC by distance in L4 (p = 0.94), or distance dependency in L2/3 (SC p = 0.68; NC p = 0.16). *E*, Scatter plot showing linear dependency of noise and signal correlations for individual cell pairs. Groups were normalized for comparison by computing z scores, and lines indicate the best linear fit (CTL $slope_{L2/3}$ = 0.13, $R^2$ = 0.012, p < $10^{-32}$; CTL $slope_{L4}$ = 0.47, $R^2$ = 0.224, p = 0; DE $slope_{L2/3}$ = 0.28, $R^2$ = 0.080, p < $10^{-152}$; DE $slope_{L4}$ = 0.24, $R^2$ = 0.057, p < $10^{-109}$). DE increased the correlation between SC and NC in L2/3 (p = 0, ANOCOVA) and decreased the correlation in L4 (p = 0, ANOCOVA).

A1 neurons after a period of visual deprivation are more likely to have similar activity during a stimulus (SC) and independent of stimulus presence (NC). In L2/3, which integrates tonotopically-organized ascending input from L4 as well as diverse cross-columnar and cross-hemispheric intracortical inputs (Schreiner and Winer, 2007; Atencio et al., 2009; Atencio and Schreiner, 2010; Chen et al., 2011; Guo et al., 2012a), DE also increased SC and NC (**Fig. 4.8a**). Our reported median SC values are similar to results previously reported ($SC_{L2/3}$ = 0.25, $SC_{L4}$ = 0.49 (Winkowski and Kanold, 2013)), but our observed noise correlation values are greater than found in previous studies and also opposite in their relationship to SC values ($NC_{L2/3}$ = 0.22, $NC_{L4}$ = 0.20 (Winkowski and Kanold, 2013)). One possible explanation for this is the longer dwell time per pixel we used in our imaging experiments, which could increase temporal integration and generate higher noise correlation values. Another alternative is that the differences in stimulus duration could drive different circuits.

The longer duration tones used previously (1000 ms, (Winkowski and Kanold, 2013)) might drive stimulus-dependent feedforward inputs more strongly, whereas the 400 ms duration tones used in the present study could drive more local responses such as recurrent inputs to amplify the signal.

Pairwise correlated activity is thought to reflect underlying neuronal connectivity and can thus depend on the spatial relationship between neurons (Levy and Reyes, 2012; Ko et al., 2013; Winkowski and Kanold, 2013; Watkins et al., 2014). We thus tested the spatial extent of correlated activity by plotting correlations as a function of distance between cell pairs (**Fig. 4.8c,d**). In control mice, we observe a steady decline in signal correlations with distance in both L2/3 and L4 (**Fig. 4.8c**). Noise correlations were more steeply affected than signal correlations by increasing distance (ANOCOVA L2/3 p=0, L4 p=0; **Fig. 4.8d**), which suggests that the probability of intralaminar connectivity between two neurons is more dependent on increasing spatial distances than the probability of receiving similar feedforward input and is consistent with previous findings (Winkowski and Kanold, 2013). After dark exposure, SC and NC both significantly decrease with distance in L2/3 and L4, but the distance dependency of correlations only changes for SC in L4 compared to controls. This decrease suggests that after DE, neurons in L4 are more likely to receive similar inputs with increasing spatial distances. This is consistent with the observed potentiation of thalamocortical input to L4 and might also suggest that while DE induces spatial refinement of intra-laminar inputs within L2/3 (Meng et al., 2015), ascending input to L4 becomes less refined.

In both L2/3 and L4 of control mice, signal and noise correlations were positively correlated (**Fig. 4.8e**), which suggests that neurons receiving similar feedforward input (SC) were more likely to share intralaminar connectivity (NC) and thus were more likely to share similar tuning preference (Ko et al., 2013; Cossell et al., 2015). DE increased the correlation between SC and NC in L2/3, and decreased the correlation in L4 (**Fig. 4.8e**), which suggests that feedforward and intralaminar inputs are differentially distributed following dark exposure. Combined with our finding that L4 receives more similar input along longer distances after DE, a decrease in SC versus NC correlation could support a conclusion that while DE causes thalamocortical input to L4 to be more widespread, this does not induce more local intralaminar connectivity, and thus SC and NC become more decorrelated. On the other hand in L2/3, DE might promote stronger local connectivity between neurons receiving the same feedforward input, which could also help auditory neurons in L2/3 to respond to lower sound thresholds.

To test whether DE pairwise correlations results are affected by increasing differences in tuning preference, we plotted correlations as a function of the BF ratio between two neurons in octaves (**Fig. 4.9a,b**). We find that across all groups, pairwise correlations decrease as frequency preference between a pair of neurons becomes more dissimilar. In L4, dark exposure decreases the relationship between correlations and BF ratio (**Fig. 4.9b, *right column***). This suggests that neurons have an increased chance of sharing connectivity with neurons that do not share similar frequency preference and further supports our conclusions that inputs to L4 neurons become less

118
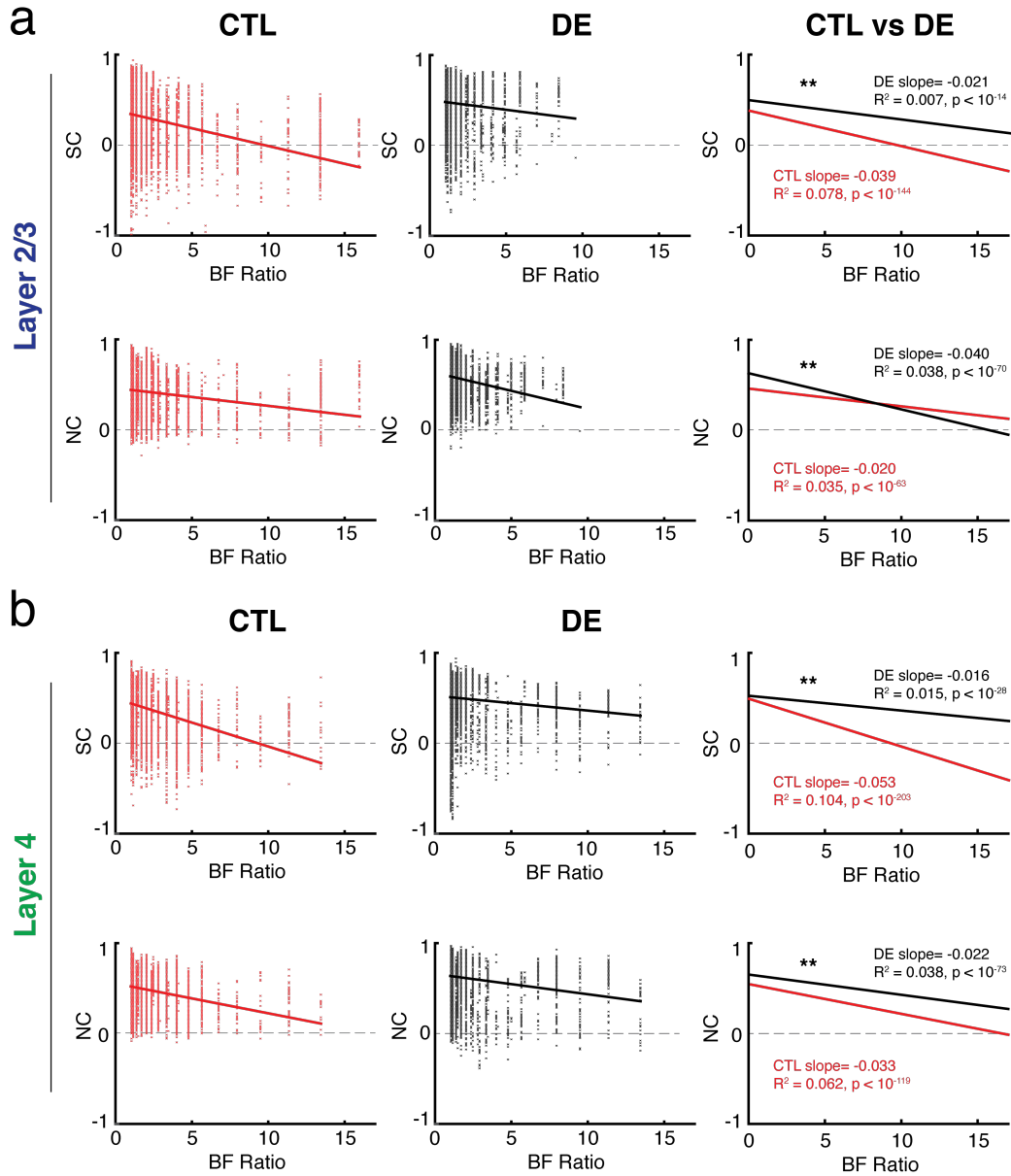
**Figure 4.9. Pairwise correlations decrease as frequency preference between neuronal pairs becomes more dissimilar.** (**a**) A scatter of correlations as a function of BF ratio (octaves) between two L2/3 neurons are plotted with a best linear fit overlaid, showing that neurons with similar tuning are more likely to have higher SC and NC. In right column, best fit slopes for CTL and DE mice are compared (p values indicate significance that individual slopes are non-zero; ** represent ANOCOVA test p<0.001 comparison between both slopes). (**b**) Correlations as a function of BF ratio are plotted for L4.

refined with DE. In contrast in L2/3, DE increases the relationship between NC and BF ratio, suggesting that intralaminar connectivity between local neurons becomes more dependent on shared tuning preference (**Fig. 4.9a,** *right column*).


## Discussion


Using *in vivo* two-photon $Ca^{2+}$-imaging we show that brief (7-10 day) periods of visual deprivation in adult mice result in robust cross-modal changes in population activity and functional organization of thalamorecipient and supragranular layers of A1. On a cellular level, we observed an increase in response reliability in L2/3 cells, but opposite effects in the level of spontaneous activity in L2/3 and L4. On the network level, we observed a decrease in spatial BF heterogeneity in both L2/3 and L4, in particular in middle frequency areas (8-16 kHz), and an increase in pairwise correlated activity.

Studies manipulating the level of intracortical inhibition have shown that feedforward projections determine initial characteristic frequency (CF) tuning preference of neurons and maintain tonotopy on a coarse scale (Kaur et al., 2004), whereas lateral intracortical inputs can either broaden spectral tuning via excitatory synapses (Kaur et al., 2004; Happel et al., 2010), or sharpen receptive fields via inhibitory inputs. Thus, the observed decrease in spatial BF heterogeneity is consistent with a potentiation of thalamocortical synapses in L4 neurons, and a refinement of inter-laminar ascending excitatory and inhibitory input from L4 to L2/3 (Petrus et al., 2014; Meng et al., 2015). The reduced BF variability we observed with

DE was most pronounced for imaging fields that were in the mid-frequency region of the tonotopic map (8-16 kHz). This frequency spectrum encompasses the low-frequency harmonics emitted by adult mice (Portfors, 2007), and represents the average peak frequency of emitted vocalizations recorded previously for normal reared and dark exposed mice (~10 kHz) (Petrus et al., 2014). Since the effects of DE on thalamocortical projections depend on hearing (Petrus et al., 2014) and since specific changes in frequency organization occur in frequency areas covering the vocal spectrum of mice, this suggests that the processing of communication-related stimuli in L2/3 might be enhanced after DE. Such a change would be consistent with the hypothesis that L2/3 networks might process complex behaviorally-relevant auditory stimuli (Nelken, 2004; Kanold et al., 2014).

In addition to our finding that DE-induced modulation of frequency heterogeneity is specific to tonotopic region, we found further differences within cells whose BFs did not match the tuning preference of the tonotopic region in which they reside. Specifically, L2/3 cells tuned to lower frequencies show decreased $IQR_{BF}$, but only those located in mid-frequency areas. While the origin of these differences is unclear, prior studies from multiple sensory cortices have shown different sub-circuits within L2/3 (Atzori et al., 2001; Yoshimura et al., 2005; Jia et al., 2010; Oviedo et al., 2010; Ko et al., 2011; Feldmeyer, 2012; Ko et al., 2013; Cossell et al., 2015). Thus, since L2/3 shows a higher degree of frequency heterogeneity than L4 (Winkowski and Kanold, 2013), we speculate that L2/3 cells that are tuned consistent with their position in the tonotopic map have a different circuit identity than those that are not.

Different spines on individual L2/3 neurons can have a wide range of frequency selectivity (Chen et al., 2011). Thus to alter the tuning of an individual cell, specific inputs can be rapidly strengthened or weakened, and A1 neurons have been shown to rapidly and transiently change their tuning when animals are attending to auditory tasks (Fritz et al., 2003). These circuit changes are likely due to the engagement of top-down circuits such as those originating in the prefrontal cortex (Fritz et al., 2010), whose activation can drive rapid A1 plasticity (Winkowski et al., 2013). This suggests that the specific changes observed here might be due to attention-based changes to behavioral relevant stimuli. Specifically, the increased noise correlations in L2/3 and L4 after DE suggest an increase in intralaminar connectivity within these layers, which is in contrast to the previously reported circuitry refinement within L2/3 (Meng et al., 2015).

Laser-scanning photostimulation to spatially map inter- and intra-laminar connectivity is limited by the direct responses of activated proximal dendrites (Meng et al., 2015), and thus this spatial resolution prevents assessment of connectivity at distances within 100 microns. As such, it is possible that while DE reduces connectivity at distances greater than 100 microns, it might also strongly increase local connections at shorter distances. Combined with previous studies, our results suggest that while frequency selectivity at CF increases (as measured 10 dB above threshold, or at the peak of the FRA; (Petrus et al., 2014)) due to potentiation of thalamocortical to L4 input and refinement of L4-L2/3 inputs, connectivity within shorter distances is differentially affected and is represented in our data as decreased frequency selectivity at 20 dB above threshold. We predict that local lateral

connections increase within spared sensory cortices following cross-modal deprivation, possibly as a homeostatic plasticity response to the decrease in long-range (>100 μm) synaptic input. Expansion of lateral connections via intracortical sprouting has been shown to occur within the somatosensory cortex following peripheral forelimb injury (Florence et al., 1998). This local growth could provide a substrate for synaptic sampling of heterogeneous inputs and can generate more complex receptive fields by widening spectral integration (Cossell et al., 2015) without affecting BF, but would only be supra-threshold in response to higher intensity stimuli. Lateral synaptic connectivity would not necessarily effect tuning at the peak of a neuron's FRA, which could depend more on the potentiation and refinement of tonotopically organized ascending input (Kaur et al., 2004).

In primary visual cortex (V1), L2/3 neurons are preferentially and reciprocally connected to neurons that share similar feature preference, while neurons with differential tuning are unlikely to share functional connectivity and are weak when they exist (Ko et al., 2013; Cossell et al., 2015). In this sensory system, weak synaptic connectivity contributes to broad sub-threshold tuning (Ko et al., 2011), but could potentially facilitate network restructuring when new environmental stimuli become behaviorally relevant (Cossell et al., 2015). Here we show that correlated activity between pairs of neurons, as a measure of connectivity, decreases as a function of the difference in their tuning similarity (**Fig. 4.9**). In L2/3 NCs, the slope of this relationship is greater after DE, and neurons tuned to different frequencies are less likely to have correlated activity. Furthermore, the correlation between SCs and NCs increases in L2/3 after DE, suggesting that neurons that share feedforward input are

123

more likely to share local synaptic connectivity. Since A1 L2/3 neurons also receive broad subthreshold inputs (Chen et al., 2011), the compensatory reorganization of A1 circuitry after DE (Goel et al., 2006; Petrus et al., 2014; Meng et al., 2015; Petrus et al., 2015) therefore involves a specific change in local synaptic connections to increase the local peak tuning similarity of neurons while broadening receptive fields at higher thresholds. The DE-induced increased local synaptic connectivity might engage synaptic remodeling mechanisms via spike-timing-dependent plasticity (STDP), which could promote strengthening of the weak, new connections if the external environment post deprivation, and therefore the relevance of auditory stimuli, is altered. However, strongest ascending connections are still preserved and prevail following a return to normal sensory conditions (light exposure; Petrus et al., 2014).

Our results suggest that cross-modal plasticity may underlie the improvements in auditory perception in humans following vision loss (Lessard et al., 1998; Roder et al., 1999; Gougoux et al., 2004; Voss et al., 2004). These results add to the mounting evidence that experience-dependent plasticity is not restricted to early developmental windows, and that cross-modal sensory experience has the power alter network circuitry and population dynamics even into adulthood. Thus it might be possible to harness this environmental manipulation in order to restore function lost as a result of impaired developmental experiences.

Methodological concerns: Overall we observe lower reliability of responses, higher noise correlations, and somewhat larger IQR$_{BF}$ than prior studies (Winkowski and

Kanold, 2013). This could be due to differences in $Ca^{2+}$ indicator (Fluo-4 vs. GCaMP6) and sound durations (1s vs. 400 ms) used. Different sound durations might drive different cortical circuits – a longer sound stimulus might recruit more feedforward-driven responses whereas a shorter duration stimulus might drive intralaminar recurrent amplification of the signal. Furthermore, previous studies that did not correct for neuropil contamination might have observed BF variability biased to lower values. Compared to the results obtained in Thy1-GCaMP6s imaged mice reported in Chapter 3, we find lower $IQR_{BF}$ values in AAV-GCaMP6 mice and increased correlated activity. Additionally, the greater BF spatial variability in L2/3 compared to L4 reported in previous studies and likewise observed in Thy1-GCaMP6s mice was not found in AAV-GCaMP6s transfected mice. It is possible that the AAV-GCaMP6s viral construct causes neurotoxic changes to neuronal circuitry and response dynamics and affects our reported data. As such, subsequent experiments will be conducted in dark-exposed Thy1-GCaMP6s mice in order to resolve these issues.

# Chapter 5: Discussion

Cortical microcircuits exhibit robust experience-dependent plasticity during critical periods of early postnatal development, and rely on acoustic experience throughout life to both assemble proper connectivity and reorganize in response to the sensory environment. In the preceding chapters of this dissertation, I have described the stages of development of mesoscale functional organization in the auditory cortex beginning with hearing onset, how this organization differs in a model of uni-modal sensory deprivation during early postnatal life, as well as how this system reorganizes in the adult in response to cross-modal sensory deprivation. I have tested the hypothesis that experience-dependent mesoscale changes are layer-specific, and found that local organization of frequency preference and pairwise correlated activity between nearby neurons are dramatically and differentially affected by sensory experience at different ages and across laminae. These findings bridge the gap between existing research on experience-dependent single-scale receptive field changes and macroscale connectivity to explain how local neuronal population activity transforms to process incoming acoustic stimuli.

## Development of sensory cortical circuitry

Prior to sensory experience, molecular gradients guide growing axons into the cortex and spontaneous waves of activity arrange rudimentary topography by evoking correlated activity between neurons and strengthening the connectivity between

coactive cells (Feller et al., 1996; Katz and Shatz, 1996; Butts, 2002; Adelsberger et al., 2005; Tritsch et al., 2007; Wang and Bergles, 2015). In the visual system, blockade of prenatal cortical activity by tetrodotoxin infusion prevented the segregation of retinogeniculate afferents into distinct layers within the LGN (Shatz and Stryker, 1988; Penn et al., 1998), indicating that these spontaneous activity patterns are necessary for preliminary circuit development. Early in development, feedforward axon collaterals arborize past columnar borders (Bender et al., 2003; Feldmeyer, 2012) and neighboring neurons are connected via gap junctions (Yao et al., 2016) without preferential connectivity (Ko et al., 2013). The intermixing of feedforward axonal fibers and diffuse non-specific intracortical connectivity likely combine to generate the detectable but frequency-overlapping tonotopy at the earliest stages of auditory development (Zhang et al., 2001, 2002; Chang and Merzenich, 2003; de Villers-Sidani et al., 2007). The presence of selective but unreliable responses I observed in L2/3 suggests feedforward input from L4 is coarsely established before onset of sensory experience, while the high noise correlations are consistent with exuberant non-specific horizontal connections between nearby neurons that have not yet had a chance to be functionally refined by acoustic input (Ko et al., 2013). Furthermore, both wide-field and two-photon imaging results confirm a heightened level of spontaneous activity at this age.

At the onset of auditory experiences with ear opening around P12, pairwise signal correlations increase in L4 as thalamocortical connections are strengthened and refined by external auditory cues (Barkat et al., 2011), and noise correlations decrease in both L4 and L2/3 consistent with intralaminar reorganization and a shift from

electrical to chemical synapses (Ko et al., 2013). The critical period (CP) is an experientially-driven epoch of circuit refinement during which the developing cortex increasingly relies on sensory experience to drive the maturation of synaptic connections into robust, precisely organized circuits and is defined based on altering the period of sensory deprivation (Insanally et al., 2009; Barkat et al., 2011; Caras and Sanes, 2015; Mowery et al., 2015). CP windows vary between different sensory cortices but also for different features of a sensory stimulus (i.e. spectral tuning vs temporal tuning). In this study, I delineate the peak of the critical period in C57BL/6 mice for spectral tuning from P15 to P16, during which neighboring neurons have very similar BF preference, respond to the most frequencies, and show high correlated activity, indicating both stronger shared inputs and local interconnectivity.

Hebbian plasticity mechanisms offer a compelling explanation for the observed activity-dependent development of connectivity, and specifically spike-timing dependent (STDP) learning rules that require a causal temporal window between pre- and post-synaptic spikes that informs synapses to strengthen or weaken (Butts and Kanold, 2010). Thalamic afferents initially target subplate neurons (Zhao et al., 2009; Kanold and Luhmann, 2010), which send strong excitatory projections to L4 and act as a teacher circuit to establish proper feedforward connectivity on the fast timescales necessary for STDP (Butts and Kanold, 2010). The critical period then involves thalamocortical afferent synapse maturation in L4 and the gradual disappearance of the transient subplate layer (Zhao et al., 2009; Kanold and Luhmann, 2010; Barkat et al., 2011). The serial relay of L4-L2/3 sensory input next drives the reorganization of L2/3 synaptic weights by strengthening the connectivity

between neurons with correlated activity responding to similar stimulus features, and eliminating synapses between uncorrelated neurons (Foeller and Feldman, 2004; Ko et al., 2013). In the somatosensory cortex, this reorganization has been shown to first drive potentiation of L4-L2/3 inputs, followed by strengthening of local cortical connectivity and an increase in synapse density (van der Bourg et al., 2016). This process forms the recurrent subnetworks characteristic of adult supragranular layers, which can amplify feedfoward signals (Douglas et al., 1995; Douglas and Martin, 2007; Happel et al., 2010) and enhance integration of diverse synaptic input to broaden the receptive fields evident in this layer (Oswald and Reyes, 2008; Atencio et al., 2009; Atencio and Schreiner, 2010).

In adult mice, I observed a consistent heterogeneous frequency preference distribution as reported previously (Bandyopadhyay et al., 2010; Rothschild et al., 2013; Winkowski and Kanold, 2013), with more local variability in L2/3 than in L4. This BF heterogeneity is present at the earliest ages imaged (P9-11), at which point it likely just represents the immature circuitry and weak synaptic strength. Notably, at the peak of the CP, spatial representation of frequency preference is most homogeneous, after which a heterogeneous organization manifests as hearing experience continues to sculpt connectivity.


**Sensory deprivation prevents refinement of cortical circuitry**

Early experience-independent processes are sufficient to segregate eye-specific thalamocortical afferents in L4 of V1 (Wiesel and Hubel, 1963) and establish thalamocortical topography in L4 of A1 prior to sensory experience (Barkat et al.,

2011). Whereas initial topography is formed without external input, sensory-evoked activity is required for refinement of cortical circuitry, which regulates fine-scale synapse reorganization and functional mapping but not large-scale anatomical remodeling of axons or dendritic branches (Fox, 1992; Feldman et al., 1999; Bender et al., 2003; Barkat et al., 2011).

Raising animals in the presence of continuous white noise masks exposure to the spectrotemporal cues required for proper A1 circuitry refinement, and indefinitely prolongs CP closure (Chang and Merzenich, 2003; de Villers-Sidani et al., 2008). The noise-rearing paradigm I use here is in contrast to monocular deprivation and whisker trimming studies, which induce competitive plasticity mechanisms that promote the potentiation of spared synapses and the weakening of deprived inputs. Furthermore, it differs from pulsed-noise exposure paradigms, which provide sufficient temporal cues to synchronize neuronal activity and terminate the CP while receptive fields and cortical organization are still immature (Zhang et al., 2002). Rather, like binocular deprivation studies (Wiesel and Hubel, 1965; Kirkwood et al., 1995), and full-whisker trimming studies (Shepherd et al., 2003), continuous noise rearing fully deprives mice of structural significance to the acoustics of their environment and drives uncorrelated activity within neuronal populations. This manipulation did not result in an overall change in auditory cortical area, consistent with full-field visual and somatosensory studies where deprivation did not prevent ocular dominance segregation or barrel formation (Wiesel and Hubel, 1965; Bender et al., 2003; Shepherd et al., 2003), but is in contrast to electrophysiological mapping of ACX noise-reared rats, which revealed expansion of tone-responsive cortical area relative

to normally-reared adults (Chang and Merzenich, 2003). Similarly to the disrupted receptive fields of cells following binocular deprivation (Wiesel and Hubel, 1963), whisker trimming (Shepherd et al., 2003), and noise-rearing (Zhang et al., 2002; Chang and Merzenich, 2003), here I find that noise-reared mice have cells that respond to tones with weakened amplitudes and with decreased frequency selectivity, and that these changes occur in both L4 and L2/3.

In contrast to the single cell developmental consistency between laminae, noise-rearing affects the mesoscale circuit organization in L2/3 and L4 in opposite ways, which suggests that sensory deprivation induces changes in these two hierarchical auditory processing layers that are reflective of distinct laminar-specific developmental stages. The increased pairwise correlated activity and response homogeneity observed in L4 of P20 noise-reared mice most resembles population responses at the peak of the CP at P15-16. This suggests that the immature feedforward thalamocortical connectivity established via sensory-independent mechanisms is retained but is prevented from undergoing sensory-driven synaptic refinement. Since feedforward projections are considered to determine initial frequency preference of neurons (Kaur et al., 2004), local homogeneity in L4 persists as a reflection of dominant thalamic projections guided before sensory input. In contrast to the developmental delays observed in L4, the increased local BF heterogeneity and decreased correlations within L2/3 are most similar to developmental stages preceding the onset of the critical period (~P12-14). This suggests that maturation of population activity in L2/3 is even more delayed, and that sensory-evoked activity might have a greater effect in L2/3 than L4 (Fox, 1992;

131

Shepherd et al., 2003; Foeller and Feldman, 2004). Some studies have even shown that deprivation induces L2/3 changes while preserving normal L4 organization (Trachtenberg et al., 2000). I propose that the circuitry changes underlying the laminar differences in population activity after noise rearing can be attributed to the serial progression of information in the canonical cortical circuit. L2/3 frequency organization is partly determined by L4-L2/3 ascending connectivity, which, like thalamocortical feedforward input, is largely established prior to sensory experience. However, patterned sensory input is required to drive the reorganization of recurrent synaptic inputs within L2/3 (Douglas et al., 1995; Douglas and Martin, 2007; Ko et al., 2013), without which the immature feedforward L4-L2/3 projections drive uncorrelated pre- and post-synaptic spikes between L4-L2/3 and L2/3-L2/3 and induce synaptic depression via STDP learning rules (Feldman, 2000; Bender et al., 2003; Celikel et al., 2004; Feldman, 2009). Furthermore, this data shows that spatial heterogeneity of frequency tuning is a developing feature of A1 that requires exposure to salient auditory cues.

## Cross-modal deprivation induces compensatory plasticity

In Chapter 4, I reveal robust changes in population activity and functional organization in L4 and L2/3 of A1 after brief visual deprivation. Previous studies found that dark exposure (DE) in adult mice had the power to change single-cell receptive fields and large-scale circuitry that is consistent with improved reliability of sound-evoked responses and increased frequency discrimination (Petrus et al., 2014; Meng et al., 2015). In L4, DE induced potentiation of thalamic input (Petrus et al.,

2014), strengthened intracortical excitatory synapses (Petrus et al., 2015), and increased spontaneous firing rates (Petrus et al., 2014). DE-induced L4 changes are consistent with my findings that signal and noise correlations increase as a function of stronger feedforward and lateral connectivity, and I likewise observed an increase in spontaneous fluorescent activity in this layer. The amplification of both incoming thalamic input and intracortical excitatory circuitry, which together can reinforce representation of thalamic information and thus CF tuning (Kaur et al., 2004; Liu et al., 2007; Happel et al., 2010; Li et al., 2013a), combine to augment neuronal receptive fields in favor of a more homogeneous BF representation. However, recurrent connections serve not just to linearly amplify feedforward thalamic signal but also integrate additional synaptic inputs and can broaden spectral tuning (Kaur et al., 2004; Li et al., 2013b). Thus, while I find local spatial representation of BF become more homogeneous with DE, the receptive fields of individual neurons become more complex and can respond to more frequencies at higher thresholds than naïve mice.

Feedforward input from L4 to L2/3 in A1 is both potentiated (Petrus et al., 2015) and refined (Meng et al., 2015) with brief DE. In contrast, DE decreases lateral L2/3-L2/3 synaptic amplitude (Goel et al., 2006; Petrus et al., 2015), refines intracortical connections (Meng et al., 2015), and decreases spontaneous fluorescent activity. Although the level of intracortical activity in L2/3 and L4 differs in response to visual deprivation, signal and noise correlated activity uniformly increase within both layers, and local spatial BF tuning becomes more homogeneous. How do we resolve these differences? Increased signal correlations in L2/3 likely reflect the

133

potentiated ascending input from L4 similarly to the changes present in L4, which also drive more similar BF tuning, but it puzzling that correlated intracortical activity increases despite decreased mEPSC amplitude of lateral connections and refinement of connectivity. Previous studies suggested that these changes are homeostatic in nature, and that DE strengthens feedforward L4-L2/3 synapses at the expense of lateral L2/3-L2/3 inputs. Here, I propose that these differences can be attributed to the spatial limitations of laser-scanning photostimulation, which prevents assessment of connectivity within 100 microns due to direct dendritic photoactivation (Watkins et al., 2014; Meng et al., 2015). Thus, in addition to lateral refinement at distances greater than 100 microns, DE might induce a redistribution of distal synapses in favor of proximal ones by either strengthening existing connections at shorter distances or encouraging sprouting of new connections. This would allow L2/3 neurons to integrate across more local synapses, each of which independently have a wide range of frequency selectivity (Chen et al., 2011), and explain the broadened tuning curves and increased noise correlations evident in L2/3, without preventing the effect of L4 input on BF tuning. Interestingly, stress has been shown to reorganize entire dendritic arbors of L2/3 neurons in prefrontal cortex of rats – distal dendritic mass decreases, with a compensatory elaboration of proximal dendrites (Wellman, 2001), and thus the changes observed in visual deprivation studies might reflect a combination of synaptic and dendritic reorganization.

## Receptive field structure as a substrate for plasticity

In the preceding developmental studies, I observed a decrease in frequency selectivity from P9 to P15, both when measured at the peak of neuronal tuning curves (at 75% peak-amplitude threshold), and further away from BF (at 60% threshold). Broad peak bandwidth persisted into adulthood, but neurons after P15 became more frequency selective at the 60% threshold. The findings at 75% threshold are consistent with microelectrode studies showing that bandwidth increases with age (Eggermont, 1996; de Villers-Sidani et al., 2007; Insanally et al., 2009), and the sharpening of frequency selectivity at 60% threshold after P15 aligns with other studies (Zhang et al., 2001; Chang and Merzenich, 2003; Chang et al., 2005). Changes in response threshold were not observed in this study before P18, and in previous studies in rat from P14 to adult (Insanally et al., 2009) and thus neuronal sensitivity to sound level are not likely to account for these differences. Therefore, these two bandwidth measures seem to resolve the discrepancies between earlier findings by suggesting that bandwidth measured at different levels reflects changes to different aspects of neuronal receptive fields.

Similarly to the critical period of plasticity in development when auditory neurons receive the most diverse synaptic input and have the broadest receptive fields, dark-exposure also decreased frequency selectivity of L4 and L2/3 neurons in this study. This is in contrast to previous studies that reported sharper CF tuning at 10 dB above threshold (Petrus et al., 2014). However, it is worth noting that Petrus et al. also looked at bandwidth 40 dB above threshold and found a small but insignificant increased bandwidth after DE in L4 neurons. Given that I see a bandwidth increase at

135

~20-30 dB above threshold, this suggests that different parts of neuronal FRA's are differentially affected by DE and implies specific circuitry changes.

The broader bandwidth observed in normal-reared P15-16 mice, P20 noise-reared mice, and dark-exposed adult mice is likely a reflection of a redistribution of synaptic weights and dendritic arborization involving both feedforward and intracortical connectivity. At these analogous stages where neuronal tuning is broadest and noise correlations are high, neurons can respond to the most frequencies present in their environment and suggests that environmental changes during this epoch would have the largest effect.

A sharpening of frequency tuning in the auditory cortex is frequently credited with improving auditory performance by enhancing frequency discrimination ability (Fitzpatrick et al., 1997; Fritz et al., 2003; O'Connell et al., 2014; Petrus et al., 2014). In learning tasks requiring attention to a particular stimulus in A1 or V1, tuning curves exhibit an increased gain to the task-related stimulus and a concomitant suppression of responses to stimuli irrelevant to the task (Okamoto et al., 2007; Lee and Middlebrooks, 2011; O'Connell et al., 2014). In these instances, sharper tuning as a result of changes in feedforward connectivity can result in higher information transmission and facilitate tone detection and discrimination given that the high-slope regions of tuning curves become steeper (Series et al., 2004; Butts and Goldman, 2006). Narrow tuning is therefore optimal for encoding a single stimulus feature (such as frequency) (Series et al., 2004), but only applies if we continue to look at A1 as solely a frequency detector. Furthermore, very narrow tuning can actually impair performance (Eurich and Wilke, 2000) by resulting in a loss of information in the

population code (Series et al., 2004). Consequently, tuning sharpening in physiological networks might not necessarily reflect improved information processing by populations of neurons. Instead, broader tuning is argued to be more informative for multi-dimensional encoding of stimulus features (Pouget et al., 1999; Zhang and Sejnowski, 1999; Eurich and Wilke, 2000; Series et al., 2004), and the relationship between tuning width and coding efficacy depends on the complexity of the encoded stimulus (Zhang and Sejnowski, 1999).

Auditory cortex has been shown to contain multi-dimensional overlapping maps encoding frequency, bandwidth, intensity, and binaural integration (Polley et al., 2006). Given that A1 consists of multiple stimulus feature processing circuits (Polley et al., 2006), broader tuning, particularly in L2/3, might be more conducive to processing higher-order auditory information such as vocalizations (Nelken, 2004; Bao et al., 2013; Kanold et al., 2014). "Combination-sensitive" neurons have been recognized in A1 that produce strong nonlinear responses to combinations of stimulus features without showing sensitivity to simple tone pips (Sadagopan and Wang, 2009; Willmore and King, 2009; Bao et al., 2013). Vocalizations such as frequency-modulated sweeps require processing of temporal and frequency components and may require neurons with more complex spectrotemporal receptive fields (Linden et al., 2003; Trujillo et al., 2011). Diverse integration of lateral inputs, which manifests as broader tuning, could facilitate processing of these higher-order stimuli and permit dynamic synaptic reorganization to adapt to changing environmental and behavioral demands (Fritz et al., 2003; Polley et al., 2006). Periods of widened spectral integration such as at the peak of the CP and following DE might therefore be

advantageous for the brain by creating an over-connected network in which neurons have more access to heterogeneously-tuned synaptic input and can rapidly adjust their tuning in order to best process the auditory stimuli present in their environment (Kaur et al., 2004; Cossell et al., 2015; Maor et al., 2016).

The similarity between CP and DE states suggests that cross-modal plasticity in adults can reinitiate a window of heightened plasticity by creating a network environment in which neurons over-sample a variety of external auditory stimuli and are primed to accommodate changes in their sensory environment. It has been suggested that higher noise correlations resulting from increased synaptic connectivity represent a transient phase during cortical circuit reorganization, whose purpose is to stimulate network restructuring (Rothschild et al., 2013). Thus, the DE-induced plasticity, like CP plasticity, might be an intermediate stage in which increased local synaptic connectivity can engage synaptic remodeling mechanisms via spike-timing-dependent plasticity (STDP). STDP could promote strengthening and weakening of specific synapses without requiring long-distance rewiring and perhaps form new functional subcircuits that are more relevant to a changing environment. In noise-reared animals with prolonged CPs, A1 remains in an undifferentiated state until the system starts to receive coherent, temporal stimulus patterns to engage specific synapses. In each of these models, the state of high local connectivity could therefore provide an ideal substrate for diverse synaptic sampling and experience-dependent plasticity (Kaur et al., 2004). However, it is critical that with dark exposure the strongest ascending connections are still preserved and allow

the system to return to its previous state following a return to normal sensory conditions (light exposure; Petrus et al., 2014).

The idea that sensory deprivation reinitiates a period of enhanced experience-dependent plasticity has been proposed for visual cortex changes in response to dark exposure (He et al., 2006; Montey and Quinlan, 2011; Eaton et al., 2016). Eaton *et al.* propose a two-step sequence in which dark exposure first stimulates a period of synaptic plasticity, which is then immediately harnessed to promote recovery from amblyopia or monocular deprivation by instructive visual training (Eaton et al., 2016). In this model, brief dark exposure in the adult (or even long-term dark rearing from birth) engages a multitude of molecular factors and plasticity mechanisms to transiently drive the system into a more immature state (He et al., 2006). The visual cortex of animals dark reared from birth or briefly visually deprived in adulthood was found to have a decreased level of $GABA_A$ receptors, an increased ratio of GluR1 relative to GluR2 in AMPA receptors, and an increased ratio of the immature NR2b subunit of NMDA receptors relative to NR2a (Goel et al., 2006; He et al., 2006). This results in a decreased strength of GABAergic inhibition relative to excitation (Morales et al., 2002; He et al., 2006). Thus, visual deprivation shifts the E/I balance in favor of excitation characteristic of CP windows, and has further been shown to effect STDP by extend the temporal integration window permissive of plasticity (Guo et al., 2012b). However, a different effect was observed cross-modally with visual deprivation, namely, reduced AMPAR-mediated excitatory synaptic transmission between lateral L2/3 connections resulting from a decreased ratio of GluR1 (Goel et al., 2006), and a potentiation and refinement of inhibitory circuitry (Meng et al.,

2015; Petrus et al., 2015). This is suggested to be a homeostatic balancing effect resulting from increased activity in auditory areas compared to the deprived visual areas, or a specific decrease in intracortical connectivity in L2/3 in response to the stronger L4 inputs this layer receives. Nevertheless, the finding that dark rearing uni-modally prevents the enhancement of inhibition that is typically attributed to CP closure (Morales et al., 2002) while cross-modally increasing inhibition (Meng et al., 2015; Petrus et al., 2015) warrants an in-depth look at the role of inhibitory circuitry in development and with sensory deprivation.

## Role of Inhibitory circuits in plasticity

The excitation-inhibition (E/I) ratio is dynamically regulated throughout life to maintain a balanced state of cortical activity. Maturation of sensory cortices is characterized by a developmental decrease in the E/I ratio (Fagiolini and Hensch, 2000; Hensch, 2005; Zhang et al., 2011) due to a developmental increase in synaptically evoked IPSCs (Zhang et al., 2011). Given that $GABA_A$ receptor conductance is already hyperpolarizing by P8 in the somatosensory cortex, this is not a reflection of the switch from an early depolarizing effect of GABAergic transmission (Zhang et al., 2011). Rather, the increased inhibitory synaptic transmission is due to an increase in total number and magnitude of GABAergic responses (Kobayashi et al., 2008) that is both essential for experience-dependent plasticity (Hensch et al., 1998), *and* is regulated by sensory experience (Morales et al., 2002). Hensch *et al.* showed that blocking $GABA_A$-mediated transmission prevented sensory-dependent reorganization of circuitry following monocular

deprivation, which suggests that inhibitory transmission is required to drive reorganization of competing synaptic inputs (Hensch et al., 1998), perhaps by correlating spiking patterns (Long et al., 2005) and increasing the chance that spikes fall within the correct temporal integration windows for STDP. Furthermore, dark rearing animals from birth prevented a developmental increase in GABAergic input, and thus sensory experience might be required for inhibitory circuit maturation (Morales et al., 2002).

During normal cortical postnatal development, the refinement of inhibitory receptive fields and connectivity occurs after excitatory connectivity (Chang et al., 2005; Gandhi et al., 2008; Dorrn et al., 2010; Sanes and Kotak, 2011), and this transition might create the optimal E/I balance required for CP sensory plasticity. Similarly to the effect of dark rearing on preventing maturation of GABA transmission and prolonging the critical period for binocularity, my noise-rearing paradigm might also result in reduced inhibitory transmission and thus delay experience-dependent reorganization until the auditory pathway receives instruction from salient acoustic input. Consistent with this hypothesis, rats raised in the presence of continuous noise were found to have broader excitatory (Chang and Merzenich, 2003; de Villers-Sidani et al., 2008) *and* inhibitory (Chang et al., 2005) receptive fields compared to normal reared rats, and gerbils with moderate conductive hearing loss in development exhibit deficiencies in inhibitory synaptic transmission (Takesian et al., 2012). The immaturity of inhibitory circuitry with continuous noise rearing is further evidenced by a decreased density and size of PV+ cells in A1 (de Villers-Sidani et al., 2008). A decrease in inhibitory transmission could also account for the

141

increased tuning bandwidth and correlated activity observed here in L4 of noise-reared mice.

In previous cross-modal plasticity studies, dark exposure refinement of excitatory L4-L2/3 ascending circuitry and L2/3-L2/3 lateral connectivity was shown to be balanced by a refinement of inhibitory connectivity through a reduction in the total cortical area driving inhibitory responses (Meng et al., 2015). While the amplitude of photoactivated IPSCs was unchanged, an additional study showed that inhibitory synaptic transmission in both L4 and L2/3 is potentiated after DE but in laminar-specific ways (Petrus et al., 2015). In L4, DE specifically increases the amplitude of PV+ evoked mIPSCs, without changing their frequency, while in L2/3 DE increases the frequency of evoked mIPSCs without changing their amplitude (Petrus et al., 2015). An increased mIPSC amplitude in L4 can occur via a postsynaptic change in GABA receptor number or conductance, whereas an increased mIPSC frequency in L2/3 can result from a change in the probability of transmitter release or increase in the readily releasable pool (Turrigiano and Nelson, 2004). Combined, the circuitry refinement and synaptic scaling suggests that while DE increases the strength of individual inhibitory synapses, the total number of functional connections are reduced, thus preserving the net connection strength (Turrigiano and Nelson, 2004; Meng et al., 2015). A refinement of ascending and lateral inhibitory connections in L2/3 might be another contributing factor to the decreased frequency selectivity I observed in L2/3 neurons after DE.

## Other factors that govern CP onset and closure

In addition to the prominent role that inhibitory circuit maturation plays in terminating the critical period, various molecular and structural factors have been implicated in regulating the temporal aspects of this window. Brain-derived neurotrophic factor (BDNF) is released as a result of locally correlated activity (Chang and Merzenich, 2003), and its expression has been shown to accelerate GABAergic innervation and maturation and thus suppress CP plasticity (Huang et al., 1999; Sale et al., 2007). Additionally, in the visual cortex an increase in intracortical myelination has been shown to consolidate neural circuitry and prevent further reorganization (McGee et al., 2005). Lastly, the structural consolidation of the extracellular matrix, particularly in surrounding PV+ inhibitory interneurons by perineuronal nets, stabilizes synapses, reduces new neurite growth, and impedes further plasticity (Hensch, 2005; McRae and Porter, 2012). Dark rearing, which delays maturation of inhibitory transmission, also inhibits the maturation of perineuronal nets (Pizzorusso et al., 2002), and protease degradation of the extracellular matrix in adulthood can reactivate plasticity after the critical period has closed (Pizzorusso et al., 2002). Remarkably, other than the maturation of myelination, these processes are controlled by experience-driven neural activity and are prevented by sensory deprivation. The onset and closure of critical period windows therefore differs by sensory modality as well as on the complexity and patterning of sensory inputs, and involves the cooperation of multiple factors.

## Conclusion

Early sensory experience is fundamental for proper structural and functional organization of the brain via robust experience-dependent plasticity mechanisms. While plasticity is most elaborate during early critical periods of development, significant environmental changes such as the loss of another sense can induce circuit reorganization in adulthood. In this dissertation, I used *in vivo* two-photon $Ca^{2+}$ imaging to investigate the mesoscale changes in functional organization and population activity that occur in thalamorecipient L4 and supragranular L2/3 in development, with sensory deprivation in the early postnatal period, and with cross-modal deprivation in adulthood. Combined, these studies show that in periods of heightened plasticity, local organization of preferred frequency tuning is most homogeneous and frequency selectivity is least refined. Periods of widened spectral selectivity might reflect transient over-connectivity and integration of diverse synaptic inputs, which could facilitate rapid reorganization in response to changing environmental and behavioral demands. Results from these studies fill crucial gaps in our understanding of experience-dependent cortical circuit development and refinement by elucidating the sensory-dependency and laminar-specificity of spatial frequency organization and neuronal population activity, and highlight a dissociation of plasticity of single-cell, mesoscale, and macroscale network properties.

# Chapter 6:  Relevance of findings to hearing disorders

According to the CDC's National Center on Birth Defects and Developmental Abnormalities, 2-3 US-born children are born with partial to full hearing loss. Hearing impairments early in life that remain untreated result in permanent abnormal organization of ACX, and lifelong speech and language disabilities (Sharma et al., 2007; Gilley et al., 2008). Furthermore, children with hearing loss are at a higher risk of falling behind in school due to impaired listening and reading skills, which can affect their academic performance, cognitive, and social skills. Later restoration of peripheral auditory input, for example by cochlear implants, is less effective in restoring language performance as neurons in the adult ACX no longer retain the ability necessary to rewire (Sharma et al., 2002; Sharma and Dorman, 2006).

## *Hearing Loss in development*

Many children endure chronic ear infections in early life. Otitis media, or inflammation of the middle ear, causes fluid in to build up in the middle ear and obstruct sound waves from properly reaching their target, the cochlea, and thus is associated with hearing loss. Children with a history of otitis media exhibit difficulty attending to auditory signals, particularly in noisy environments (Moore et al., 1991). Children born with cleft palate have recurrent ear infections due to deformed soft palate muscles that prevent proper functioning of the Eustachian tubes (Sharma and Nanda, 2009). Hearing loss is a well-known complication of cleft palate due to the

145

higher incidence of fluid accumulation in the middle ear, which causes a high prevalence of speech and language difficulties that can also lead to reading and academic impairments (Kral et al., 2001). Furthermore, hearing impairments in children are frequently attributed to misbehavior and/or attention disorders, since deficient language comprehension can manifest as ignoring the speaker.

Early hearing disorders can often be treated with hearing aids or in the case of cleft palate, be surgically corrected, but impairments must first be detected and thus early postnatal hearing screening programs are critical. Cochlear implants can facilitate language development in children with hearing loss but the age of implantation determines scale of success. Optimal implantation age is between 3.5 years (Sharma et al., 2002) and 5 years (Fryauf-Bertschy et al., 1997), whereas later implantation can result in insufficient activation of language areas and poorer performance on speech discrimination.

## Cross-modal plasticity in adulthood

There is converging evidence that deprivation of one sensory modality leads to enhancement in the spared modality (Frasnelli et al., 2011). Humans that are blind from birth can effectively develop an accurate representation of space, can localize binaural sounds as efficiently as sighted individuals, and are more adept at localizing sounds monaurally (Lessard et al., 1998). Furthermore, blind individuals can more skillfully localize sounds in their periphery (Roder et al., 1999; Voss et al., 2004). Together, these findings suggest that humans deprived of visual input from early life develop compensatory strategies to balance the sensory offset, but that these

146

enhancements emerge during more complex tasks (Frasnelli et al., 2011). Cross-modal plasticity is not just limited to loss of vision from birth, as late-onset blind subjects still show enhancement of spatial abilities (Voss et al., 2004), although there is some evidence that early-onset blind individuals outperform late-onset blind individuals on a variety of auditory perception tasks (Wan et al., 2010). Most relevant to the studies performed in this dissertation, even brief visual deprivation in humans can improve auditory perception, which return to baseline after visual experience resumes (Page et al., 2016).

The research presented in this dissertation serves to highlight the robust cortical circuitry changes occurring in the short time frame after hearing onset that rely on hearing ability, and thus emphasizes the importance of early preventative intervention in children born with hearing loss. Furthermore, it provides insight into the effectiveness of cross-modal plasticity in stimulating ACX circuit plasticity in adulthood, which perhaps can be harnessed to restore function lost in early life. The more we understand how a normal brain responds to and processes sensory input, the more suited we are to detect and correct sensory deficits.

# Bibliography

Adelsberger H, Garaschuk O, Konnerth A (2005) Cortical calcium waves in resting newborn mice. Nat Neurosci 8:988-990.

Allendoerfer KL, Shatz CJ (1994) The subplate, a transient neocortical structure: its role in the development of connections between thalamus and cortex. Annu Rev Neurosci 17:185-218.

Atencio CA, Schreiner CE (2010) Columnar connectivity and laminar processing in cat primary auditory cortex. PLoS One 5:e9521.

Atencio CA, Sharpee TO, Schreiner CE (2009) Hierarchical computation in the canonical auditory cortical circuit. Proc Natl Acad Sci U S A 106:21894-21899.

Atzori M, Lei S, Evans DI, Kanold PO, Phillips-Tansey E, McIntyre O, McBain CJ (2001) Differential synaptic processing separates stationary from transient inputs to the auditory cortex. Nat Neurosci 4:1230-1237.

Averbeck BB, Latham PE, Pouget A (2006) Neural correlations, population coding and computation. Nat Rev Neurosci 7:358-366.

Bandyopadhyay S, Shamma SA, Kanold PO (2010) Dichotomy of functional organization in the mouse auditory cortex. Nat Neurosci 13:361-368.

Bao S, Chan VT, Merzenich MM (2001) Cortical remodelling induced by activity of ventral tegmental dopamine neurons. Nature 412:79-83.

Bao S, Chang EF, Davis JD, Gobeske KT, Merzenich MM (2003) Progressive degradation and subsequent refinement of acoustic representations in the adult auditory cortex. J Neurosci 23:10765-10775.

Bao S, Chang EF, Teng CL, Heiser MA, Merzenich MM (2013) Emergent categorical representation of natural, complex sounds resulting from the early post-natal sound environment. Neuroscience 248:30-42.

Barbour DL, Callaway EM (2008) Excitatory local connections of superficial neurons in rat auditory cortex. J Neurosci 28:11174-11185.

Barkat TR, Polley DB, Hensch TK (2011) A critical period for auditory thalamocortical connectivity. Nat Neurosci 14:1189-1194.

Bender KJ, Rangel J, Feldman DE (2003) Development of columnar topography in the excitatory layer 4 to layer 2/3 projection in rat barrel cortex. J Neurosci 23:8759-8770.

Binzegger T, Douglas RJ, Martin KA (2004) A quantitative map of the circuit of cat primary visual cortex. J Neurosci 24:8441-8453.

Bizley JK, Nodal FR, Nelken I, King AJ (2005) Functional organization of ferret auditory cortex. Cereb Cortex 15:1637-1653.

Briggs F, Usrey WM (2008) Emerging views of corticothalamic function. Curr Opin Neurobiol 18:403-407.

Bruno RM, Sakmann B (2006) Cortex is driven by weak but synchronously active thalamocortical synapses. Science 312:1622-1627.

Butts DA (2002) Retinal waves: implications for synaptic learning rules during development. Neuroscientist 8:243-253.

Butts DA, Goldman MS (2006) Tuning curves, neuronal variability, and sensory coding. PLoS Biol 4:e92.

Butts DA, Kanold PO (2010) The applicability of spike time dependent plasticity to development. Front Synaptic Neurosci 2:30.

Campbell RA, Schulz AL, King AJ, Schnupp JW (2010) Brief sounds evoke prolonged responses in anesthetized ferret auditory cortex. J Neurophysiol 103:2783-2793.

Caras ML, Sanes DH (2015) Sustained Perceptual Deficits from Transient Sensory Deprivation. J Neurosci 35:10831-10842.

Carrasco MM, Trujillo M, Razak K (2013) Development of response selectivity in the mouse auditory cortex. Hear Res 296:107-120.

Castro JB, Kandler K (2010) Changing tune in auditory cortex. Nat Neurosci 13:271-273.

Catalano SM, Shatz CJ (1998) Activity-dependent cortical target selection by thalamic axons. Science 281:559-562.

Celikel T, Szostak VA, Feldman DE (2004) Modulation of spike timing by sensory deprivation during induction of cortical map plasticity. Nat Neurosci 7:534-541.

Chance FS, Nelson SB, Abbott LF (1999) Recurrent cortical amplification produces complex cell responses. In: Advances in neural information processing systems 11 (Kearns MS, Solla SA, Cohn DA, eds), pp 90-96. Cambridge, MA: MIT Press.

Chang EF, Merzenich MM (2003) Environmental noise retards auditory cortical development. Science 300:498-502.

Chang EF, Bao S, Imaizumi K, Schreiner CE, Merzenich MM (2005) Development of spectral and temporal response selectivity in the auditory cortex. Proc Natl Acad Sci U S A 102:16460-16465.

Chen Q, Cichon J, Wang W, Qiu L, Lee SJ, Campbell NR, Destefino N, Goard MJ, Fu Z, Yasuda R, Looger LL, Arenkiel BR, Gan WB, Feng G (2012) Imaging neural activity using Thy1-GCaMP transgenic mice. Neuron 76:297-308.

Chen TW, Wardill TJ, Sun Y, Pulver SR, Renninger SL, Baohan A, Schreiter ER, Kerr RA, Orger MB, Jayaraman V, Looger LL, Svoboda K, Kim DS (2013) Ultrasensitive fluorescent proteins for imaging neuronal activity. Nature 499:295-300.

Chen X, Leischner U, Rochefort NL, Nelken I, Konnerth A (2011) Functional mapping of single spines in cortical neurons in vivo. Nature 475:501-505.

Chen-Bee CH, Zhou Y, Jacobs NS, Lim B, Frostig RD (2012) Whisker array functional representation in rat barrel cortex: transcendence of one-to-one topography and its underlying mechanism. Front Neural Circuits 6:93.

Cossell L, Iacaruso MF, Muir DR, Houlton R, Sader EN, Ko H, Hofer SB, Mrsic-Flogel TD (2015) Functional organization of excitatory synaptic strength in primary visual cortex. Nature 518:399-403.

Crair MC, Gillespie DC, Stryker MP (1998) The role of visual experience in the development of columns in cat visual cortex. Science 279:566-570.

Crowley JC, Katz LC (1999) Development of ocular dominance columns in the absence of retinal input. Nat Neurosci 2:1125-1130.

Cruikshank SJ, Rose HJ, Metherate R (2002) Auditory thalamocortical synaptic transmission in vitro. J Neurophysiol 87:361-384.

Dana H, Chen TW, Hu A, Shields BC, Guo C, Looger LL, Kim DS, Svoboda K (2014) Thy1-GCaMP6 transgenic mice for neuronal population imaging in vivo. PLoS One 9:e108697.

de Villers-Sidani E, Chang EF, Bao S, Merzenich MM (2007) Critical period window for spectral tuning defined in the primary auditory cortex (A1) in the rat. J Neurosci 27:180-189.

de Villers-Sidani E, Simpson KL, Lu YF, Lin RC, Merzenich MM (2008) Manipulating critical period closure across different sectors of the primary auditory cortex. Nat Neurosci 11:957-965.

DeWeese MR, Wehr M, Zador AM (2003) Binary spiking in auditory cortex. J Neurosci 23:7940-7949.

Dorr A, Sled JG, Kabani N (2007) Three-dimensional cerebral vasculature of the CBA mouse brain: a magnetic resonance imaging and micro computed tomography study. Neuroimage 35:1409-1423.

Dorrn AL, Yuan K, Barker AJ, Schreiner CE, Froemke RC (2010) Developmental sensory experience balances cortical excitation and inhibition. Nature 465:932-936.

Douglas RJ, Martin KA (2007) Recurrent neuronal circuits in the neocortex. Curr Biol 17:R496-500.

Douglas RJ, Markram H, Martin KA (2004) Neocortex. In: The Synaptic Organization of the Brain, Fifth Edition (Shepherd GM, ed), pp 499-558. New York: Oxford University Press.

Douglas RJ, Koch C, Mahowald M, Martin KA, Suarez HH (1995) Recurrent excitation in neocortical circuits. Science 269:981-985.

Eaton NC, Sheehan HM, Quinlan EM (2016) Optimization of visual training for full recovery from severe amblyopia in adults. Learn Mem 23:99-103.

Echteler SM, Arjmand E, Dallos P (1989) Developmental alterations in the frequency map of the mammalian cochlea. Nature 341:147-149.

Edeline JM, Pham P, Weinberger NM (1993) Rapid development of learning-induced receptive field plasticity in the auditory cortex. Behav Neurosci 107:539-551.

Eggermont J (1996) Differential maturation rates for response parameters in cat primary auditory cortex. Auditory Neuroscience 2:309-327.

Elyada YM, Mizrahi A (2015) Becoming a mother-circuit plasticity underlying maternal behavior. Curr Opin Neurobiol 35:49-56.

Eurich CW, Wilke SD (2000) Multidimensional encoding strategy of spiking neurons. Neural Comput 12:1519-1529.

Fagiolini M, Hensch TK (2000) Inhibitory threshold for critical-period activation in primary visual cortex. Nature 404:183-186.

Fagiolini M, Pizzorusso T, Berardi N, Domenici L, Maffei L (1994) Functional postnatal development of the rat primary visual cortex and the role of visual experience: dark rearing and monocular deprivation. Vision Res 34:709-720.

Feldman DE (2000) Timing-based LTP and LTD at vertical inputs to layer II/III pyramidal cells in rat barrel cortex. Neuron 27:45-56.

Feldman DE (2009) Synaptic mechanisms for plasticity in neocortex. Annu Rev Neurosci 32:33-55.

Feldman DE, Nicoll RA, Malenka RC (1999) Synaptic plasticity at thalamocortical synapses in developing rat somatosensory cortex: LTP, LTD, and silent synapses. J Neurobiol 41:92-101.

Feldmeyer D (2012) Excitatory neuronal connectivity in the barrel cortex. Front Neuroanat 6:24.

Feldmeyer D, Egger V, Lubke J, Sakmann B (1999) Reliable synaptic connections between pairs of excitatory layer 4 neurones within a single 'barrel' of developing rat somatosensory cortex. J Physiol 521 Pt 1:169-190.

Feller MB, Wellis DP, Stellwagen D, Werblin FS, Shatz CJ (1996) Requirement for cholinergic synaptic transmission in the propagation of spontaneous retinal waves. Science 272:1182-1187.

Fitzpatrick DC, Batra R, Stanford TR, Kuwada S (1997) A neuronal population code for sound localization. Nature 388:871-874.

Florence SL, Taub HB, Kaas JH (1998) Large-scale sprouting of cortical connections after peripheral injury in adult macaque monkeys. Science 282:1117-1121.

Foeller E, Feldman DE (2004) Synaptic basis for developmental plasticity in somatosensory cortex. Curr Opin Neurobiol 14:89-95.

Fox K (1992) A critical period for experience-dependent synaptic plasticity in rat barrel cortex. J Neurosci 12:1826-1838.

Frasnelli J, Collignon O, Voss P, Lepore F (2011) Crossmodal plasticity in sensory loss. Prog Brain Res 191:233-249.

Fritz J, Elhilali M, Shamma S (2005) Active listening: task-dependent plasticity of spectrotemporal receptive fields in primary auditory cortex. Hear Res 206:159-176.

Fritz J, Shamma S, Elhilali M, Klein D (2003) Rapid task-related plasticity of spectrotemporal receptive fields in primary auditory cortex. Nat Neurosci 6:1216-1223.

Fritz JB, David SV, Radtke-Schuller S, Yin P, Shamma SA (2010) Adaptive, behaviorally gated, persistent encoding of task-relevant auditory information in ferret frontal cortex. Nat Neurosci 13:1011-1019.

Fryauf-Bertschy H, Tyler RS, Kelsay DM, Gantz BJ, Woodworth GG (1997) Cochlear implant use by prelingually deafened children: the influences of age at implant and length of device use. J Speech Lang Hear Res 40:183-199.

Gandhi SP, Yanagawa Y, Stryker MP (2008) Delayed plasticity of inhibitory neurons in developing visual cortex. Proc Natl Acad Sci U S A 105:16797-16802.

Garrett ME, Nauhaus I, Marshel JH, Callaway EM (2014) Topography and areal organization of mouse visual cortex. J Neurosci 34:12587-12600.

Ghosh A, Shatz CJ (1992) Involvement of subplate neurons in the formation of ocular dominance columns. Science 255:1441-1443.

Ghosh A, Shatz CJ (1993) A role for subplate neurons in the patterning of connections from thalamus to neocortex. Development 117:1031-1047.

Ghosh A, Antonini A, McConnell SK, Shatz CJ (1990) Requirement for subplate neurons in the formation of thalamocortical connections. Nature 347:179-181.

Gil Z, Connors BW, Amitai Y (1999) Efficacy of thalamocortical and intracortical synaptic connections: quanta, innervation, and reliability. Neuron 23:385-397.

Gilley PM, Sharma A, Dorman MF (2008) Cortical reorganization in children with cochlear implants. Brain Res 1239:56-65.

Glascock JJ, Osman EY, Coady TH, Rose FF, Shababi M, Lorson CL (2011) Delivery of therapeutic agents through intracerebroventricular (ICV) and intravenous (IV) injection in mice. J Vis Exp.

Goel A, Jiang B, Xu LW, Song L, Kirkwood A, Lee HK (2006) Cross-modal regulation of synaptic AMPA receptors in primary sensory cortices by visual experience. Nat Neurosci 9:1001-1003.

Goldstein MH, Jr., Abeles M, Daly RL, McIntosh J (1970) Functional architecture in cat primary auditory cortex: tonotopic organization. J Neurophysiol 33:188-197.

Goncalves JT, Anstey JE, Golshani P, Portera-Cailliau C (2013) Circuit level defects in the developing neocortex of Fragile X mice. Nat Neurosci 16:903-909.

Gougoux F, Lepore F, Lassonde M, Voss P, Zatorre RJ, Belin P (2004) Neuropsychology: pitch discrimination in the early blind. Nature 430:309.

Guo W, Chambers AR, Darrow KN, Hancock KE, Shinn-Cunningham BG, Polley DB (2012a) Robustness of cortical topography across fields, laminae, anesthetic states, and neurophysiological signal types. J Neurosci 32:9159-9172.

Guo Y, Huang S, de Pasquale R, McGehrin K, Lee HK, Zhao K, Kirkwood A (2012b) Dark exposure extends the integration window for spike-timing-dependent plasticity. J Neurosci 32:15027-15035.

Hackett TA, Barkat TR, O'Brien BM, Hensch TK, Polley DB (2011) Linking topography to tonotopy in the mouse auditory thalamocortical circuit. J Neurosci 31:2983-2995.

Happel MF, Jeschke M, Ohl FW (2010) Spectral integration in primary auditory cortex attributable to temporally precise convergence of thalamocortical and intracortical input. J Neurosci 30:11114-11127.

Harris KD, Quiroga RQ, Freeman J, Smith SL (2016) Improving data quality in neuronal population recordings. Nat Neurosci 19:1165-1174.

He HY, Hodos W, Quinlan EM (2006) Visual deprivation reactivates rapid ocular dominance plasticity in adult visual cortex. J Neurosci 26:2951-2955.

Hensch TK (2005) Critical period plasticity in local cortical circuits. Nat Rev Neurosci 6:877-888.

Hensch TK, Fagiolini M, Mataga N, Stryker MP, Baekkeskov S, Kash SF (1998) Local GABA circuit control of experience-dependent plasticity in developing visual cortex. Science 282:1504-1508.

Hires SA, Tian L, Looger LL (2008) Reporting neural activity with genetically encoded calcium indicators. Brain Cell Biol 36:69-86.

Hoerder-Suabedissen A, Molnar Z (2015) Development, evolution and pathology of neocortical subplate neurons. Nat Rev Neurosci 16:133-146.

Hromadka T, Deweese MR, Zador AM (2008) Sparse representation of sounds in the unanesthetized auditory cortex. PLoS Biol 6:e16.

Hu H, Gan J, Jonas P (2014) Interneurons. Fast-spiking, parvalbumin(+) GABAergic interneurons: from cellular design to microcircuit function. Science 345:1255263.

Huang ZJ, Kirkwood A, Pizzorusso T, Porciatti V, Morales B, Bear MF, Maffei L, Tonegawa S (1999) BDNF regulates the maturation of inhibition and the critical period of plasticity in mouse visual cortex. Cell 98:739-755.

Hubel DH, Wiesel TN (1962) Receptive fields, binocular interaction and functional architecture in the cat's visual cortex. J Physiol 160:106-154.

Hubel DH, Wiesel TN (1970) The period of susceptibility to the physiological effects of unilateral eye closure in kittens. J Physiol 206:419-436.

Hubel DH, Wiesel TN (1977) Ferrier lecture. Functional architecture of macaque monkey visual cortex. Proc R Soc Lond B Biol Sci 198:1-59.

Insanally MN, Kover H, Kim H, Bao S (2009) Feature-dependent sensitive periods in the development of complex sound representation. J Neurosci 29:5456-5462.

Issa JB, Haeffele BD, Agarwal A, Bergles DE, Young ED, Yue DT (2014) Multiscale optical Ca2+ imaging of tonal organization in mouse auditory cortex. Neuron 83:944-959.

Jia H, Rochefort NL, Chen X, Konnerth A (2010) Dendritic organization of sensory input to cortical neurons in vivo. Nature 464:1307-1312.

Kadia SC, Wang X (2003) Spectral integration in A1 of awake primates: neurons with single- and multipeaked tuning characteristics. J Neurophysiol 89:1603-1622.

Kalmbach AS, Waters J (2012) Brain surface temperature under a craniotomy. J Neurophysiol 108:3138-3146.

Kanold PO (2004) Transient microcircuits formed by subplate neurons and their role in functional development of thalamocortical connections. Neuroreport 15:2149-2153.

Kanold PO (2009) Subplate neurons: crucial regulators of cortical development and plasticity. Front Neuroanat 3:16.

Kanold PO, Shatz CJ (2006) Subplate neurons regulate maturation of cortical inhibition and outcome of ocular dominance plasticity. Neuron 51:627-638.

Kanold PO, Luhmann HJ (2010) The subplate and early cortical circuits. Annu Rev Neurosci 33:23-48.

Kanold PO, Nelken I, Polley DB (2014) Local versus global scales of organization in auditory cortex. Trends Neurosci 37:502-510.

Kanold PO, Kara P, Reid RC, Shatz CJ (2003) Role of subplate neurons in functional maturation of visual cortical columns. Science 301:521-525.

Katz LC, Shatz CJ (1996) Synaptic activity and the construction of cortical circuits. Science 274:1133-1138.

Kaur S, Lazar R, Metherate R (2004) Intracortical pathways determine breadth of subthreshold frequency receptive fields in primary auditory cortex. J Neurophysiol 91:2551-2567.

Kerlin AM, Andermann ML, Berezovskii VK, Reid RC (2010) Broadly tuned response properties of diverse inhibitory neuron subtypes in mouse visual cortex. Neuron 67:858-871.

Keuroghlian AS, Knudsen EI (2007) Adaptive auditory plasticity in developing and adult animals. Prog Neurobiol 82:109-121.

Kilgard MP, Merzenich MM (1998) Cortical map reorganization enabled by nucleus basalis activity. Science 279:1714-1718.

Kim JY, Grunke SD, Levites Y, Golde TE, Jankowsky JL (2014) Intracerebroventricular viral injection of the neonatal mouse brain for persistent and widespread neuronal transduction. J Vis Exp:51863.

King AJ, Parsons CH (1999) Improved auditory spatial acuity in visually deprived ferrets. Eur J Neurosci 11:3945-3956.

King J, Insanally M, Jin M, Martins AR, D'Amour J A, Froemke RC (2015) Rodent auditory perception: Critical band limitations and plasticity. Neuroscience 296:55-65.

Kirkwood A, Lee HK, Bear MF (1995) Co-regulation of long-term potentiation and experience-dependent synaptic plasticity in visual cortex by age and experience. Nature 375:328-331.

Ko H, Hofer SB, Pichler B, Buchanan KA, Sjostrom PJ, Mrsic-Flogel TD (2011) Functional specificity of local synaptic connections in neocortical networks. Nature 473:87-91.

Ko H, Cossell L, Baragli C, Antolik J, Clopath C, Hofer SB, Mrsic-Flogel TD (2013) The emergence of functional microcircuits in visual cortex. Nature 496:96-100.

Kobayashi M, Hamada T, Kogo M, Yanagawa Y, Obata K, Kang Y (2008) Developmental profile of GABAA-mediated synaptic transmission in pyramidal cells of the somatosensory cortex. Eur J Neurosci 28:849-861.

Kotak VC, Takesian AE, Sanes DH (2008) Hearing loss prevents the maturation of GABAergic transmission in the auditory cortex. Cereb Cortex 18:2098-2108.

Kral A, Hartmann R, Tillein J, Heid S, Klinke R (2001) Delayed maturation and sensitive periods in the auditory cortex. Audiol Neurootol 6:346-362.

Kratz MB, Manis PB (2015) Spatial organization of excitatory synaptic inputs to layer 4 neurons in mouse primary auditory cortex. Front Neural Circuits 9:17.

Kremkow J, Jin J, Wang Y, Alonso JM (2016) Principles underlying sensory map topography in primary visual cortex. Nature 533:52-57.

Lee CC, Middlebrooks JC (2011) Auditory cortex spatial sensitivity sharpens during task performance. Nat Neurosci 14:108-114.

Lessard N, Pare M, Lepore F, Lassonde M (1998) Early-blind human subjects localize sound sources better than sighted subjects. Nature 395:278-280.

Levy RB, Reyes AD (2012) Spatial profile of excitatory and inhibitory synaptic connectivity in mouse primary auditory cortex. J Neurosci 32:5609-5619.

Li LY, Li YT, Zhou M, Tao HW, Zhang LI (2013a) Intracortical multiplication of thalamocortical signals in mouse auditory cortex. Nat Neurosci 16:1179-1181.

Li LY, Ji XY, Liang F, Li YT, Xiao Z, Tao HW, Zhang LI (2014) A feedforward inhibitory circuit mediates lateral refinement of sensory representation in upper layer 2/3 of mouse primary auditory cortex. J Neurosci 34:13670-13683.

Li YT, Ibrahim LA, Liu BH, Zhang LI, Tao HW (2013b) Linear transformation of thalamocortical input by intracortical excitation. Nat Neurosci 16:1324-1330.

Linden JF, Liu RC, Sahani M, Schreiner CE, Merzenich MM (2003) Spectrotemporal structure of receptive fields in areas AI and AAF of mouse auditory cortex. J Neurophysiol 90:2660-2675.

Liu BH, Wu GK, Arbuckle R, Tao HW, Zhang LI (2007) Defining cortical frequency tuning with recurrent excitatory circuitry. Nat Neurosci 10:1594-1600.

Long MA, Cruikshank SJ, Jutras MJ, Connors BW (2005) Abrupt maturation of a spike-synchronizing mechanism in neocortex. J Neurosci 25:7309-7316.

Looger LL, Griesbeck O (2012) Genetically encoded neural activity indicators. Curr Opin Neurobiol 22:18-23.

Maor I, Shalev A, Mizrahi A (2016) Distinct Spatiotemporal Response Properties of Excitatory Versus Inhibitory Neurons in the Mouse Auditory Cortex. Cereb Cortex.

McConnell SK, Ghosh A, Shatz CJ (1989) Subplate neurons pioneer the first axon pathway from the cerebral cortex. Science 245:978-982.

McGee AW, Yang Y, Fischer QS, Daw NW, Strittmatter SM (2005) Experience-driven plasticity of visual cortex limited by myelin and Nogo receptor. Science 309:2222-2226.

McRae PA, Porter BE (2012) The perineuronal net component of the extracellular matrix in plasticity and epilepsy. Neurochem Int 61:963-972.

Meng X, Kao JP, Lee HK, Kanold PO (2015) Visual Deprivation Causes Refinement of Intracortical Circuits in the Auditory Cortex. Cell Rep 12:955-964.

Merzenich MM, Brugge JF (1973) Representation of the cochlear partition of the superior temporal plane of the macaque monkey. Brain Res 50:275-296.

Merzenich MM, Knight PL, Roth GL (1975) Representation of cochlea within primary auditory cortex in the cat. J Neurophysiol 38:231-249.

Mikaelian DO, Ruben RJ (1965) Development of hearing in the normal CBA-J mouse: correlation of physiological observations with behavioral responses and with cochlear anatomy. Acta Otolaryngol 59:451-461.

Mills DM, Rubel EW (1998) Development of the base of the cochlea: place code shift in the gerbil. Hear Res 122:82-96.

Molnar Z, Blakemore C (1995) How do thalamic axons find their way to the cortex? Trends Neurosci 18:389-397.

Molnar Z, Adams R, Blakemore C (1998) Mechanisms underlying the early establishment of thalamocortical connections in the rat. J Neurosci 18:5723-5745.

Montey KL, Quinlan EM (2011) Recovery from chronic monocular deprivation following reactivation of thalamocortical plasticity by dark exposure. Nat Commun 2:317.

Moore AK, Wehr M (2013) Parvalbumin-expressing inhibitory interneurons in auditory cortex are well-tuned for frequency. J Neurosci 33:13713-13723.

Moore DR, Aitkin LM (1975) Rearing in an acoustically unusual environment - effects on neural auditory responses. Neurosci Lett 1:29-34.

Moore DR, Hutchings ME, Meyer SE (1991) Binaural masking level differences in children with a history of otitis media. Audiology 30:91-101.

Morales B, Choi SY, Kirkwood A (2002) Dark rearing alters the development of GABAergic transmission in visual cortex. J Neurosci 22:8084-8090.

Morel A, Garraghty PE, Kaas JH (1993) Tonotopic organization, architectonic fields, and connections of auditory cortex in macaque monkeys. J Comp Neurol 335:437-459.

Moshitch D, Las L, Ulanovsky N, Bar-Yosef O, Nelken I (2006) Responses of neurons in primary auditory cortex (A1) to pure tones in the halothane-anesthetized cat. J Neurophysiol 95:3756-3769.

Mower GD (1991) The effect of dark rearing on the time course of the critical period in cat visual cortex. Brain Res Dev Brain Res 58:151-158.

Mowery TM, Kotak VC, Sanes DH (2015) Transient Hearing Loss Within a Critical Period Causes Persistent Changes to Cellular Properties in Adult Auditory Cortex. Cereb Cortex 25:2083-2094.

Nathanson JL, Yanagawa Y, Obata K, Callaway EM (2009) Preferential labeling of inhibitory and excitatory cortical neurons by endogenous tropism of adeno-associated virus and lentivirus vectors. Neuroscience 161:441-450.

Nelken I (2004) Processing of complex stimuli and natural scenes in the auditory cortex. Curr Opin Neurobiol 14:474-480.

Nimmerjahn A, Helmchen F (2012) In vivo labeling of cortical astrocytes with sulforhodamine 101 (SR101). Cold Spring Harb Protoc 2012:326-334.

O'Connell MN, Barczak A, Schroeder CE, Lakatos P (2014) Layer specific sharpening of frequency tuning by selective attention in primary auditory cortex. J Neurosci 34:16496-16508.

Oh SW et al. (2014) A mesoscale connectome of the mouse brain. Nature 508:207-214.

Ohki K, Chung S, Ch'ng YH, Kara P, Reid RC (2005) Functional imaging with cellular resolution reveals precise micro-architecture in visual cortex. Nature 433:597-603.

Okamoto H, Stracke H, Wolters CH, Schmael F, Pantev C (2007) Attention improves population-level frequency tuning in human auditory cortex. J Neurosci 27:10383-10390.

Oswald AM, Reyes AD (2008) Maturation of intrinsic and synaptic properties of layer 2/3 pyramidal neurons in mouse auditory cortex. J Neurophysiol 99:2998-3008.

Oswald AM, Reyes AD (2011) Development of inhibitory timescales in auditory cortex. Cereb Cortex 21:1351-1361.

Oviedo HV, Bureau I, Svoboda K, Zador AM (2010) The functional asymmetry of auditory cortex is reflected in the organization of local cortical circuits. Nat Neurosci 13:1413-1420.

Packer AM, Russell LE, Dalgleish HW, Hausser M (2015) Simultaneous all-optical manipulation and recording of neural circuit activity with cellular resolution in vivo. Nat Methods 12:140-146.

Page S, Sharp A, Landry SP, Champoux F (2016) Short-term visual deprivation can enhance spatial release from masking. Neurosci Lett.

Peinado A, Yuste R, Katz LC (1993) Gap junctional communication and the development of local circuits in neocortex. Cereb Cortex 3:488-498.

Penn AA, Riquelme PA, Feller MB, Shatz CJ (1998) Competition in retinogeniculate patterning driven by spontaneous activity. Science 279:2108-2112.

Peron SP, Freeman J, Iyer V, Guo C, Svoboda K (2015) A Cellular Resolution Map of Barrel Cortex Activity during Tactile Behavior. Neuron 86:783-799.

Petrus E, Rodriguez G, Patterson R, Connor B, Kanold PO, Lee HK (2015) Vision loss shifts the balance of feedforward and intracortical circuits in opposite directions in mouse primary auditory and visual cortices. J Neurosci 35:8790-8801.

Petrus E, Isaiah A, Jones AP, Li D, Wang H, Lee HK, Kanold PO (2014) Crossmodal induction of thalamocortical potentiation leads to enhanced information processing in the auditory cortex. Neuron 81:664-673.

Pizzorusso T, Medini P, Berardi N, Chierzi S, Fawcett JW, Maffei L (2002) Reactivation of ocular dominance plasticity in the adult visual cortex. Science 298:1248-1251.

Polley DB, Steinberg EE, Merzenich MM (2006) Perceptual learning directs auditory cortical map reorganization through top-down influences. J Neurosci 26:4970-4982.

Polley DB, Thompson JH, Guo W (2013) Brief hearing loss disrupts binaural integration during two early critical periods of auditory cortex development. Nat Commun 4:2547.

Polley DB, Read HL, Storace DA, Merzenich MM (2007) Multiparametric auditory receptive field organization across five cortical fields in the albino rat. J Neurophysiol 97:3621-3638.

Popescu MV, Polley DB (2010) Monaural deprivation disrupts development of binaural selectivity in auditory midbrain and cortex. Neuron 65:718-731.

Portfors CV (2007) Types and functions of ultrasonic vocalizations in laboratory rats and mice. J Am Assoc Lab Anim Sci 46:28-34.

Pouget A, Deneve S, Ducom JC, Latham PE (1999) Narrow versus wide tuning curves: What's best for a population code? Neural Comput 11:85-90.

Rasmussen R, Nedergaard M, Petersen NC (2016) Sulforhodamine 101, a widely used astrocyte marker, can induce cortical seizure-like activity at concentrations commonly used. Sci Rep 6:30433.

Ratzlaff EH, Grinvald A (1991) A tandem-lens epifluorescence macroscope: hundred-fold brightness advantage for wide-field imaging. J Neurosci Methods 36:127-137.

Rauschecker JP, Kniepert U (1994) Auditory localization behaviour in visually deprived cats. Eur J Neurosci 6:149-160.

Read HL, Winer JA, Schreiner CE (2002) Functional architecture of auditory cortex. Curr Opin Neurobiol 12:433-440.

Reale RA, Imig TJ (1980) Tonotopic organization in auditory cortex of the cat. J Comp Neurol 192:265-291.

Roder B, Teder-Salejarvi W, Sterr A, Rosler F, Hillyard SA, Neville HJ (1999) Improved auditory spatial tuning in blind humans. Nature 400:162-166.

Romand R (1987) Tonotopic evolution during development. Hear Res 28:117-123.

Romand R, Ehret G (1990) Development of tonotopy in the inferior colliculus. I. Electrophysiological mapping in house mice. Brain Res Dev Brain Res 54:221-234.

Rose T, Goltstein PM, Portugues R, Griesbeck O (2014) Putting a finishing touch on GECIs. Front Mol Neurosci 7:88.

Rothschild G, Nelken I, Mizrahi A (2010) Functional organization and population dynamics in the mouse primary auditory cortex. Nat Neurosci 13:353-360.

Rothschild G, Cohen L, Mizrahi A, Nelken I (2013) Elevated correlations in neuronal ensembles of mouse auditory cortex following parturition. J Neurosci 33:12851-12861.

Rutkowski RG, Weinberger NM (2005) Encoding of learned importance of sound by magnitude of representational area in primary auditory cortex. Proc Natl Acad Sci U S A 102:13664-13669.

Sadagopan S, Wang X (2009) Nonlinear spectrotemporal interactions underlying selectivity for complex sounds in auditory cortex. J Neurosci 29:11192-11202.

Sale A, Maya Vetencourt JF, Medini P, Cenni MC, Baroncelli L, De Pasquale R, Maffei L (2007) Environmental enrichment in adulthood promotes amblyopia recovery through a reduction of intracortical inhibition. Nat Neurosci 10:679-681.

Sanes DH, Constantine-Paton M (1983) Altered activity patterns during development reduce neural tuning. Science 221:1183-1185.

Sanes DH, Constantine-Paton M (1985) The sharpening of frequency tuning curves requires patterned activity during development in the mouse, Mus musculus. J Neurosci 5:1152-1166.

Sanes DH, Bao S (2009) Tuning up the developing auditory CNS. Curr Opin Neurobiol 19:188-199.

Sanes DH, Kotak VC (2011) Developmental plasticity of auditory cortical inhibitory synapses. Hear Res 279:140-148.

Sato TR, Gray NW, Mainen ZF, Svoboda K (2007) The functional microarchitecture of the mouse barrel cortex. PLoS Biol 5:e189.

Schoonover CE, Tapia JC, Schilling VC, Wimmer V, Blazeski R, Zhang W, Mason CA, Bruno RM (2014) Comparative strength and dendritic organization of thalamocortical and corticocortical synapses onto excitatory layer 4 neurons. J Neurosci 34:6746-6758.

Schreiner CE, Winer JA (2007) Auditory cortex mapmaking: principles, projections, and plasticity. Neuron 56:356-365.

Schreiner CE, Polley DB (2014) Auditory map plasticity: diversity in causes and consequences. Curr Opin Neurobiol 24:143-156.

Schreiner CE, Read HL, Sutter ML (2000) Modular organization of frequency integration in primary auditory cortex. Annu Rev Neurosci 23:501-529.

Series P, Latham PE, Pouget A (2004) Tuning curve sharpening for orientation selectivity: coding efficiency and the impact of correlations. Nat Neurosci 7:1129-1135.

Sharma A, Dorman MF (2006) Central auditory development in children with cochlear implants: clinical implications. Adv Otorhinolaryngol 64:66-88.

Sharma A, Dorman MF, Spahr AJ (2002) A sensitive period for the development of the central auditory system in children with cochlear implants: implications for age of implantation. Ear Hear 23:532-539.

Sharma A, Gilley PM, Dorman MF, Baldwin R (2007) Deprivation-induced cortical reorganization in children with cochlear implants. Int J Audiol 46:494-499.

Sharma RK, Nanda V (2009) Problems of middle ear and hearing in cleft children. Indian J Plast Surg 42 Suppl:S144-148.

Shatz CJ, Luskin MB (1986) The relationship between the geniculocortical afferents and their cortical target cells during development of the cat's primary visual cortex. J Neurosci 6:3655-3668.

Shatz CJ, Stryker MP (1988) Prenatal tetrodotoxin infusion blocks segregation of retinogeniculate afferents. Science 242:87-89.

Shepherd GM, Pologruto TA, Svoboda K (2003) Circuit analysis of experience-dependent plasticity in the developing rat barrel cortex. Neuron 38:277-289.

Shnerson A, Pujol R (1983) Development: anatomy, electrophysiology, and behavior. In: The Auditory Psychobiology of the Mouse (Willot J, ed), pp 395-425. Springfield, IL: Charles C. Thomas.

Sitdikova G, Zakharov A, Janackova S, Gerasimova E, Lebedeva J, Inacio AR, Zaynutdinova D, Minlebaev M, Holmes GL, Khazipov R (2014) Isoflurane suppresses early cortical activity. Ann Clin Transl Neurol 1:15-26.

Smith GB, Sederberg A, Elyada YM, Van Hooser SD, Kaschube M, Fitzpatrick D (2015) The development of cortical circuits for motion discrimination. Nat Neurosci 18:252-261.

Steel K, Niaussat M, Bock GR (1983) The Genetics of Hearing. In: The Auditory Psychobiology of the Mouse (Willot J, ed), pp 341-394. Springfield, IL: Charles C. Thomas.

Stiebler I, Neulist R, Fichtel I, Ehret G (1997) The auditory cortex of the house mouse: left-right differences, tonotopic organization and quantitative analysis of frequency representation. J Comp Physiol A 181:559-571.

Stosiek C, Garaschuk O, Holthoff K, Konnerth A (2003) In vivo two-photon calcium imaging of neuronal networks. Proc Natl Acad Sci U S A 100:7319-7324.

Suter BA, O'Connor T, Iyer V, Petreanu LT, Hooks BM, Kiritani T, Svoboda K, Shepherd GM (2010) Ephus: multipurpose data acquisition software for neuroscience experiments. Front Neural Circuits 4:100.

Takahashi K, Hishida R, Kubota Y, Kudoh M, Takahashi S, Shibuki K (2006) Transcranial fluorescence imaging of auditory cortical plasticity regulated by acoustic environments in mice. Eur J Neurosci 23:1365-1376.

Takesian AE, Kotak VC, Sanes DH (2012) Age-dependent effect of hearing loss on cortical inhibitory synapse function. J Neurophysiol 107:937-947.

Tian L, Hires SA, Mao T, Huber D, Chiappe ME, Chalasani SH, Petreanu L, Akerboom J, McKinney SA, Schreiter ER, Bargmann CI, Jayaraman V, Svoboda K, Looger LL (2009) Imaging neural activity in worms, flies and mice with improved GCaMP calcium indicators. Nat Methods 6:875-881.

Timney B, Mitchell DE, Cynader M (1980) Behavioral evidence for prolonged sensitivity to effects of monocular deprivation in dark-reared cats. J Neurophysiol 43:1041-1054.

Tolner EA, Sheikh A, Yukin AY, Kaila K, Kanold PO (2012) Subplate neurons promote spindle bursts and thalamocortical patterning in the neonatal rat somatosensory cortex. J Neurosci 32:692-702.

Trachtenberg JT, Trepel C, Stryker MP (2000) Rapid extragranular plasticity in the absence of thalamocortical plasticity in the developing primary visual cortex. Science 287:2029-2032.

Tritsch NX, Yi E, Gale JE, Glowatzki E, Bergles DE (2007) The origin of spontaneous activity in the developing auditory system. Nature 450:50-55.

Trujillo M, Measor K, Carrasco MM, Razak KA (2011) Selectivity for the rate of frequency-modulated sweeps in the mouse auditory cortex. J Neurophysiol 106:2825-2837.

Turrigiano GG, Nelson SB (2004) Homeostatic plasticity in the developing nervous system. Nat Rev Neurosci 5:97-107.

van der Bourg A, Yang JW, Reyes-Puerta V, Laurenczy B, Wieckhorst M, Stuttgen MC, Luhmann HJ, Helmchen F (2016) Layer-Specific Refinement of Sensory Coding in Developing Mouse Barrel Cortex. Cereb Cortex.

Van der Loos H, Woolsey TA (1973) Somatosensory cortex: structural alterations following early injury to sense organs. Science 179:395-398.

Viswanathan S, Bandyopadhyay S, Kao JP, Kanold PO (2012) Changing microcircuits in the subplate of the developing cortex. J Neurosci 32:1589-1601.

Voss P, Lassonde M, Gougoux F, Fortin M, Guillemot JP, Lepore F (2004) Early- and late-onset blind individuals show supra-normal auditory abilities in far-space. Curr Biol 14:1734-1738.

Wan CY, Wood AG, Reutens DC, Wilson SJ (2010) Early but not late-blindness leads to enhanced auditory perception. Neuropsychologia 48:344-348.

Wang HC, Bergles DE (2015) Spontaneous activity in the developing auditory system. Cell Tissue Res 361:65-75.

Wang X (2007) Neural coding strategies in auditory cortex. Hear Res 229:81-93.

Watkins PV, Kao JP, Kanold PO (2014) Spatial pattern of intra-laminar connectivity in supragranular mouse auditory cortex. Front Neural Circuits 8:15.

Wellman CL (2001) Dendritic reorganization in pyramidal neurons in medial prefrontal cortex after chronic corticosterone administration. J Neurobiol 49:245-253.

Wess J, Depireux DA, Kanold PO (2011) Sound evoked responses in neonatal subplate neurons in auditory cortex. Association for Research in Otolaryngology Poster.

Wiesel TN, Hubel DH (1963) Single-Cell Responses in Striate Cortex of Kittens Deprived of Vision in One Eye. J Neurophysiol 26:1003-1017.

Wiesel TN, Hubel DH (1965) Comparison of the effects of unilateral and bilateral eye closure on cortical unit responses in kittens. J Neurophysiol 28:1029-1040.

Willmore BD, King AJ (2009) Auditory cortex: representation through sparsification? Curr Biol 19:R1123-1125.

Willott JF, Shnerson A (1978) Rapid development of tuning characteristics of inferior colliculus neurons of mouse pups. Brain Res 148:230-233.

Winkowski DE, Kanold PO (2013) Laminar transformation of frequency organization in auditory cortex. J Neurosci 33:1498-1508.

Winkowski DE, Bandyopadhyay S, Shamma SA, Kanold PO (2013) Frontal cortex activation causes rapid plasticity of auditory cortical processing. J Neurosci 33:18134-18148.

Woolsey CW, EM. (1942) Topical projection of nerve fibers from local regions of the cochlea to the cerebral cortex of the cat. Bull Johns Hopkins Hosp 71:315-344.

Woolsey TA, Van der Loos H (1970) The structural organization of layer IV in the somatosensory region (SI) of mouse cerebral cortex. The description of a cortical field composed of discrete cytoarchitectonic units. Brain Res 17:205-242.

Wu GK, Tao HW, Zhang LI (2011) From elementary synaptic circuits to information processing in primary auditory cortex. Neurosci Biobehav Rev 35:2094-2104.

Wu GK, Arbuckle R, Liu BH, Tao HW, Zhang LI (2008) Lateral sharpening of cortical frequency tuning by approximately balanced inhibition. Neuron 58:132-143.

Yang JW, Hanganu-Opatz IL, Sun JJ, Luhmann HJ (2009) Three patterns of oscillatory activity differentially synchronize developing neocortical networks in vivo. J Neurosci 29:9011-9025.

Yao XH, Wang M, He XN, He F, Zhang SQ, Lu W, Qiu ZL, Yu YC (2016) Electrical coupling regulates layer 1 interneuron microcircuit formation in the neocortex. Nat Commun 7:12229.

Yoshimura Y, Dantzker JL, Callaway EM (2005) Excitatory cortical neurons form fine-scale functional networks. Nature 433:868-873.

Zhang K, Sejnowski TJ (1999) Neuronal tuning: To sharpen or broaden? Neural Comput 11:75-84.

Zhang LI, Bao S, Merzenich MM (2001) Persistent and specific influences of early acoustic environments on primary auditory cortex. Nat Neurosci 4:1123-1130.

Zhang LI, Bao S, Merzenich MM (2002) Disruption of primary auditory cortex by synchronous auditory inputs during a critical period. Proc Natl Acad Sci U S A 99:2309-2314.

Zhang Z, Jiao YY, Sun QQ (2011) Developmental maturation of excitation and inhibition balance in principal neurons across four layers of somatosensory cortex. Neuroscience 174:10-25.

Zhao C, Kao JP, Kanold PO (2009) Functional excitatory microcircuits in neonatal cortex connect thalamus and layer 4. J Neurosci 29:15479-15488.